

# Multi-Grid Monte Carlo via $XY$ Embedding

## I. General Theory and Two-Dimensional $O(N)$ -Symmetric Nonlinear $\sigma$ -Models

Tereza Mendes  
*Department of Physics*  
*New York University*  
*4 Washington Place*  
*New York, NY 10003 USA*  
 MENDES@MAFALDA.PHYSICS.NYU.EDU

Andrea Pelissetto  
*Dipartimento di Fisica*  
*Università degli Studi di Pisa*  
*Pisa 56100, ITALIA*  
 PELISSET@SUNTHPI1.DIFI.UNIPI.IT

Alan D. Sokal  
*Department of Physics*  
*New York University*  
*4 Washington Place*  
*New York, NY 10003 USA*  
 SOKAL@NYU.EDU

October 31, 2018

### Abstract

We introduce a variant of the multi-grid Monte Carlo (MGMC) method, based on the embedding of an  $XY$  model into the target model, and we study its mathematical properties for a variety of nonlinear  $\sigma$ -models. We then apply the method to the two-dimensional  $O(N)$ -symmetric nonlinear  $\sigma$ -models (also called  $N$ -vector models) with  $N = 3, 4, 8$  and study its dynamic critical behavior. Using lattices up to  $256 \times 256$ , we find dynamic critical exponents  $z_{int, \mathcal{M}^2} \approx 0.70 \pm 0.08, 0.60 \pm 0.07, 0.52 \pm 0.10$  for  $N = 3, 4, 8$ , respectively (subjective 68% confidence intervals). Thus, for these asymptotically free models, critical slowing-down is greatly reduced compared to local algorithms, but not completely eliminated; and the dynamic critical exponent does apparently vary with  $N$ . We also analyze the static data for  $N = 8$  using a finite-size-scaling extrapolation method. The correlation length  $\xi$  agrees with the four-loop asymptotic-freedom prediction to within  $\approx 1\%$  over the interval  $12 \lesssim \xi \lesssim 650$ .

# 1 Introduction

By now it is widely recognized [1, 2, 3, 4] that better simulation algorithms, with strongly reduced critical slowing-down, are needed for high-precision Monte Carlo studies of statistical-mechanical systems near critical points and of quantum field theories (such as QCD) near the continuum limit. One promising class of such algorithms is *multi-grid Monte Carlo* (MGMC) [5, 6, 7, 8, 9, 10, 11, 12, 13, 14, 15, 16, 17, 18, 19, 20, 21, 22, 23, 24]: this is a collective-mode approach that introduces block updates (of fixed shape but variable amplitude) on all length scales. The basic ingredients of the method are<sup>1</sup>:

1) *Interpolation operator*: This is a rule specifying the shape of the block update. The interpolations most commonly used are *piecewise-constant* (square-wave updates) and *piecewise-linear* (pyramidal-wave updates).

2) *Cycle control parameter  $\gamma$* : This is an integer number that determines the way in which the different block sizes are visited. In general, blocks of linear size  $2^l$  are updated  $\gamma^l$  times per iteration. Thus, in the W-cycle ( $\gamma = 2$ ) more emphasis is placed on large length scales than in the V-cycle ( $\gamma = 1$ ).

3) *Basic (smoothing) iteration*: This is the local Monte Carlo update that is performed on each level. Typically one chooses to use *heat-bath* updating if the distribution can be sampled in some simple way, and *Metropolis* updating otherwise.

4) *Implementation*: The computations can be implemented either in the *recursive multi-grid* style using explicit coarse-grid fields [25, 26, 5, 6, 7, 8, 9], or in the *unigrid* style using block updates acting directly on the fine-grid fields [27, 11, 12, 13, 14, 15]. For a  $d$ -dimensional system of linear size  $L$ , the computational labor per iteration is

$$\text{Work(MG)} \sim \begin{cases} L^d & \text{for } \gamma < 2^d \\ L^d \log L & \text{for } \gamma = 2^d \\ L^{\log_2 \gamma} & \text{for } \gamma > 2^d \end{cases} \quad (1.1)$$

for the recursive multi-grid approach, and

$$\text{Work(UG)} \sim \begin{cases} L^d \log L & \text{for } \gamma = 1 \\ L^{d + \log_2 \gamma} & \text{for } \gamma > 1 \end{cases} \quad (1.2)$$

for the unigrid approach. Thus, the unigrid implementation is marginally more expensive for a V-cycle, but prohibitively more expensive for a W-cycle.

The efficiency of the MGMC method can be analyzed rigorously in the case of the Gaussian (free-field) model, for which it can be proven [5, 6, 28] that critical slowing-down is completely eliminated. That is, the *autocorrelation time*  $\tau$  is bounded as the correlation length  $\xi$  and the lattice size  $L$  tend to infinity, so that the *dynamic critical exponent*  $z$  is zero.<sup>2</sup> More precisely, the algorithm with piecewise-linear interpolation exhibits  $z = 0$  for both the V-cycle and the W-cycle, while the algorithm with piecewise-constant interpolation has  $z = 0$  only for the W-cycle (the piecewise-constant V-cycle has  $z = 1$ ).

---

<sup>1</sup> See [6] for details.

<sup>2</sup> See [4] for a pedagogical discussion of the various autocorrelation times and their associated dynamic critical exponents.

One is therefore motivated to apply MGMC to “nearly Gaussian” systems; one might hope that critical slowing-down would likewise be completely eliminated (possibly modulo a logarithm) or at least greatly reduced compared to the  $z \approx 2$  of local algorithms. In particular, we are interested in applying MGMC to asymptotically free two-dimensional  $\sigma$ -models, such as the  $N$ -vector models [also called  $O(N)$ -invariant  $\sigma$ -models] for  $N > 2$ , the  $SU(N)$  and  $SO(N)$  principal chiral models, and the  $RP^{N-1}$  and  $CP^{N-1}$   $\sigma$ -models.<sup>3</sup>

In view of the rigorous results for the Gaussian case, we want to investigate two questions:

1) Is  $z = 0$  for all asymptotically free two-dimensional  $\sigma$ -models? If not, does  $z$  vary from one asymptotically free model to another?

2) Is the algorithm with piecewise-constant interpolation and a W-cycle as efficient (at least in order of magnitude) as the one with piecewise-linear interpolation and a V-cycle, i.e. is  $z_{PC,W}$  equal to  $z_{PL,V}$  for these models?

The key design choice in a MGMC algorithm is that of the interpolation operator; indeed, this choice determines most of the remaining ingredients. If one chooses a “smooth” interpolation such as piecewise-linear, then it is usually impossible to implement true recursive MGMC, as there is no simple form for the induced coarse-grid Hamiltonians.<sup>4</sup> Therefore one is obliged to use the unigrid style, a V-cycle, and Metropolis updating. We call this the “German” approach [10, 11, 12, 13, 14, 15]. On the other hand, if one chooses a “crude” interpolation such as piecewise-constant, then one is obliged to use a W-cycle in order to have a chance at  $z < 1$ ; but piecewise-constant interpolation usually gives rise to a simple coarse-grid Hamiltonian (typically a slight generalization of the fine-grid Hamiltonian<sup>5</sup>), so

---

<sup>3</sup> In [6, Section IX.C] we conjectured that that for asymptotically free theories — which are “almost Gaussian” except at very long distances — the critical slowing-down should be completely eliminated except for a possible logarithm. However, when we made a numerical study of MGMC in the two-dimensional 4-vector model [8], we found to our surprise that the dynamic critical exponent is *not* zero:  $z_{int,\mathcal{M}^2} = 0.60 \pm 0.07$  (subjective 68% confidence interval). We then produced [8, Section 4.1] a heuristic explanation of this fact, based on the logarithmically decaying deviations from Gaussianness in an asymptotically free theory.

Shortly thereafter, Richard Brower (private communication) pointed out to us that if our explanation is correct, it follows that for a *one*-dimensional  $\sigma$ -model — in which the deviations from Gaussianness decay much more rapidly, namely as a power law — the critical slowing-down should be *completely* eliminated, i.e. we should have  $z_{MGMC} = 0$  (with *no* logarithm). We hardly doubted that this would be the case, but we decided to make an empirical test to settle the matter once and for all. We have recently [9] reported numerical evidence suggesting that the critical slowing-down is *not* in fact completely eliminated in the one-dimensional  $O(4)$ -symmetric  $\sigma$ -model, but is rather logarithmic:  $\tau_{int,\mathcal{M}^2} \sim \log \xi$ . It goes without saying that we have no idea why this is the case.

<sup>4</sup> In particular, this occurs for the nonlinear  $\sigma$ -models. The trouble is that concepts like “an update of half the magnitude ...” have no natural meaning in a nonlinear manifold; and whatever precise definition one chooses, one is left with a horribly nonlinear expression for the coarse-grid Hamiltonian.

<sup>5</sup> For example, consider a model in which the fields  $\{g_x\}$  are unitary matrices, and in which the block update is left-multiplication  $g_x^{new} = h_y g_x^{old}$  where  $x$  is a fine-grid site,  $y$  is a coarse-grid site,  $h_y$  is the coarse-grid field, and  $x \in B_y \equiv$  the fine-grid block corresponding to coarse-grid site  $y$ . Then, if the Hamiltonian on grid  $l$  is

$$H_l(g) = \sum_{\langle xx' \rangle} \text{Re tr}(\alpha_{xx'} g_x^\dagger g_{x'}) ,$$

the induced Hamiltonian on grid  $l+1$  will be

$$H_{l+1}(h) = \sum_{\langle yy' \rangle} \text{Re tr}(\alpha'_{yy'} h_y^\dagger h_{y'}) ,$$

that one can use the recursive multi-grid style and, at least in principle, heat-bath updating. This is the approach taken by our group [5, 6, 7, 8, 9].

The “German” version has the advantage of being easy to implement for diverse models, but its use of Metropolis updates introduces several free parameters that have to be adjusted<sup>6</sup>, making it more difficult to test systematically. “Our” version has no free parameters, but its implementation is cumbersome and model-dependent, in the sense that the program (and in particular the heat-bath subroutine) has to be drastically rewritten for each distinct model. For example, among the  $N$ -vector models, the only ones that can be handled conveniently by our “direct” MGMC method are  $N = 2$  [7] and  $N = 4$  [8], by exploiting the isomorphism with the  $U(1)$  and  $SU(2)$  groups, respectively.<sup>7</sup>

With this problem in mind, we have developed a new implementation of MGMC that combines some of the advantages of both methods; in particular, it can be used conveniently for a large class of  $\sigma$ -models with very little modification of the program.<sup>8</sup> The idea is to *embed* angular variables  $\{\theta_x\}$  into the given  $\sigma$ -model, and then update the resulting induced  $XY$  model by our standard (piecewise-constant, W-cycle, heat-bath, recursive) MGMC method. We do not claim that this approach is superior in practice to the “German” method — that remains to be determined — but we do think that it is well suited for the systematic study of the dynamic critical behavior of MGMC algorithms.

In the simplest cases, the induced  $XY$  Hamiltonian takes the form

$$\mathcal{H}_{embed} = - \sum_{\langle xx' \rangle} [\alpha_{xx'} \cos(\theta_x - \theta_{x'}) + \beta_{xx'} \sin(\theta_x - \theta_{x'})] , \quad (1.3)$$

where the induced couplings  $\{\alpha_{xx'}, \beta_{xx'}\}$  depend on the current configuration  $\{\varphi_x^{old}\}$  of the original model. Such a “generalized  $XY$  Hamiltonian” is easily simulated by MGMC; indeed, the coarse-grid Hamiltonians in  $XY$ -model MGMC are inevitably of the form (1.3), even when the fine-grid Hamiltonian is the standard  $XY$  model  $\alpha_{xx'} \equiv \alpha \geq 0$ ,  $\beta_{xx'} \equiv 0$  [6, 7]. So one may just as easily start from (1.3) already on the finest grid.

---

where the coarse-grid couplings  $\{\alpha'_{yy'}\}$  are given in terms of fine-grid couplings  $\{\alpha_{xx'}\}$  by

$$\alpha'_{yy'} = \sum_{\langle xx' \rangle: x \in B_y, x' \in B_{y'}} g_{x'} \alpha_{xx'} g_x^\dagger .$$

(Remark: In this paper grid 0 is the finest grid, and grid  $l$  maps to blocks of linear size  $2^l$ . This notation is opposite to that used in [6, 7, 8]; it now seems to us to be more natural.)

<sup>6</sup> For each block size  $2^l$ , one must choose the Metropolis hit size  $t_l$  and the number  $N_l$  of Metropolis hits per site. As shown by Grabenstein and Pinn [19, 20, 22], for smooth interpolations in Gaussian and “near-Gaussian” models (such as  $\sigma$ -models) it is natural to take  $t_l = t_0 2^{-(d-2)l/2}$  and  $N_l = N_0$ ; this is expected to ensure an acceptance fraction roughly independent of  $l$ . So it suffices to choose  $t_0$  and  $N_0$ .

<sup>7</sup> For general  $N$ -vector models, our direct MGMC method is still applicable, but one must first “lift” the theory from the manifold  $S^{N-1}$  to the group  $SO(N)$ , as described in [6, Section IV] and [8, Section 2]. One then has the problem of writing an efficient heat-bath subroutine for generating random variables  $R \in SO(N)$  with probability density  $\sim \exp \text{tr}(AR)$ , where  $A$  is a general real  $N \times N$  matrix. For  $N \geq 3$  this seems to be quite messy.

<sup>8</sup> We devised this approach after extensive discussions with Martin Hasenbusch and Steffen Meyer at the Lattice '92 conference in Amsterdam. In particular, the idea of  $XY$  embedding is made explicit in their work: see equations (5)/(6) in [14] and equations (5)–(9) in [15].

For future reference, let us call the Hamiltonian (1.3) *ferromagnetic* if  $\alpha_{xx'} \geq 0$  and  $\beta_{xx'} = 0$  for all bonds  $\langle xx' \rangle$ ; let us call it *unfrustrated* if there exists a configuration  $\{\theta_x\}$  that simultaneously minimizes the bond energy  $-\alpha_{xx'} \cos(\theta_x - \theta_{x'}) + \beta_{xx'} \sin(\theta_x - \theta_{x'})$  on all bonds  $\langle xx' \rangle$ .

In models with isotensor or adjoint-representation couplings, the induced XY model will in some cases have also “isospin-2” terms:

$$\begin{aligned} \mathcal{H}_{embed} = & - \sum_{\langle xx' \rangle} [\alpha_{xx'} \cos(\theta_x - \theta_{x'}) + \beta_{xx'} \sin(\theta_x - \theta_{x'}) \\ & + \gamma_{xx'} \cos(2\theta_x - 2\theta_{x'}) + \delta_{xx'} \sin(2\theta_x - 2\theta_{x'})] . \end{aligned} \quad (1.4)$$

We shall call such a Hamiltonian ferromagnetic if  $\alpha_{xx'}, \gamma_{xx'} \geq 0$  and  $\beta_{xx'} = \delta_{xx'} = 0$  for all bonds  $\langle xx' \rangle$ ; we call it unfrustrated if there exists a configuration  $\{\theta_x\}$  that simultaneously minimizes the bond energy  $-\alpha_{xx'} \cos(\theta_x - \theta_{x'}) + \beta_{xx'} \sin(\theta_x - \theta_{x'}) + \gamma_{xx'} \cos(2\theta_x - 2\theta_{x'}) + \delta_{xx'} \sin(2\theta_x - 2\theta_{x'})$  on all bonds  $\langle xx' \rangle$ .

Already in a previous paper, we noted in passing [29, pp. 516–517] the possibility of XY-embedding MGMC; we argued, however, that it is *no better* than direct MGMC, because the updates in XY-embedding MGMC are simply a subset of those available in direct MGMC. This is true, but it is also true that XY-embedding MGMC is likely to be *no worse* than direct MGMC (except for a constant factor), at least for asymptotically free  $\sigma$ -models: this is because, in such a model, the spin waves along different axes in internal-spin space are weakly coupled.<sup>9</sup> And XY-embedding MGMC can be much more convenient to implement than direct MGMC.

One might wonder why we have bothered studying MGMC algorithms for two-dimensional  $N$ -vector models, when Wolff’s [30] cluster algorithm already succeeds in completely eliminating the critical slowing-down for these models [30, 31, 32, 29, 33]. The reason is that the success of generalized Wolff-type embedding algorithms appears to be limited to  $N$ -vector models (and possibly also  $RP^{N-1}$  models) [29], while MGMC can be expected to behave qualitatively similarly for all asymptotically free  $\sigma$ -models.<sup>10</sup> Therefore, we want to understand systematically the dynamic critical behavior of MGMC in asymptotically free  $\sigma$ -models. We have started with the  $N$ -vector models because of their simplicity, but our eye is ultimately on more general  $\sigma$ -models, such as those taking values in  $SU(N)$  [14, 34, 35] or  $CP^{N-1}$  [14, 15].

The plan of this paper is as follows: In Section 2 we introduce XY embeddings for a variety of nonlinear  $\sigma$ -models, and we analyze their mathematical properties. In Section 3 we report our numerical data on the XY-embedding MGMC algorithm for the two-dimensional  $N$ -vector models with  $N = 3, 4, 8$ . In Section 4 we analyze our static data for the  $N = 8$  case, using a finite-size-scaling extrapolation method [36, 37, 38, 39, 40] and comparing the results

---

<sup>9</sup> It would be very interesting to study direct versus XY-embedding MGMC also in *non*-asymptotically-free  $\sigma$ -models, such as the *three*-dimensional  $N$ -vector model (e.g. with  $N = 4$ ). Of course, the dynamic critical behavior of MGMC in such a model is an open question even in the XY case  $N = 2$ .

<sup>10</sup> Additional difficulties might arise in models that have important discrete excitations (i.e. vortices) in addition to spin waves: for example, the  $RP^{N-1}$  model, the  $SO(N)$  chiral model, and the adjoint  $SU(N)$  chiral model. These difficulties would be analogous to the mediocre performance of MGMC in the two-dimensional XY model in the high-temperature (vortex) phase [7, 16].

to the four-loop asymptotic-freedom predictions [41]. In Section 5 we analyze our dynamic data for  $N = 3, 4, 8$ , using traditional finite-size-scaling plots to extract the dynamic critical exponents  $z_{int, \mathcal{M}^2}$ . In Section 6 we discuss our findings.

A brief preliminary version of this work appeared in [34]. In a subsequent paper [35] we will report results for  $XY$ -embedding MGMC applied to the two-dimensional  $SU(3)$  principal chiral model.

## 2 $XY$ Embedding

In this section we introduce  $XY$  embeddings for a variety of nonlinear  $\sigma$ -models, and we analyze their mathematical properties. In particular, for each model and each choice of embedding, we want to answer the following two questions:

- (a) Is the induced  $XY$  Hamiltonian of the *simple form* (1.3) [as opposed to the “mixed isospin-1/isospin-2” form (1.4)]? This question is relevant because it is much easier to write an MGMC program (and in particular a heat-bath subroutine) for (1.3) than for (1.4).
- (b) Is the induced  $XY$  Hamiltonian *unfrustrated*? This question *may* be relevant to the dynamic critical behavior of the resulting algorithm (at any rate we want to *find out* whether it is relevant).

After making some general comments on embedding algorithms (Section 2.1), we introduce the models and the embeddings and compute the induced  $XY$  Hamiltonians (Section 2.2). Next we ask whether or not these induced  $XY$  Hamiltonians are frustrated (Section 2.3). We also discuss some alternative embeddings (Section 2.4). Finally, we summarize our results (Section 2.5).

### 2.1 Generalities on Embedding Algorithms

The general idea of embedding algorithms [4, 29] is the following: “Foliate” the configuration space of the original model into “leaves” isomorphic to the configuration space of some “embedded” model (which may be an Ising model,  $XY$  model, etc.). The Monte Carlo process then moves around the current leaf, using any legitimate Monte Carlo algorithm for simulating the conditional probability distribution of the original model restricted to that leaf; this conditional probability distribution (which of course depends on the current configuration of the original model) defines the induced Hamiltonian for the embedded model.<sup>11</sup> Of course, one must combine this procedure with other moves, or with different foliations, in order to make the algorithm ergodic.

Clearly, the updates available in an embedding algorithm with a specified foliation are a *subset* of all the updates available in a general Monte Carlo algorithm for the original model. So embedding never enlarges the space of possible algorithms; if anything, it restricts it. And the smaller the “leaves” of the foliation, the slower the algorithm is likely to move through

---

<sup>11</sup> This same structure arises in the coarse-grid updates of MGMC algorithms; we have termed it “partial resampling” [1, 5, 6].

the configuration space. The advantage of embedding is, rather, that the embedded model may be much *simpler* than the original model. As a result, it may be easier to invent a good algorithm for updating the embedded model than for updating the original model; or even if good algorithms for both models can be invented, the former algorithm may be easier to implement in practice. Thus, embedding may even lead to a *loss* in efficiency compared to alternative algorithms; but if this loss is not too great, it may be outweighed by the *simplicity* of programming and by the *flexibility* of the method (which is important in case we want to apply the method systematically to several similar models).

The dynamic critical behavior of an embedding algorithm is determined by the combined effect of two *completely distinct* issues:

- i) How well the chosen embedding succeeds in “encoding” the important large-scale collective modes of the original model into the embedded variables.
- ii) How well the chosen algorithm for updating the embedded model succeeds in its task.

Thus, if the physically relevant large-scale collective motions of the original model cannot be obtained by motions *within* a leaf, then the embedding algorithm will have severe critical slowing-down *no matter what* method is used to update the embedded variables. On the other hand, if the embedding algorithm with a *particular* choice of updating method for the embedded model shows severe critical slowing-down, this does *not* necessarily mean that the embedding *per se* works badly: the poor performance might be due to slow decorrelation in the inner-loop subroutine for updating the embedded model, and could possibly be remedied by switching to a better inner-loop algorithm.

To study question (i) independently of question (ii), it is conceptually useful to consider the *idealized embedding algorithm* [29], in which a new configuration on the current leaf is chosen, *independent of the old configuration*, with probabilities given by the conditional probability distribution restricted to that leaf. Of course, such an algorithm is not practical, but that is not its role. Rather, it serves as a standard of comparison (and presumed lower bound on the autocorrelation time) for *all* algorithms based on the given embedding. To approximate in practice the idealized embedding algorithm, we can update the embedded model by  $N_{hit}$  hits of some chosen algorithm, and extrapolate to  $N_{hit} = \infty$ .<sup>12</sup> To be sure, this test procedure can be very time-consuming; we have implemented it in our work on generalized Wolff-type embedding algorithms [29], for which the embedded variables are Ising spins.

Here, by contrast, the embedded variables are  $XY$  spins, and we suspect [29, p. 517] that the idealized embedding algorithm will have *no* critical slowing-down (because of the weak coupling between spin waves along different internal-spin axes in an asymptotically free  $\sigma$ -model). This prediction should, of course, be carefully tested; but in this initial study we have for simplicity restricted attention to the “practical” algorithm having  $N_{hit} = 1$ . We want to know whether the  $XY$ -embedding MGMC algorithm lies in the same dynamic universality class as the direct MGMC algorithm for the same model; and we want to know whether (and how) the dynamic critical exponents vary from one asymptotically free model to another.

---

<sup>12</sup> Preferably we would perform simulations for successively increasing values of  $N_{hit}$  until the autocorrelation time is constant within error bars. However, this may not always be feasible.

There is one situation in which one might worry that the practical ( $N_{hit} = 1$ )  $XY$ -embedding MGMC algorithm could behave poorly even though the idealized ( $N_{hit} = \infty$ ) algorithm would behave well: this is when the induced  $XY$  Hamiltonian is strongly frustrated, so that it has multiple ground states (or approximate ground states) separated by large energy barriers. In such a situation, the MGMC moves, which are basically spin waves, would probably be insufficient to surmount these energy barriers and to find the distant ground states.<sup>13</sup> We have therefore taken care to investigate, for each of our  $XY$  embeddings, whether the induced  $XY$  Hamiltonian is frustrated or not. (This is a natural theoretical question in any case: one wants to know the properties of the induced  $XY$  Hamiltonian. It is also relevant for *analytical* applications of  $XY$  embedding, such as the proof of correlation inequalities [42, 43, 44].) It turns out that in the case of  $N$ -vector models the induced  $XY$  Hamiltonian is unfrustrated, while for  $SU(N)$  chiral models it is generically frustrated. Nevertheless,  $XY$ -embedding MGMC performs well (dynamic critical exponents  $z$  in the range 0.4–0.7) in *both* cases [34, 35]. We think this is because the induced  $XY$  Hamiltonian in the  $SU(N)$  case is only *weakly* frustrated as  $\beta \rightarrow \infty$ ; we intend to study this point in more detail in a subsequent paper devoted specifically to  $SU(N)$  chiral models [35].

Let us now define our notation for nonlinear  $\sigma$ -models. The original model will have field variables (“spins”)  $\varphi_x$  living on lattice sites  $x \in \mathbb{Z}^d$  and taking values in a compact manifold (“target space”)  $M$ .<sup>14</sup> The Hamiltonian  $\mathcal{H}$  of this model will have a global symmetry group  $G$ , i.e.  $\mathcal{H}(\{\varphi_x\}) = \mathcal{H}(\{g\varphi_x\})$  for all  $g \in G$  and all field configurations  $\{\varphi_x\}$ . We shall assume that  $G$  is a compact Lie group with Lie algebra  $\mathfrak{g}$ , and that  $G$  acts transitively on  $M$ .

It is worth mentioning a useful heuristic principle for finding candidates for “good” embedding algorithms [29, p. 517]; this principle includes as special cases both the Wolff-type embedding of Ising spins and the multi-grid-type embedding of spin waves. The idea is to take an exact *global* symmetry of the model (global reflection in the case of Wolff, global rotation in the case of multi-grid) and to apply it in an *inhomogeneous* way (constant on clusters in the case of Wolff, constant on blocks in the case of multi-grid). In other words, one picks a subgroup  $H \subset G$  (possibly all of  $G$ ) and then embeds a model taking values in  $H$ , via the update  $\varphi_x^{new} = h_x \varphi_x^{old}$ . Because  $H$  is an exact global symmetry of the original model, the energy cost of such an update is *zero* whenever the field  $\{h_x\}$  is constant (independent of  $x$ ). Therefore, if  $\{h_x\}$  is “almost constant” (e.g. constant on a large block), then the energy cost is only a “surface term”.<sup>15</sup>

Let us mention, finally, that embedding algorithms can be written in two alternate (but physically equivalent) parametrizations. On the one hand, the embedded variables  $\{h_x\}$  can be considered as *updates* to the current values  $\{\varphi_x^{old}\}$  of the original spins; this is the interpretation taken in the formula  $\varphi_x^{new} = h_x \varphi_x^{old}$ . On the other hand, in *some* models the embedded variables can be taken to be a *subset of the new values*  $\{\varphi_x^{new}\}$  of the original

---

<sup>13</sup> A similar problem occurs in MGMC for the ordinary two-dimensional  $XY$  model just above the Kosterlitz-Thouless critical temperature: the MGMC moves are inefficient at creating and destroying vortices [7, 16].

<sup>14</sup> We shall use the notation  $\varphi_x$  for generic discussions. When discussing specific models we shall use standard notations:  $\sigma_x$  for real unit vectors,  $\mathbf{z}_x$  for complex unit vectors,  $U_x$  for  $SU(N)$  matrices, etc.

<sup>15</sup> The principle of looking for collective-mode updates whose energy cost is only a “surface term” is also made explicit by Grabenstein and Pinn [22, 23].



spins: for example, in the  $N$ -vector model the embedded variable  $\theta_x$  can be taken to be the angle of certain components of  $\varphi_x^{new}$  with respect to some fixed basis [see (2.30) ff. for details]. The first parametrization always exists, while the second one exists only in some cases (e.g. in  $N$ -vector models but apparently not in  $SU(N)$  models). The advantage of the second parametrization, when it does exist, is that certain properties of the embedded Hamiltonian (e.g. nonfrustration) are more manifest. When both parametrizations exist, they are related by a gauge transformation with gauge group  $H$ .

## 2.2 XY Embedding: Some Examples

### 2.2.1 Embedded Variables as Updates

The basic idea of our algorithm is to embed angular variables  $\{\theta_x\}$  into the given  $\sigma$ -model; we then update the resulting induced XY model by our standard (piecewise-constant, W-cycle, heat-bath, recursive) MGMC method.

Consider, therefore, a  $\sigma$ -model with target manifold  $M$  and global symmetry group  $G$ ; we assume that  $G$  is a connected compact Lie group with Lie algebra  $\mathfrak{g}$ , and that  $G$  acts transitively on  $M$ . The idea behind XY embedding is to choose randomly a  $U(1)$  subgroup  $H \subset G$ , and to apply a “rotation”  $\theta_x$  in this subgroup to the original spin variable  $\varphi_x \in M$ . Thus, the angular variables  $\theta_x$  are *updates* to the original variables  $\varphi_x$ . More precisely, we define the updated variable  $\varphi_x^{new}$  by

$$\varphi_x^{new} = e^{i\theta_x R T R^{-1}} \varphi_x^{old} = R e^{i\theta_x T} R^{-1} \varphi_x^{old}, \quad (2.1)$$

where  $R$  is a random element of  $G$ , and  $T$  is a fixed nonzero element (to be specified later) of the Lie algebra  $\mathfrak{g}$ . The embedded XY model consisting of the spins  $\{\theta_x\}$  is then simulated using the induced Hamiltonian

$$\mathcal{H}_{embed}(\{\theta_x\}) = \mathcal{H}(\{\varphi_x^{new}\}), \quad (2.2)$$

with initial condition  $\theta_x = 0$  (i.e.  $\varphi_x^{new} = \varphi_x^{old}$ ) for all  $x$ . At each iteration of the algorithm, a new random matrix  $R$  is chosen.

In general the induced XY Hamiltonian (2.2) can be extremely complicated (and thus impractical to simulate by true recursive MGMC). However, if the original Hamiltonian  $\mathcal{H}$  is sufficiently “nice” *and* one makes a clever choice of the generator  $T$ , then in some cases the induced XY Hamiltonian can be reasonably simple. Thus, we shall always choose the matrix  $T$  to have all its eigenvalues in the set  $\{-1, 0, 1\}$ . This implies that

$$e^{i\theta T} = T^2 \cos \theta + iT \sin \theta + (I - T^2), \quad (2.3)$$

where  $I$  is the identity matrix.

Let us now illustrate the method in five models:

- 1) The  $N$ -vector model:  $M = S^{N-1}$ ,  $G = SO(N)$ . The original variables  $\sigma_x$  are unit vectors in  $\mathbb{R}^N$ , and the original Hamiltonian is

$$\mathcal{H}_{N-vector} = -\beta \sum_{\langle xx' \rangle} \sigma_x \cdot \sigma_{x'}. \quad (2.4)$$

- 2) The  $SU(N)$  principal chiral model:  $M = SU(N)$ ,  $G = SU(N) \times SU(N)$ . The original variables  $U_x$  of this model are  $SU(N)$  matrices, and the original Hamiltonian is

$$\mathcal{H}_{SU(N)} = -\beta \sum_{\langle xx' \rangle} \text{Re tr}(U_x^\dagger U_{x'}) . \quad (2.5)$$

[Similar methods apply to other principal chiral models, e.g.  $SO(N)$ .]

- 3) The mixed isovector/isotensor model:  $M = S^{N-1}$ ,  $G = SO(N)$ . This model generalizes the  $N$ -vector model: the original variables  $\boldsymbol{\sigma}_x$  are again unit vectors in  $\mathbb{R}^N$ , but the Hamiltonian is now

$$\mathcal{H}_{mixed}(\{\boldsymbol{\sigma}\}) = -\beta_V \sum_{\langle xx' \rangle} \boldsymbol{\sigma}_x \cdot \boldsymbol{\sigma}_{x'} - \frac{\beta_T}{2} \sum_{\langle xx' \rangle} (\boldsymbol{\sigma}_x \cdot \boldsymbol{\sigma}_{x'})^2 . \quad (2.6)$$

[If  $\beta_T = 0$ , this is the  $N$ -vector model. If  $\beta_V = 0$ , this is the pure isotensor model, which has a local  $Z_2$  gauge group; it can therefore be thought of as taking values in  $M = RP^{N-1} \equiv S^{N-1}/Z_2$ .<sup>16</sup>]

- 4) The complex mixed isovector/isotensor model:  $M = S^{2N-1}$ ,  $G = U(N) \subset SO(2N)$ . The original variables  $\mathbf{z}_x$  are unit vectors in  $\mathbb{C}^N$ , and the original Hamiltonian is

$$\mathcal{H}_{mixed}(\{\mathbf{z}\}) = -\beta_V \sum_{\langle xx' \rangle} \text{Re}(\mathbf{z}_x^* \cdot \mathbf{z}_{x'}) - \frac{\beta_T}{2} \sum_{\langle xx' \rangle} |\mathbf{z}_x^* \cdot \mathbf{z}_{x'}|^2 . \quad (2.7)$$

[If  $\beta_T = 0$ , this is  $2N$ -vector model written in complex notation. If  $\beta_V = 0$ , this is the pure complex isotensor model, which has a global  $SU(N)$  symmetry group and a local  $U(1)$  gauge group; it can therefore be thought of as taking values in  $M = CP^{N-1} \equiv S^{2N-1}/U(1)$ .<sup>17</sup>]

- 5) The mixed fundamental/adjoint  $SU(N)$  principal chiral model:  $M = SU(N)$ ,  $G = SU(N) \times SU(N)$ . Again the original variables  $U_x$  of this model are  $SU(N)$  matrices, and the Hamiltonian is

$$\mathcal{H}_{SU(N)}(\{U\}) = -\beta_F \sum_{\langle xx' \rangle} \text{Re tr}(U_x^\dagger U_{x'}) - \beta_A \sum_{\langle xx' \rangle} \text{tr}_A(U_x^\dagger U_{x'}) , \quad (2.8)$$

where of course

$$\text{tr}_A(U) = |\text{tr}(U)|^2 - 1 . \quad (2.9)$$

---

<sup>16</sup> Note also the special case  $N = 4$  and  $\beta_V = 0$ : since  $RP^3 \simeq SO(3)$  via the correspondence

$$(V_x)_{ij} = (2\sigma_x^{(0)2} - 1)\delta_{ij} + 2\sigma_x^{(i)}\sigma_x^{(j)} + 2\sigma_x^{(0)}\varepsilon_{ijk}\sigma_x^{(k)} ,$$

where  $\boldsymbol{\sigma}_x \in S^3$  and  $V_x \in SO(3)$ , we have  $\text{tr}(V_x^T V_x) = 4(\boldsymbol{\sigma}_x \cdot \boldsymbol{\sigma}_x)^2 - 1$ , so that the  $RP^3$  model (with *this* choice of lattice action) is equivalent to the  $SO(3)$  principal chiral model.

<sup>17</sup> Note also the special case  $N = 2$  and  $\beta_V = 0$ : since  $CP^1 \simeq S^2$  via the correspondence  $\boldsymbol{\sigma}_x = \mathbf{z}_x^* \boldsymbol{\tau} \mathbf{z}_x$  where  $\boldsymbol{\tau}$  are the Pauli matrices, we have  $|\mathbf{z}_x^* \cdot \mathbf{z}_{x'}|^2 = (1 + \boldsymbol{\sigma}_x \cdot \boldsymbol{\sigma}_{x'})/2$ , so that the  $CP^1$  model (with *this* choice of lattice action) is equivalent to the standard 3-vector model.

[If  $\beta_A = 0$ , this is the usual  $SU(N)$  chiral model. If  $\beta_F = 0$ , this is the pure adjoint chiral model, which has a global  $SU(N) \times SU(N)$  symmetry group and a local  $Z_N$  gauge group; it can therefore be thought of as taking values in  $M = SU(N)/Z_N$ .<sup>18</sup>]

For models 1 and 3, the symmetry group is  $SO(N)$ , and the update is

$$\boldsymbol{\sigma}_x^{new} = e^{i\theta_x R T R^{-1}} \boldsymbol{\sigma}_x^{old} = R e^{i\theta_x T} R^{-1} \boldsymbol{\sigma}_x^{old}, \quad (2.10)$$

where  $R$  is a random  $SO(N)$  matrix and  $iT$  is a fixed antisymmetric  $N \times N$  real matrix. As mentioned above, we want  $T$  to have eigenvalues in  $\{\pm 1, 0\}$ . It follows that  $T$  has  $k$  eigenvalues  $+1$ ,  $k$  eigenvalues  $-1$ , and  $N - 2k$  eigenvalues  $0$ , for some integer  $k$  satisfying  $1 \leq k \leq \lfloor N/2 \rfloor$ . Here we shall choose  $k = 1$ ; the subgroup  $H$  generated by  $R T R^{-1}$  is then rotation in a single plane in  $\mathbb{R}^N$ . (Other choices of  $T$  will be discussed in Section 2.4.1 below.) Without loss of generality (because of the random choice of  $R$ ) we can take

$$T = \begin{pmatrix} 0 & i & 0 & & \\ -i & 0 & 0 & \cdots & \\ 0 & 0 & 0 & & \\ & \vdots & & \ddots & \end{pmatrix}. \quad (2.11)$$

We then have the following induced Hamiltonians:

*Model 1 (N-vector model):* The induced XY Hamiltonian is

$$\mathcal{H}_{embed} = - \sum_{\langle xx' \rangle} [\alpha_{xx'} \cos(\theta_x - \theta_{x'}) + \beta_{xx'} \sin(\theta_x - \theta_{x'})] + \text{const}, \quad (2.12)$$

where the induced couplings  $\{\alpha_{xx'}, \beta_{xx'}\}$  are given by

$$\alpha_{xx'} = \beta \boldsymbol{\sigma}_x \cdot R T^2 R^{-1} \boldsymbol{\sigma}_{x'} \quad (2.13a)$$

$$\beta_{xx'} = \beta \boldsymbol{\sigma}_x \cdot R (-iT) R^{-1} \boldsymbol{\sigma}_{x'} \quad (2.13b)$$

(and for simplicity we have dropped the superscript *old* on the  $\boldsymbol{\sigma}$ 's). For the  $k = 1$  update with the explicit choice (2.11) for  $T$ , we have

$$\alpha_{xx'} = \beta \left[ (R^{-1} \boldsymbol{\sigma}_x)_1 (R^{-1} \boldsymbol{\sigma}_{x'})_1 + (R^{-1} \boldsymbol{\sigma}_x)_2 (R^{-1} \boldsymbol{\sigma}_{x'})_2 \right] \quad (2.14a)$$

$$\beta_{xx'} = \beta \left[ (R^{-1} \boldsymbol{\sigma}_x)_1 (R^{-1} \boldsymbol{\sigma}_{x'})_2 - (R^{-1} \boldsymbol{\sigma}_x)_2 (R^{-1} \boldsymbol{\sigma}_{x'})_1 \right] \quad (2.14b)$$

Note that these couplings are in general *disordered* and *non-ferromagnetic*. However, we shall show below that they are *unfrustrated*: that is, they are  $U(1)$ -gauge-equivalent to a ferromagnetic set of couplings.

---

<sup>18</sup>Note also the special case  $N = 2$ : since  $SU(2) \simeq S^3$  via the correspondence  $U_x = \sigma_x^{(0)} I + i \vec{\sigma}_x \cdot \vec{\tau}$  where  $\boldsymbol{\sigma}_x \equiv (\sigma_x^{(0)}, \vec{\sigma}_x) \in S^3$  and  $\vec{\tau}$  are the Pauli matrices, we have  $\text{tr}(U_x^\dagger U_{x'}) = 2 \boldsymbol{\sigma}_x \cdot \boldsymbol{\sigma}_{x'}$ , so that the  $SU(2)$  mixed fundamental/adjoint model is equivalent to the  $N = 4$  mixed isovector/isotensor model.

*Model 3 (mixed isovector/isotensor model):* The induced  $XY$  Hamiltonian is

$$\begin{aligned} \mathcal{H}_{embed} = & - \sum_{\langle xx' \rangle} [\alpha_{xx'} \cos(\theta_x - \theta_{x'}) + \beta_{xx'} \sin(\theta_x - \theta_{x'}) \\ & + \gamma_{xx'} \cos(2\theta_x - 2\theta_{x'}) + \delta_{xx'} \sin(2\theta_x - 2\theta_{x'})] + \text{const} , \end{aligned} \quad (2.15)$$

with the induced couplings  $\{\alpha_{xx'}, \beta_{xx'}, \gamma_{xx'}, \delta_{xx'}\}$  given by

$$\alpha_{xx'} = (\beta_V + \beta_T c_{xx'}) a_{xx'} \quad (2.16a)$$

$$\beta_{xx'} = (\beta_V + \beta_T c_{xx'}) b_{xx'} \quad (2.16b)$$

$$\gamma_{xx'} = \frac{\beta_T}{4} (a_{xx'}^2 - b_{xx'}^2) \quad (2.16c)$$

$$\delta_{xx'} = \frac{\beta_T}{2} a_{xx'} b_{xx'} \quad (2.16d)$$

where we have defined

$$a_{xx'} = \boldsymbol{\sigma}_x \cdot R T^2 R^{-1} \boldsymbol{\sigma}_{x'} \quad (2.17a)$$

$$b_{xx'} = \boldsymbol{\sigma}_x \cdot R(-iT) R^{-1} \boldsymbol{\sigma}_{x'} \quad (2.17b)$$

$$c_{xx'} = \boldsymbol{\sigma}_x \cdot R(I - T^2) R^{-1} \boldsymbol{\sigma}_{x'} \quad (2.17c)$$

For the  $k = 1$  update with the explicit choice (2.11) for  $T$ , we get

$$a_{xx'} = [(R^{-1} \boldsymbol{\sigma}_x)_1 (R^{-1} \boldsymbol{\sigma}_{x'})_1 + (R^{-1} \boldsymbol{\sigma}_x)_2 (R^{-1} \boldsymbol{\sigma}_{x'})_2] \quad (2.18a)$$

$$b_{xx'} = [(R^{-1} \boldsymbol{\sigma}_x)_1 (R^{-1} \boldsymbol{\sigma}_{x'})_2 - (R^{-1} \boldsymbol{\sigma}_x)_2 (R^{-1} \boldsymbol{\sigma}_{x'})_1] \quad (2.18b)$$

$$c_{xx'} = \sum_{i=3}^N (R^{-1} \boldsymbol{\sigma}_x)_i (R^{-1} \boldsymbol{\sigma}_{x'})_i \quad (2.18c)$$

Note that for  $N \geq 3$  we have in general  $c_{xx'} \neq 0$ , so that  $\alpha_{xx'}, \beta_{xx'} \neq 0$  even in the pure isotensor model.<sup>19</sup>

For models 2 and 5, the symmetry group is  $SU(N)_{left} \times SU(N)_{right}$ , but we shall exploit here only the left-multiplication subgroup. Thus, we shall take as our update

$$U_x^{new} = e^{i\theta_x R T R^{-1}} U_x^{old} = R e^{i\theta_x T} R^{-1} U_x^{old} , \quad (2.19)$$

where  $R$  is a random  $SU(N)$  matrix and  $T$  is a fixed traceless Hermitian matrix with eigenvalues in  $\{\pm 1, 0\}$ . It follows that  $T$  has  $k$  eigenvalues  $+1$ ,  $k$  eigenvalues  $-1$ , and  $N - 2k$  eigenvalues  $0$ , where  $1 \leq k \leq \lfloor N/2 \rfloor$ . As before, we shall choose  $k = 1$  (see Section 2.4.1 for other choices). Without loss of generality we can take

$$T = \begin{pmatrix} 1 & 0 & 0 & \\ 0 & -1 & 0 & \cdots \\ 0 & 0 & 0 & \\ \vdots & & & \ddots \end{pmatrix} . \quad (2.20)$$

---

<sup>19</sup> However, if  $N$  is even we may choose the *alternate* embedding with  $k = N/2$ : this yields  $T^2 = I$  and hence  $c_{xx'} = 0$ . With *this* embedding, the pure isotensor model ( $\beta_V = 0$ ) has  $\alpha_{xx'} = \beta_{xx'} = 0$ . For further discussion, see Section 2.4.1.

We then have the following induced Hamiltonians:

*Model 2 (SU(N) principal chiral model):* The induced XY Hamiltonian is again of the form (2.12), with couplings

$$\alpha_{xx'} = \beta \operatorname{Re} \operatorname{tr}(U_x^\dagger R T^2 R^{-1} U_{x'}) \quad (2.21a)$$

$$\beta_{xx'} = \beta \operatorname{Re} \operatorname{tr}(U_x^\dagger R(-iT)R^{-1}U_{x'}) = \beta \operatorname{Im} \operatorname{tr}(U_x^\dagger R T R^{-1}U_{x'}) \quad (2.21b)$$

For the  $k = 1$  update with the explicit choice (2.20) for  $T$ , we have

$$\alpha_{xx'} = \beta \left[ \operatorname{Re}(R^{-1} U_{x'} U_x^\dagger R)_{11} + \operatorname{Re}(R^{-1} U_{x'} U_x^\dagger R)_{22} \right] \quad (2.22a)$$

$$\beta_{xx'} = \beta \left[ \operatorname{Im}(R^{-1} U_{x'} U_x^\dagger R)_{11} - \operatorname{Im}(R^{-1} U_{x'} U_x^\dagger R)_{22} \right] \quad (2.22b)$$

Note that these couplings are in general *disordered* and *non-ferromagnetic*; moreover, as will be seen in the next subsection, they are also generically *frustrated*, in contrast to what happens for the  $N$ -vector models.

*Model 5 (mixed fundamental/adjoint SU(N) chiral model):* The induced XY Hamiltonian is again of the form (2.15), with couplings

$$\alpha_{xx'} = \operatorname{Re} [(\beta_F + 2\beta_A c_{xx'}^*) a_{xx'}] \quad (2.23a)$$

$$\beta_{xx'} = \operatorname{Re} [(\beta_F + 2\beta_A c_{xx'}^*) b_{xx'}] \quad (2.23b)$$

$$\gamma_{xx'} = \frac{\beta_A}{2} (|a_{xx'}|^2 - |b_{xx'}|^2) \quad (2.23c)$$

$$\delta_{xx'} = \beta_A \operatorname{Re}(a_{xx'} b_{xx'}^*) \quad (2.23d)$$

where we have defined

$$a_{xx'} = \operatorname{tr}[U_x^\dagger R T^2 R^{-1} U_{x'}] \quad (2.24a)$$

$$b_{xx'} = \operatorname{tr}[U_x^\dagger R(-iT)R^{-1}U_{x'}] \quad (2.24b)$$

$$c_{xx'} = \operatorname{tr}[U_x^\dagger R(I - T^2)R^{-1}U_{x'}] \quad (2.24c)$$

Note that for  $N = 2$  we have  $T^2 = I$  and hence  $c_{xx'} = 0$ . On the other hand, for  $N \geq 3$  we have in general  $c_{xx'} \neq 0$ , so that  $\alpha_{xx'}, \beta_{xx'} \neq 0$  even in the pure adjoint model.<sup>20</sup>

*Model 4 (complex mixed isovector/isotensor model):* The symmetry group is  $U(N)$ , and we take the update to be

$$\mathbf{z}_x^{\text{new}} = e^{i\theta_x R T R^{-1}} \mathbf{z}_x^{\text{old}} = R e^{i\theta_x T} R^{-1} \mathbf{z}_x^{\text{old}}, \quad (2.25)$$

where  $R$  is a random  $SU(N)$  matrix and  $T$  is a fixed Hermitian matrix with eigenvalues in  $\{\pm 1, 0\}$ .<sup>21</sup> It follows that  $T$  has  $k$  eigenvalues  $+1$ ,  $l$  eigenvalues  $-1$ , and  $N - k - l$  eigenvalues

<sup>20</sup> However, if  $N$  is even we may choose the *alternate* embedding with  $k = N/2$ : this yields  $T^2 = I$  and hence  $c_{xx'} = 0$ . With *this* embedding, the pure adjoint model ( $\beta_F = 0$ ) has  $\alpha_{xx'} = \beta_{xx'} = 0$ .

<sup>21</sup> Note that  $T$  is *not* required to be traceless, even in the pure  $CP^{N-1}$  model ( $\beta_V = 0$ ). Of course, in this latter model the  $U(1)$  subgroup of  $U(N)$  is a local gauge group, so only the traceless part of  $T$  [i.e.  $T - (N^{-1} \operatorname{tr} T)I$ ] plays an interesting dynamical role. In particular, two update matrices  $T$  and  $T'$  that differ by a multiple of the identity give rise to physically equivalent embeddings (differing only by a gauge transformation) and identical induced XY Hamiltonians.

0, for suitable integers  $k$  and  $l$ . Here we shall choose  $k = 1$ ,  $l = 0$  (see also [15]); without loss of generality we can take

$$T = \begin{pmatrix} 1 & 0 & 0 & \\ 0 & 0 & 0 & \cdots \\ 0 & 0 & 0 & \\ \vdots & & & \ddots \end{pmatrix}. \quad (2.26)$$

The evaluation of the embedded Hamiltonian is analogous to model 3; it is of the form (2.15), with couplings

$$\alpha_{xx'} = \text{Re}[(\beta_V + \beta_T c_{xx'}^*) a_{xx'}] \quad (2.27a)$$

$$\beta_{xx'} = \text{Re}[(\beta_V + \beta_T c_{xx'}^*) b_{xx'}] \quad (2.27b)$$

$$\gamma_{xx'} = \frac{\beta_T}{4} (|a_{xx'}|^2 - |b_{xx'}|^2) \quad (2.27c)$$

$$\delta_{xx'} = \frac{\beta_T}{2} \text{Re}(a_{xx'} b_{xx'}^*) \quad (2.27d)$$

where we have defined

$$a_{xx'} = \mathbf{z}_x^* \cdot RT^2 R^{-1} \mathbf{z}_{x'} \quad (2.28a)$$

$$b_{xx'} = \mathbf{z}_x^* \cdot R(-iT) R^{-1} \mathbf{z}_{x'} \quad (2.28b)$$

$$c_{xx'} = \mathbf{z}_x^* \cdot R(I - T^2) R^{-1} \mathbf{z}_{x'} \quad (2.28c)$$

Note that because of the particular choice (2.26) of  $T$ , we have  $T^2 = T$  and hence  $b_{xx'} = -ia_{xx'}$ , which implies that  $\gamma_{xx'} = \delta_{xx'} = 0$ . So, perhaps surprisingly, the embedded Hamiltonian is of the simple form (2.12) in spite of the isotensor couplings in (2.7). This happens whenever all the complex rotations are in the same direction, i.e. either  $l = 0$  (hence  $T^2 = T$ ) or  $k = 0$  (hence  $T^2 = -T$ ). In these cases we have

$$\mathbf{z}_x^* \cdot \mathbf{z}_{x'} = A_{xx'} e^{\pm i(\theta_x - \theta_{x'})} + B_{xx'} , \quad (2.29)$$

without double-angle terms.<sup>22</sup>

### 2.2.2 Alternate Interpretation

For the two models taking values in  $S^{N-1}$  — viz. the  $N$ -vector and mixed isovector/isotensor models — there is a simpler and more natural way of specifying the embedding of angular variables. The embedding is clearly given by choosing randomly a two-dimensional subspace  $P \subset \mathbb{R}^N$  and then rotating only the component of  $\boldsymbol{\sigma}_x$  in  $P$ . [From (2.10)/(2.11) we see that  $P$  is the image of the 1–2 plane under the rotation  $R$ .] To be precise, let us decompose each vector  $\boldsymbol{\sigma}_x$  into its parts parallel and perpendicular to the plane  $P$ :

$$\boldsymbol{\sigma}_x = \boldsymbol{\sigma}_x^{\parallel} + \boldsymbol{\sigma}_x^{\perp}. \quad (2.30)$$

---

<sup>22</sup>There is another interesting possibility: If we take  $k + l = N$ , we have  $T^2 = I$  and hence  $c_{xx'} = 0$ . With this embedding, the pure isotensor model ( $\beta_V = 0$ ) has  $\alpha_{xx'} = \beta_{xx'} = 0$ . Of course, this embedding is gauge-equivalent to one with  $k' = k$ ,  $l' = 0$  and  $\theta_x$  replaced by  $2\theta_x$  (see footnote 21). For further discussion, see Section 2.4.1.

We then fix  $\{\sigma_x^\perp\}$  at their current values, and consider only  $\{\sigma_x^\parallel\}$  as dynamical variables. Substituting (2.30) into the original  $N$ -vector Hamiltonian (2.4), we get

$$\mathcal{H}_{N\text{-vector}} = -\beta \sum_{\langle xx' \rangle} \sigma_x \cdot \sigma_{x'} = -\beta \sum_{\langle xx' \rangle} \sigma_x^\parallel \cdot \sigma_{x'}^\parallel + \text{const} . \quad (2.31)$$

The angular variables  $\{\theta_x\}$  can then be defined in either of two convenient ways:

- 1) Let  $\{\theta_x\}$  be the angles of  $\sigma_x^\parallel$  with respect to the some fixed basis vectors in the plane  $P$ . In this case  $\sigma_x^\parallel \cdot \sigma_{x'}^\parallel = |\sigma_x^\parallel| |\sigma_{x'}^\parallel| \cos(\theta_x - \theta_{x'})$ , so that the embedding has the form (2.12), with couplings

$$\alpha_{xx'} = \beta |\sigma_x^\parallel| |\sigma_{x'}^\parallel| \quad (2.32a)$$

$$\beta_{xx'} = 0 \quad (2.32b)$$

and the embedded model is simulated starting from the present configuration for the angles (call it  $\{\bar{\theta}_x\}$ ). These couplings are clearly ferromagnetic (provided that  $\beta \geq 0$ ). This is the embedding implementation that is used in our MGMC program.

- 2) Alternatively, we can take  $\{\theta_x\}$  to be the angles of  $\sigma_x^\parallel$  with respect to its present orientation (given by  $\{\bar{\theta}_x\}$  in the previous coordinates). In this case the couplings are given by

$$\alpha_{xx'} = \beta |\sigma_x^\parallel| |\sigma_{x'}^\parallel| \cos(\bar{\theta}_x - \bar{\theta}_{x'}) \quad (2.33a)$$

$$\beta_{xx'} = -\beta |\sigma_x^\parallel| |\sigma_{x'}^\parallel| \sin(\bar{\theta}_x - \bar{\theta}_{x'}) \quad (2.33b)$$

and the embedded model is simulated starting from  $\theta_x \equiv 0$ . This is the approach taken in (2.10)–(2.14) above; and of course (2.33) is identical to (2.14).

The sets of couplings (2.32) and (2.33) are related by a  $U(1)$  gauge transformation: namely, the angle  $\theta_x^{(1)}$  in the “first” variables is equal to  $\theta_x^{(2)} + \bar{\theta}_x$  in the “latter” variables, for all  $x$ . Therefore, the couplings (2.14)/(2.33), though in general non-ferromagnetic, are nevertheless *unfrustrated*, since they are  $U(1)$ -gauge-equivalent to the ferromagnetic couplings (2.32).

For the mixed isovector/isotensor model we can use the same decomposition (2.30), but the embedded Hamiltonian becomes somewhat more complicated. In interpretation #2, the induced  $XY$  Hamiltonian has already been given in (2.15)–(2.18). In interpretation #1, we get

$$\begin{aligned} \mathcal{H}_{embed} \equiv & - \sum_{\langle xx' \rangle} \left[ (\beta_V + \beta_T \sigma_x^\perp \cdot \sigma_{x'}^\perp) |\sigma_x^\parallel| |\sigma_{x'}^\parallel| \cos(\theta_x - \theta_{x'}) \right. \\ & \left. + \frac{\beta_T}{4} |\sigma_x^\parallel|^2 |\sigma_{x'}^\parallel|^2 \cos(2\theta_x - 2\theta_{x'}) \right] + \text{const} . \end{aligned} \quad (2.34)$$

The couplings are clearly ferromagnetic if  $\beta_V \geq \beta_T \geq 0$ .

**Remark.** A similar representation can be employed for the *complex* mixed isovector/isotensor model with the choice (2.26) of  $T$ . The embedding is specified by choosing

a random complex direction  $\mathbf{v} \in \mathbb{C}^N$  (in fact  $\mathbf{v} = R\mathbf{e}_1$ ) and then rotating only the component of  $\mathbf{z}_x$  along  $\mathbf{v}$ . That is, we decompose  $\mathbf{z}_x = \mathbf{z}_x^\parallel + \mathbf{z}_x^\perp$  with

$$\mathbf{z}_x^\parallel = (\mathbf{z}_x \cdot \mathbf{v}^*) \mathbf{v}. \quad (2.35)$$

The analogue of interpretation #1 is obtained by defining

$$\theta_x = \arg(\mathbf{z}_x \cdot \mathbf{v}^*). \quad (2.36)$$

The induced  $XY$  Hamiltonian is of the form (2.12) (“single-angle” couplings only), with

$$\alpha_{xx'} = [\beta_V + \beta_T \operatorname{Re}(\mathbf{z}_x^{\perp*} \cdot \mathbf{z}_{x'}^\perp)] |\mathbf{z}_x^\parallel| |\mathbf{z}_{x'}^\parallel| \quad (2.37a)$$

$$\beta_{xx'} = -\beta_T \operatorname{Im}(\mathbf{z}_x^{\perp*} \cdot \mathbf{z}_{x'}^\perp) |\mathbf{z}_x^\parallel| |\mathbf{z}_{x'}^\parallel| \quad (2.37b)$$

However, these couplings are not in general ferromagnetic, even if  $\beta_V \geq \beta_T \geq 0$ , since  $\mathbf{z}_x^{\perp*} \cdot \mathbf{z}_{x'}^\perp$  need not be real. In fact, we shall show in the next section that they are in general frustrated, except in the pure  $CP^1$  model ( $N = 2$ ,  $\beta_V = 0$ ). In interpretation #2 we have the expression (2.27), with

$$a_{xx'} = i b_{xx'} = \mathbf{z}_x^{\parallel*} \cdot \mathbf{z}_{x'}^\parallel = |\mathbf{z}_x^\parallel| |\mathbf{z}_{x'}^\parallel| e^{-i(\bar{\theta}_x - \bar{\theta}_{x'})} \quad (2.38a)$$

$$c_{xx'} = \mathbf{z}_x^{\perp*} \cdot \mathbf{z}_{x'}^\perp \quad (2.38b)$$

and hence

$$\alpha_{xx'} = \operatorname{Re}[(\beta_V + \beta_T \mathbf{z}_x^\perp \cdot \mathbf{z}_{x'}^{\perp*}) \mathbf{z}_x^{\parallel*} \cdot \mathbf{z}_{x'}^\parallel] \quad (2.39a)$$

$$\beta_{xx'} = \operatorname{Im}[(\beta_V + \beta_T \mathbf{z}_x^\perp \cdot \mathbf{z}_{x'}^{\perp*}) \mathbf{z}_x^{\parallel*} \cdot \mathbf{z}_{x'}^\parallel] \quad (2.39b)$$

$$\gamma_{xx'} = \delta_{xx'} = 0 \quad (2.39c)$$

## 2.3 Frustration

Although our original models (2.4)–(2.8) are ferromagnetic and translation-invariant, we have seen that the corresponding induced  $XY$  Hamiltonians are generically non-ferromagnetic and non-translation-invariant: they contain both  $\cos(\theta_x - \theta_{x'})$  and  $\sin(\theta_x - \theta_{x'})$  terms, with coefficients of arbitrary sign. This raises the question of whether the induced  $XY$  Hamiltonians may be frustrated. Recall that a Hamiltonian<sup>23</sup> is said to be *unfrustrated* if there exists a configuration of the field variables that simultaneously minimizes the energy on each bond.

One case is easy: any *ferromagnetic*  $XY$  Hamiltonian is obviously unfrustrated, since any configuration  $\theta_x \equiv \text{constant}$  (independent of  $x$ ) simultaneously minimizes the energy on each bond. Furthermore, any  $XY$  Hamiltonian that is  $U(1)$ -gauge-equivalent to a ferromagnetic Hamiltonian is also unfrustrated. Thus, the induced  $XY$  Hamiltonian for the  $N$ -vector model is unfrustrated: it is either ferromagnetic (interpretation #1) or gauge-equivalent to

---

<sup>23</sup> More precisely, frustration is not a property of a Hamiltonian *per se*, but of a specific *decomposition* of that Hamiltonian into “elementary bonds”. Here we shall always consider the elementary terms in the Hamiltonian to be the *complete* energy associated with a *single* bond  $\langle xx' \rangle$ .



a ferromagnetic one (interpretation #2). This is also true for the mixed isovector/isotensor model with  $\beta_V \geq \beta_T \geq 0$  because of (2.34).<sup>24</sup>

For the  $SU(N)$  principal chiral models, however, the situation is less clear, as no manifestly ferromagnetic representation appears to be available. Here we shall show that no such representation can exist: the induced  $XY$  Hamiltonians are in general *frustrated* for all  $N \geq 2$ . We shall also locate the underlying cause of this frustration.

**Remark.** When we say that the induced  $XY$  Hamiltonians are “in general frustrated”, what we mean is that there *exist* configurations  $\{\varphi_x^{old}\}$  of the original model (which we shall present explicitly) for which the induced  $XY$  Hamiltonians are frustrated. We conjecture that in fact a much stronger statement is true, namely that the induced  $XY$  Hamiltonians are *generically* frustrated, in the sense that frustration occurs for *all* configurations  $\{\varphi_x^{old}\}$  except those lying on a lower-dimensional submanifold of the configuration space. We expect that this can be proven by suitable modifications of our examples, but we have not attempted to do so.

To test whether the generalized  $XY$  model (2.12) is frustrated, we consider the product around a plaquette of the quantity  $\alpha_{xx'} - i\beta_{xx'}$ . If this product is real and positive for *all* plaquettes, then the model is unfrustrated.<sup>25</sup> Conversely, if for some plaquette the product is *not* real and positive, then the model is frustrated. This is because we can rewrite (2.12) as

$$\mathcal{H}_{embed} = - \sum_{\langle xx' \rangle} \text{Re} \left[ (\alpha_{xx'} - i\beta_{xx'}) e^{i(\theta_x - \theta_{x'})} \right] = - \sum_{\langle xx' \rangle} \text{Re} \left[ \rho_{xx'} e^{i(\phi_{xx'} + \theta_x - \theta_{x'})} \right], \quad (2.40)$$

where  $\rho_{xx'} \equiv (\alpha_{xx'}^2 + \beta_{xx'}^2)^{1/2} \geq 0$  and  $\phi_{xx'} = \arg(\alpha_{xx'} - i\beta_{xx'})$ ; to minimize the energy on bond  $\langle xx' \rangle$  we need

$$\theta_{x'} = \theta_x + \phi_{xx'} \quad (2.41)$$

(provided that  $\rho_{xx'} \neq 0$ ). This can be done simultaneously for all bonds  $\langle xx' \rangle$  if and only if for each plaquette we have

$$\sum_{\square} \phi_{xx'} = 0 \pmod{2\pi}, \quad (2.42)$$

or, equivalently,

$$\prod_{\square} (\alpha_{xx'} - i\beta_{xx'}) \text{ real and positive.} \quad (2.43)$$

Let us now use the criterion (2.43) to test for frustration in our various models:

*Model 2 ( $SU(N)$  principal chiral model):* We shall prove frustration for all  $N \geq 2$ , by showing that (2.43) does *not* in general hold for the embedding (2.19)–(2.22). Without loss of generality we can take  $R = I$ . We begin with the simplest case  $N = 2$ .

In the case of  $SU(2)$  matrices, it is easy to show that for our choice of  $T$  we get from (2.21) the simple form

$$\alpha_{xx'} - i\beta_{xx'} = 2\beta (U_x U_{x'}^\dagger)_{11}. \quad (2.44)$$

---

<sup>24</sup>For a more complete discussion of the mixed case, see Section 2.4.1.

<sup>25</sup> In periodic boundary conditions this statement is not quite correct: one should also insist that this product be real and positive for “Polyakov loops” that wind around the lattice by periodicity.

Then we want to show that around a plaquette with sites  $A, B, C, D$  the product

$$(U_A U_B^\dagger)_{11} (U_B U_C^\dagger)_{11} (U_C U_D^\dagger)_{11} (U_D U_A^\dagger)_{11} \quad (2.45)$$

is not necessarily real and positive. It suffices to take  $U_A = U_D = I$  and general  $U_B$  and  $U_C$ :

$$U_B = \begin{pmatrix} \alpha & \beta \\ -\beta^* & \alpha^* \end{pmatrix} \quad (2.46a)$$

$$U_C = \begin{pmatrix} \gamma & \delta \\ -\delta^* & \gamma^* \end{pmatrix} \quad (2.46b)$$

where  $|\alpha|^2 + |\beta|^2 = |\gamma|^2 + |\delta|^2 = 1$ . We get for the product in (2.45)

$$|\alpha|^2 |\gamma|^2 + \alpha^* \beta \gamma \delta^*. \quad (2.47)$$

Although the first term is real and positive, the second is free to have an imaginary part (for example, take  $\alpha = \cos \theta$ ,  $\beta = \sin \theta$ ,  $\gamma = \cos \theta'$ ,  $\delta = i \sin \theta'$ ), and therefore the couplings are in general frustrated.

This example can be immediately extended to  $SU(N)$  for  $N \geq 3$ : it suffices to take matrices  $U$  which are block-diagonal, in which the uppermost  $2 \times 2$  block is as above, and the lowermost  $(N-2) \times (N-2)$  block is an arbitrary  $SU(N-2)$  matrix. Thus, for all  $N \geq 2$  our  $SU(N)$  algorithm leads in general to a *frustrated* induced  $XY$  model.

The presence of frustration even in the  $SU(2)$  case may seem surprising, as there is an isomorphism relating the  $SU(2)$  chiral model to the 4-vector model, and we know that the embedding (2.10)/(2.11) for  $N$ -vector models is unfrustrated. The explanation is that the  $SU(2)$  embedding (2.19) does *not* map into the 4-vector embedding (2.10)/(2.11), but rather into a *different* embedding! Let us work this out in detail, using the isomorphism

$$U = s_0 I + i \vec{s} \cdot \vec{\sigma} \quad (2.48)$$

between  $U \in SU(2)$  and  $\mathbf{s} = (s_0, s_1, s_2, s_3) \in S^3 \subset \mathbb{R}^4$ ; here  $I$  is the  $2 \times 2$  identity matrix,  $\vec{\sigma}$  represents the Pauli matrices, and we use the symbol  $\vec{s}$  to denote the 3-vector  $(s_1, s_2, s_3)$ . The Hamiltonian (2.5) for the  $SU(2)$  chiral model corresponds to the Hamiltonian (2.4) for the 4-vector model, with the identification  $\beta_{4\text{-vector}} = 2\beta_{SU(2)}$ .

Let us now work out the update at a single site  $x$  (for simplicity we suppress the subscript  $x$  from the notation). We have

$$RTR^{-1} = \vec{a} \cdot \vec{\sigma} \quad (2.49)$$

for some unit vector  $\vec{a} \in \mathbb{R}^3$ . Substituting (2.48) and (2.49) in (2.19), we get

$$s_0^{\text{new}} I + i \vec{s}^{\text{new}} \cdot \vec{\sigma} = (\cos \theta + i \vec{a} \cdot \vec{\sigma} \sin \theta) (s_0^{\text{old}} I + i \vec{s}^{\text{old}} \cdot \vec{\sigma}) \quad (2.50)$$

and hence

$$s_0^{\text{new}} = (\cos \theta) s_0^{\text{old}} - (\sin \theta) \vec{a} \cdot \vec{s}^{\text{old}} \quad (2.51a)$$

$$\vec{s}^{\text{new}} = (\cos \theta) \vec{s}^{\text{old}} + (\sin \theta) [s_0^{\text{old}} \vec{a} - (\vec{a} \times \vec{s}^{\text{old}})] \quad (2.51b)$$

where we have used

$$(\vec{a} \cdot \vec{\sigma})(\vec{s} \cdot \vec{\sigma}) = \vec{a} \cdot \vec{s} + i(\vec{a} \times \vec{s}) \cdot \vec{\sigma}. \quad (2.52)$$

For example, if we choose  $\vec{a} = (1, 0, 0)$ , we have

$$s_0^{new} = (\cos \theta) s_0^{old} - (\sin \theta) s_1^{old} \quad (2.53a)$$

$$s_1^{new} = (\sin \theta) s_0^{old} + (\cos \theta) s_1^{old} \quad (2.53b)$$

$$s_2^{new} = (\cos \theta) s_2^{old} + (\sin \theta) s_3^{old} \quad (2.53c)$$

$$s_3^{new} = -(\sin \theta) s_2^{old} + (\cos \theta) s_3^{old} \quad (2.53d)$$

and we can see that this corresponds to *two* coupled rotations for the 4-vector  $\mathbf{s}$ : a counter-clockwise rotation on the plane defined by the 0-direction and  $\vec{a}$ , and a clockwise rotation on the plane orthogonal to this one. By contrast, our standard 4-vector update (2.10), with  $T$  given by the  $k = 1$  choice (2.11), corresponds to a rotation in one plane only. Clearly, the  $SU(2)$  update (2.53) corresponds to the 4-vector update (2.10) with  $T$  given instead by the  $k = 2$  choice

$$T = \begin{pmatrix} 0 & i & 0 & 0 \\ -i & 0 & 0 & 0 \\ 0 & 0 & 0 & -i \\ 0 & 0 & i & 0 \end{pmatrix}. \quad (2.54)$$

The induced  $XY$  Hamiltonian is then (2.12) with the couplings

$$\alpha_{xx'} = 2\beta \left[ |\boldsymbol{\sigma}_x^\parallel| |\boldsymbol{\sigma}_{x'}^\parallel| \cos(\bar{\theta}_x^\parallel - \bar{\theta}_{x'}^\parallel) + |\boldsymbol{\sigma}_x^\perp| |\boldsymbol{\sigma}_{x'}^\perp| \cos(\bar{\theta}_x^\perp - \bar{\theta}_{x'}^\perp) \right] \quad (2.55a)$$

$$\beta_{xx'} = -2\beta \left[ |\boldsymbol{\sigma}_x^\parallel| |\boldsymbol{\sigma}_{x'}^\parallel| \sin(\bar{\theta}_x^\parallel - \bar{\theta}_{x'}^\parallel) - |\boldsymbol{\sigma}_x^\perp| |\boldsymbol{\sigma}_{x'}^\perp| \sin(\bar{\theta}_x^\perp - \bar{\theta}_{x'}^\perp) \right] \quad (2.55b)$$

where  $\bar{\theta}_x^\parallel$  and  $\bar{\theta}_x^\perp$  are the initial angles of  $\boldsymbol{\sigma}_x^\parallel \equiv (s_0, s_1)$  and  $\boldsymbol{\sigma}_x^\perp \equiv (s_2, s_3)$ , respectively. These couplings are clearly frustrated, since although there exist gauge transformations that will make the “parallel” or the “perpendicular” part of the couplings become ferromagnetic separately, we cannot in general make them *simultaneously* ferromagnetic (unless by chance we had  $\bar{\theta}_x^\parallel = \bar{\theta}_x^\perp$  for all  $x$ , or some similar degenerate situation). For example, consider a plaquette  $ABCD$  with angles  $(\bar{\theta}_x^\parallel, \bar{\theta}_x^\perp)$  given by  $(\theta, 0), (0, 0), (0, 0), (0, 0)$ , respectively. Then the product of

$$\alpha_{xx'} - i\beta_{xx'} = 2\beta \left[ |\boldsymbol{\sigma}_x^\parallel| |\boldsymbol{\sigma}_{x'}^\parallel| e^{i(\bar{\theta}_x^\parallel - \bar{\theta}_{x'}^\parallel)} + |\boldsymbol{\sigma}_x^\perp| |\boldsymbol{\sigma}_{x'}^\perp| e^{-i(\bar{\theta}_x^\perp - \bar{\theta}_{x'}^\perp)} \right] \quad (2.56)$$

around the plaquette will have a complex part proportional to

$$i \sin \theta |\boldsymbol{\sigma}_A^\parallel| |\boldsymbol{\sigma}_A^\perp| (|\boldsymbol{\sigma}_B^\parallel| |\boldsymbol{\sigma}_D^\perp| - |\boldsymbol{\sigma}_D^\parallel| |\boldsymbol{\sigma}_B^\perp|), \quad (2.57)$$

which can clearly be nonzero.

**Remark.** The  $k = 2$  4-vector update with both rotations clockwise, namely

$$T = \begin{pmatrix} 0 & i & 0 & 0 \\ -i & 0 & 0 & 0 \\ 0 & 0 & 0 & i \\ 0 & 0 & -i & 0 \end{pmatrix}, \quad (2.58)$$

corresponds to the *right*  $SU(2)$  update

$$U^{new} = U^{old} e^{i\theta \vec{a} \cdot \vec{\sigma}} . \quad (2.59)$$

*Model 5 (mixed fundamental/adjoint  $SU(N)$  chiral model)*: Let us now show, using (2.23), that frustration occurs also for the mixed fundamental/adjoint  $SU(2)$  chiral model whenever  $\beta_A \geq 0$  (and  $\beta_F, \beta_A$  are not both zero). The point is that for  $SU(2)$  matrices we have  $c_{xx'} = 0$  and  $a_{xx'}, b_{xx'}$  both real; it follows that

$$\alpha_{xx'} - i\beta_{xx'} = \beta_F (a_{xx'} - ib_{xx'}) \quad (2.60a)$$

$$\gamma_{xx'} - i\delta_{xx'} = \frac{\beta_A}{2} (a_{xx'} - ib_{xx'})^2 \quad (2.60b)$$

Hence, if we write the induced  $XY$  Hamiltonian in terms of “frustration angles”,

$$\mathcal{H}_{embed} = - \sum_{\langle xx' \rangle} \text{Re} \left[ (\alpha_{xx'} - i\beta_{xx'}) e^{i(\theta_x - \theta_{x'})} + (\gamma_{xx'} - i\delta_{xx'}) e^{2i(\theta_x - \theta_{x'})} \right] \quad (2.61a)$$

$$= - \sum_{\langle xx' \rangle} \text{Re} \left[ \rho_{xx'} e^{i(\phi_{xx'} + \theta_x - \theta_{x'})} + \rho'_{xx'} e^{i(\phi'_{xx'} + 2\theta_x - 2\theta_{x'})} \right] , \quad (2.61b)$$

we have  $\phi'_{xx'} = 2\phi_{xx'} \pmod{2\pi}$  provided that  $\beta_A \geq 0$ . It follows that the presence or absence of frustration can be determined solely by looking at  $\prod_{\square} (\alpha_{xx'} - i\beta_{xx'})$ . And as we have already seen, for certain configurations this product has a nonzero imaginary part.

To extend this proof to  $SU(N)$  with  $N \geq 2$ , we take (when  $R = I$ ) the matrices  $U$  to be block-diagonal, in which the uppermost  $2 \times 2$  block is as above, and the lowermost  $(N-2) \times (N-2)$  block is the *identity matrix*. We then have each  $c_{xx'} = N-2$ , so that the only change in the foregoing argument is that, in (2.60a), the prefactor  $\beta_F$  is replaced by  $\beta_F + 2\beta_A(N-2)$ .

*Model 4 (complex mixed isovector/isotensor model)*: Likewise, we can show that the complex mixed isovector/isotensor model with the choice (2.26) of  $T$  leads to a frustrated induced  $XY$  model in the following two cases:

- (i) For all  $N \geq 2$ , provided that  $\beta_V, \beta_T \neq 0$ . Without loss of generality we can take  $R = I$ , hence

$$\mathbf{v} = (1, 0, 0, \dots) . \quad (2.62)$$

Consider the product of  $\alpha_{xx'} - i\beta_{xx'}$  around a plaquette. We have, from (2.39),

$$\alpha_{xx'} - i\beta_{xx'} = [\beta_V + \beta_T(\mathbf{z}_x^{\perp*} \cdot \mathbf{z}_{x'}^{\perp})] \mathbf{z}_x^{\parallel} \cdot \mathbf{z}_{x'}^{\parallel*} . \quad (2.63)$$

Now consider, on the plaquette  $ABCD$ , the configuration

$$\mathbf{z}_A = \mathbf{z}_D = (1, 0, 0, \dots) \quad (2.64a)$$

$$\mathbf{z}_B = (\cos \lambda, \sin \lambda, 0, \dots) \quad (2.64b)$$

$$\mathbf{z}_C = (\cos \tau, i \sin \tau, 0, \dots) \quad (2.64c)$$

We get

$$\prod_{\square} (\alpha_{xx'} - i\beta_{xx'}) = \cos^2 \lambda \cos^2 \tau \beta_V^3 (\beta_V + i\beta_T \sin \lambda \sin \tau) , \quad (2.65)$$

which shows that the embedding is *frustrated* if we take  $\sin \lambda, \sin \tau, \cos \lambda, \cos \tau \neq 0$ .

(ii) For all  $N \geq 3$ , whenever  $\beta_T \neq 0$ . Consider, on the plaquette  $ABCD$  the configuration

$$\mathbf{z}_A = \mathbf{z}_D = (\cos \lambda, \sin \lambda, 0, 0, \dots) \quad (2.66a)$$

$$\mathbf{z}_B = \frac{1}{\sqrt{3}}(1, 1, 1, 0, \dots) \quad (2.66b)$$

$$\mathbf{z}_C = \frac{1}{\sqrt{3}}(1, 1, i, 0, \dots) \quad (2.66c)$$

Then, using (2.63) we get

$$\prod_{\square} (\alpha_{xx'} - i\beta_{xx'}) = \frac{\cos^4 \lambda}{9} (\beta_V + \beta_T \sin^2 \lambda) \left( \beta_V + \beta_T \frac{\sin \lambda}{\sqrt{3}} \right)^2 \times \left[ \beta_V + \frac{\beta_T}{3}(1 + i) \right]. \quad (2.67)$$

This has a nonzero imaginary part whenever  $\beta_T \neq 0$ , provided we choose  $\lambda$  so that the first three factors are nonvanishing; therefore the embedding is frustrated.

The remaining cases are unfrustrated:

- (iii) If  $\beta_T = 0$ , this is equivalent to the  $2N$ -vector model with our standard  $k = 1$  update.
- (iv) If  $N = 2$  and  $\beta_V = 0$ , this is the  $CP^1$  model, which is equivalent to the 3-vector model (see footnote 17); and it is easily seen that the update corresponds to our standard  $k = 1$  update for this latter model. The nonfrustration can also be seen directly from (2.63), once one notes that  $\mathbf{z}_x^{\parallel}$  and  $\mathbf{z}_x^{\perp}$  are both one-dimensional.

## 2.4 Alternative XY Embeddings

### 2.4.1 Embeddings with $k \neq 1$

Thus far we have been concentrating on the embeddings in which the matrix  $T$  has only one eigenvalue equal to +1, i.e. the cases  $k = 1$ . Here we shall examine the cases with  $k > 1$ ; in particular we shall investigate the occurrence of frustration.

Note first that we must always have  $N \geq 2k$  (or  $N \geq k + l$  in the case of the complex mixed isovector/isotensor model). For each model, therefore, we shall begin by investigating the minimal cases  $N = 2k$  (or  $N = k + l$ ). Once frustration has been proven for such a case, the proof can be immediately extended to all higher values of  $N$  for the same fixed  $k$  (and  $l$ ): For the vector models, it suffices to extend the chosen configuration with zeros in the last  $N - 2k$  (or  $N - k - l$ ) components; then  $a_{xx'}$  and  $b_{xx'}$  are unchanged, while  $c_{xx'} \equiv 0$ , so that the couplings are unchanged (even if  $\beta_T \neq 0$ ). For the  $SU(N)$  matrix models, we can take (when  $R = I$ ) the matrices  $U$  to be block-diagonal, with the uppermost  $2k \times 2k$  block being as previously constructed, and the lowermost  $(N - 2k) \times (N - 2k)$  block being the *identity matrix*; then  $a_{xx'}$  and  $b_{xx'}$  are unchanged, while  $c_{xx'} \equiv N - 2$ , so that the only change in the reasoning is to replace  $\beta_F$  by  $\beta_F + 2\beta_A(N - 2)$  in the formulae for  $\alpha_{xx'}$  and  $\beta_{xx'}$ .

Let us now consider separately the various models:

*Model 1 (N-vector model):* For  $k = 1$  we have shown that the embedding is unfrustrated. For  $k = 2$  the minimal case is  $N = 4$ : we have already discussed this case in the preceding subsection, and have shown that the induced  $XY$  Hamiltonian (2.55) is in general *frustrated* because the couplings are a sum of contributions written in terms of unrelated angles. The same argument applies for general  $k \geq 2$  and  $N = 2k$ : the update consists of  $k$  plane rotations and leads to couplings that are a sum of  $k$  contributions written in terms of unrelated angles. Finally, as explained above, the proof of frustration immediately extends to  $N > 2k$ . Hence *all* cases with  $k \geq 2$  lead to frustration.

*Model 2 (SU(N) principal chiral model):* For  $k = 1$  we have shown frustration for all  $N \geq 2$ . Next consider  $k \geq 2$  and  $N = 2k$ . If we look at configurations that are block-diagonal (in the same basis in which  $T$  is block-diagonal) in which each of the  $k$  blocks is an  $SU(2)$  matrix, we get couplings that are the sum of  $k$  terms each of which is as in (2.55). In other words, the couplings are a sum of  $2k$  contributions written in terms of unrelated angles, so they are in general frustrated. Finally, as explained above, the proof immediately extends to  $N > 2k$ . Hence *all* cases lead to frustration.

*Model 3 (mixed isovector/isotensor model):* For  $k = 1$  we have shown that the couplings are unfrustrated if  $\beta_V \geq \beta_T \geq 0$ . For general  $k$ , the couplings (2.16) lead to

$$\alpha_{xx'} - i\beta_{xx'} = (\beta_V + \beta_T c_{xx'}) (a_{xx'} - ib_{xx'}) \quad (2.68a)$$

$$\gamma_{xx'} - i\delta_{xx'} = \frac{\beta_T}{4} (a_{xx'} - ib_{xx'})^2 \quad (2.68b)$$

Hence, if we write the induced  $XY$  Hamiltonian in terms of “frustration angles” as in (2.61), we have  $\phi'_{xx'} = 2\phi_{xx'} \pmod{2\pi}$  provided that  $\beta_T \geq 0$ . Hence the presence or absence of frustration can be determined solely by looking at  $\prod_{\square} (\alpha_{xx'} - i\beta_{xx'})$ . This product consists of two factors: the product of  $a_{xx'} - ib_{xx'}$  around the plaquette, which we have already studied in connection with the pure  $N$ -vector model; and the product of  $\beta_V + \beta_T c_{xx'}$ , which is always real but may in some cases be negative. The cases with  $N = 2k$  are simple, since we have  $T^2 = I$  and hence  $c_{xx'} = 0$ , so that the problem is reduced to that of frustration for the pure  $N$ -vector model: frustration occurs whenever  $k \geq 2$ . The proof extends immediately to  $N > 2k$ , as explained before.

The only cases left to investigate are the mixed models with  $\beta_T > \beta_V \geq 0$  for  $k = 1$  and  $N \geq 3$ . Now, for  $k = 1$  we have already seen that  $\prod (a_{xx'} - ib_{xx'})$  is real and positive, so that the model will be unfrustrated if and only if  $\prod (\beta_V + \beta_T c_{xx'})$  is positive. Let us treat separately the cases  $\beta_V = 0$  and  $\beta_V > 0$ :

*Case (a):  $\beta_V = 0$  (pure  $RP^{N-1}$  model).* The criterion for nonfrustration is

$$\prod_{\square} c_{xx'} = \prod_{\square} \sigma_x^{\perp} \cdot \sigma_{x'}^{\perp} \geq 0. \quad (2.69)$$

Two distinct situations then arise:

- (i)  $N = 3$ : Here the vectors  $\sigma_x^{\perp}$  are one-dimensional, so that the product (2.69) is manifestly nonnegative (each  $\sigma_x^{\perp}$  occurs exactly twice in the product). Therefore, the model is unfrustrated.

- (ii)  $N \geq 4$ : For these cases one can easily find configurations with  $\prod \sigma_x^\perp \cdot \sigma_{x'}^\perp < 0$ : take, for example, on a plaquette  $ABCD$  the configuration

$$\sigma_A^\perp = r_A (1, 0, 0, \dots) \quad (2.70a)$$

$$\sigma_B^\perp = r_B (\cos \theta_B, \sin \theta_B, 0, \dots) \quad (2.70b)$$

$$\sigma_C^\perp = r_C (\cos \theta_C, \sin \theta_C, 0, \dots) \quad (2.70c)$$

$$\sigma_D^\perp = r_D (\cos \theta_D, \sin \theta_D, 0, \dots) \quad (2.70d)$$

with all  $r_i > 0$ . Then, we have frustration whenever the product

$$\cos \theta_B \cos(\theta_C - \theta_B) \cos(\theta_D - \theta_C) \cos \theta_D \quad (2.71)$$

is negative, e.g. for  $\theta_B = \pi/3$ ,  $\theta_C = 2\pi/3$  and  $\theta_D = \pi$ . We thus prove that all  $RP^{N-1}$  models with  $N \geq 4$  are frustrated when  $k = 1$ .

*Case (b):*  $\beta_V > 0$ . For any  $N \geq 3$  and any values  $\beta_T > \beta_V > 0$ , we can find configurations such that  $\prod(\beta_V + \beta_T c_{xx'})$  is negative. For example, take a configuration such that  $\sigma_A^\perp, \sigma_B^\perp, \sigma_C^\perp, \sigma_D^\perp$  are all colinear, with  $\sigma_A^\perp, \sigma_B^\perp, \sigma_C^\perp > 0$  and  $\sigma_D^\perp < 0$  relative to some fixed orientation of this line. Then, whenever  $\sigma_A^\perp > \sigma_C^\perp$  and

$$\frac{\beta_V}{\beta_T \sigma_A^\perp} < |\sigma_D^\perp| < \frac{\beta_V}{\beta_T \sigma_C^\perp}, \quad (2.72)$$

we have  $\prod(\beta_V + \beta_T c_{xx'}) < 0$ .

In summary, the mixed isovector/isotensor models are frustrated except for two cases with  $k = 1$ : (a)  $\beta_V \geq \beta_T \geq 0$  for any  $N$ , and (b) the pure  $RP^2$  model.

**Remark.** As mentioned in footnote 16, the case  $N = 4$  and  $\beta_V = 0$  (namely the  $RP^3$  model) is equivalent to the  $SO(3)$  principal chiral model. It is interesting to write the  $k = 2$   $RP^3$  update in  $SO(3)$  language. Recall that a 4-vector  $s = (s_0, \vec{s}) \in S^3$  maps into a matrix  $V \in SO(3)$  via

$$(V_x)_{ij} = (2s_0^2 - 1)\delta_{ij} + 2s_i s_j + 2s_0 \varepsilon_{ijk} s_k. \quad (2.73)$$

Now, one case of the  $k = 2$  update for the  $RP^3$  model is given by (2.51). Using (2.73), we see that this translates into

$$V^{new} = e^{2i\theta \vec{a} \cdot \vec{J}} V^{old}, \quad (2.74)$$

where  $\vec{J}$  are the generators of the  $\mathfrak{so}(3)$  algebra, i.e.  $(J_i)_{jk} = -i\varepsilon_{ijk}$ . This is the standard left-update for the  $SO(3)$  chiral model [analogous to (2.19) for the  $SU(N)$  chiral model] except that the angle is doubled. This explains why the induced  $XY$  Hamiltonian has only “isospin-2” terms (see footnote 19).

*Model 4 (complex mixed isovector/isotensor model):* Let us start by considering the embeddings with  $l = 0$ , so that  $T^2 = T$ . (The cases with  $k = 0$ ,  $T^2 = -T$  are trivially equivalent.) All such embeddings have  $\gamma_{xx'} = \delta_{xx'} = 0$  and

$$\alpha_{xx'} - i\beta_{xx'} = [\beta_V + \beta_T (\mathbf{z}_x^\perp \cdot \mathbf{z}_{x'}^\perp)] \mathbf{z}_x^\parallel \cdot \mathbf{z}_{x'}^\parallel, \quad (2.75)$$

where  $\mathbf{z}_x^\parallel$  (resp.  $\mathbf{z}_x^\perp$ ) denotes the first  $k$  (resp. last  $N - k$ ) components of  $\mathbf{z}_x$ . We can prove frustration in three cases:

- (i) If  $N \geq k \geq 2$  and  $\beta_V \neq 0$ . It suffices to choose configurations with  $\mathbf{z}_x^\perp \equiv 0$ . Then the couplings are those of a  $k \geq 2$  update for the  $2k$ -vector model, hence frustrated.
- (ii) If  $N \geq k + 2$  and  $\beta_T \neq 0$ . The proof is identical to that of case (ii) in Section 2.3, if in (2.66) we insert  $k - 1$  zeros between the first and second coordinates.
- (iii) If  $N = k + 1 \geq 3$ ,  $\beta_V = 0$  and  $\beta_T \neq 0$ . This is a pure  $CP^{N-1}$  model, and adding a multiple of the identity to  $T$  corresponds to a  $U(1)$  gauge transformation. So the case  $k = N - 1, l = 0$  is gauge-equivalent to  $k = 0, l = 1$ , which was proven to be frustrated for  $N \geq 3$  in case (ii) of Section 2.3.

The only remaining case with  $k \geq 2$  is  $N = k, \beta_V = 0$ : this is a mere gauge transformation of the  $CP^{N-1}$  model, and the induced  $XY$  Hamiltonian is zero.

For cases with  $k, l \neq 0$  we no longer have  $\gamma_{xx'}, \delta_{xx'} = 0$ , and a more careful analysis is needed. We have been able to obtain a result only for the pure  $CP^{N-1}$  model ( $\beta_V = 0$ ). Consider first the minimal case  $N = k + l$ : here we have  $T^2 = I$  and hence  $c_{xx'} = 0$ , so that  $\alpha_{xx'} = \beta_{xx'} = 0$ . The criterion for frustration is then given in terms of

$$\gamma_{xx'} - i\delta_{xx'} = \beta_T (\mathbf{z}_x^+ \cdot \mathbf{z}_{x'}^{+*}) (\mathbf{z}_x^{-*} \cdot \mathbf{z}_{x'}^-), \quad (2.76)$$

where  $\mathbf{z}_x^+$  (resp.  $\mathbf{z}_x^-$ ) denotes the first  $k$  (resp. the last  $l$ ) components of  $\mathbf{z}_x$ . For  $k = l = 1$  this is manifestly unfrustrated, as  $\prod(\gamma_{xx'} - i\delta_{xx'}) = \prod |\mathbf{z}_x^+|^2 |\mathbf{z}_x^-|^2 \geq 0$ ; but for all cases with  $k \geq 2$  and/or  $l \geq 2$  it is easy to devise frustrated configurations, by the same method as was used for the  $RP^{N-1}$  models with  $N \geq 4$ .<sup>26</sup> Finally, the proof of frustration extends to  $N > k + l$ , as explained earlier.

The remaining cases of the  $CP^{N-1}$  models are  $k = 1, l = 1$  with  $N \geq 3$ . Let  $z_x^+$  (resp.  $z_x^-$ ) denote the first (resp. second) component of  $\mathbf{z}_x$ , and let  $\mathbf{z}_x^\perp$  denote the last  $N - 2$  components.

- (a) Suppose we choose a configuration with  $z_x^- \equiv 0$ . From (2.28) we then have  $b_{xx'} = -ia_{xx'}$ , so that  $\gamma_{xx'} = \delta_{xx'} = 0$  and

$$\alpha_{xx'} - i\beta_{xx'} = \beta_T (\mathbf{z}_x^\perp \cdot \mathbf{z}_{x'}^\perp) (z_x^+ z_{x'}^{+*}). \quad (2.77)$$

For  $N \geq 4$  it is easy to devise frustrated configurations, by the same method as was used for the  $RP^{N-1}$  models with  $N \geq 4$ .

- (b) For  $N = 3$  we can construct a frustrated configuration as follows: consider on a plaquette  $ABCD$  the configuration

$$\mathbf{z}_A = \frac{1}{\sqrt{2}} (1, 0, e^{i\mu}) \quad (2.78a)$$

$$\mathbf{z}_B = \frac{1}{\sqrt{3}} (1, 1, e^{i\nu}) \quad (2.78b)$$

---

<sup>26</sup> *Alternate proof:* The  $CP^{N-1}$  model with  $N = k + l$  is gauge-equivalent to one with  $k' = k, l' = 0$  and  $\theta_x$  replaced by  $2\theta_x$  (see footnotes 21 and 22). Hence this is unfrustrated for  $k = 1$  and frustrated for  $k \geq 2$ , as proven in Section 2.3.



$$\mathbf{z}_C = \frac{1}{\sqrt{3}}(1, 1, 1) \quad (2.78c)$$

$$\mathbf{z}_D = \frac{1}{\sqrt{3}}(1, 1, e^{i\sigma}) \quad (2.78d)$$

with  $\mu, \nu, \sigma$  real and  $-\pi/2 < \nu, \sigma < \pi/2$ . Then for the links  $BC$  and  $CD$  we have from (2.27)/(2.28) (noting that  $T$  is the diagonal matrix  $\{1, -1, 0\}$ ) that  $\beta_{xx'} = \delta_{xx'} = 0$  and  $\alpha_{xx'}, \gamma_{xx'} > 0$ , so that the unique minimum of the Hamiltonian for these links occurs at  $\theta_B = \theta_C = \theta_D$ . For the links  $DA$  and  $AB$  we have that  $\gamma_{xx'} = \delta_{xx'} = 0$  and

$$(\alpha_{DA} - i\beta_{DA})(\alpha_{AB} - i\beta_{AB}) = \frac{\beta_T^2}{36} e^{i(\nu-\sigma)}. \quad (2.79)$$

Therefore, this configuration is frustrated unless  $\nu = \sigma$ .

So the  $CP^{N-1}$  models with  $k = l = 1$  are frustrated for all  $N \geq 3$ .

*Model 5 (mixed fundamental/adjoint  $SU(N)$  chiral model):* For  $k = 1$  all mixed models are frustrated. Therefore, for  $k \geq 2$  all mixed models will be likewise frustrated, since for  $N = 2k$  we can take configurations that are block-diagonal formed by  $SU(2)$  matrices; and we can extend the proof to  $N > 2k$  as before.

#### 2.4.2 Two-Sided Update for $SU(N)$

In view of the results in Sections 2.3 and 2.4.1 concerning the frustration in the  $SU(N)$  case, one might ask: Can we find a *different* update for the  $SU(N)$  chiral model that would yield unfrustrated couplings for the induced  $XY$  model? One possibility is to make a simultaneous rotation on both the left and the right:

$$U_x^{new} = R e^{i\theta_x T} R^{-1} U_x^{old} S e^{i\theta_x T} S^{-1} \quad (2.80)$$

where  $R, S$  are random  $SU(N)$  matrices and  $T$  is a fixed traceless Hermitian matrix with eigenvalues in  $\{\pm 1, 0\}$ . In general  $T$  has  $k$  eigenvalues  $+1$ ,  $k$  eigenvalues  $-1$ , and  $N - 2k$  eigenvalues  $0$ , for some integer  $k$  satisfying  $1 \leq k \leq \lfloor N/2 \rfloor$ .

Inserting (2.80) into the chiral-model Hamiltonian (2.5) and using (2.3), we find that the induced  $XY$  Hamiltonian is of the “isovector/isotensor” form (2.15), with couplings

$$\alpha_{xx'} = \beta \{ \text{Re tr}[V_x^\dagger T^2 V_{x'}(I - T^2)] + \text{Re tr}[V_x^\dagger(I - T^2)V_{x'}T^2] \} \quad (2.81a)$$

$$\beta_{xx'} = \beta \{ \text{Im tr}[V_x^\dagger T V_{x'}(I - T^2)] + \text{Im tr}[V_x^\dagger(I - T^2)V_{x'}T] \} \quad (2.81b)$$

$$\gamma_{xx'} = \frac{\beta}{2} [\text{Re tr}(V_x^\dagger T^2 V_{x'} T^2) + \text{Re tr}(V_x^\dagger T V_{x'} T)] \quad (2.81c)$$

$$\delta_{xx'} = \frac{\beta}{2} [\text{Im tr}(V_x^\dagger T V_{x'} T^2) + \text{Im tr}(V_x^\dagger T^2 V_{x'} T)] \quad (2.81d)$$

where

$$V_x \equiv R^{-1} U_x^{old} S. \quad (2.82)$$

One interesting case is that in which  $N$  is even and  $k = N/2$ : then  $T$  has only eigenvalues  $\pm 1$  (and not also 0), so that

$$T^2 = I. \quad (2.83)$$

It follows that  $\alpha_{xx'} = \beta_{xx'} = 0$ , so that the induced  $XY$  Hamiltonian becomes again, after a relabeling  $\theta_x \rightarrow \theta_x/2$ , a “pure isovector”  $XY$  Hamiltonian (2.12).

For  $N = 2$  (and hence  $k = 1$ ) we can rewrite the update (2.80) in 4-vector notation. With  $T$  given by (2.20), let  $RTS^{-1} = \vec{a} \cdot \vec{\sigma}$  and  $STS^{-1} = \vec{b} \cdot \vec{\sigma}$ . We have

$$s_0^{new} = s_0^{old} (\cos^2 \theta - \vec{a} \cdot \vec{b} \sin^2 \theta) - \vec{s}^{old} \cdot [(\vec{a} + \vec{b}) \sin \theta \cos \theta + \vec{a} \times \vec{b} \sin^2 \theta] \quad (2.84a)$$

$$\begin{aligned} \vec{s}^{new} = & s_0^{old} [(\vec{a} + \vec{b}) \sin \theta \cos \theta - \vec{a} \times \vec{b} \sin^2 \theta] + \vec{s}^{old} (\cos^2 \theta + \vec{a} \cdot \vec{b} \sin^2 \theta) \\ & - [(\vec{s}^{old} \cdot \vec{a}) \vec{b} + (\vec{s}^{old} \cdot \vec{b}) \vec{a}] \sin^2 \theta + \vec{s}^{old} \times (\vec{a} - \vec{b}) \sin \theta \cos \theta \end{aligned} \quad (2.84b)$$

With the special choice  $\vec{a} = \vec{b}$  (which can be obtained from  $R = S$  among other choices), we get

$$s_0^{new} = s_0^{old} \cos 2\theta - \vec{s}^{old} \cdot \vec{a} \sin 2\theta \quad (2.85a)$$

$$\vec{s}^{new} = s_0^{old} \vec{a} (\sin 2\theta) + (\vec{s}^{old} \cdot \vec{a}) \vec{a} \cos 2\theta + [\vec{s}^{old} - (\vec{s}^{old} \cdot \vec{a}) \vec{a}] \quad (2.85b)$$

which corresponds to a single rotation of angle  $2\theta$  in the plane defined by the 0-direction and  $\vec{a}$ . Likewise, the choice  $\vec{a} = -\vec{b}$  yields

$$s_0^{new} = s_0^{old} \quad (2.86a)$$

$$\vec{s}^{new} = [\vec{s}^{old} - (\vec{s}^{old} \cdot \vec{a}) \vec{a}] \cos 2\theta + (\vec{s}^{old} \times \vec{a}) \sin 2\theta + (\vec{s}^{old} \cdot \vec{a}) \vec{a} \quad (2.86b)$$

which corresponds to a single rotation of angle  $2\theta$  in the plane perpendicular to the 0-direction and to  $\vec{a}$ . With more general choices of  $R$  and  $S$ , we obtain rotations of angle  $2\theta$  in an arbitrary two-dimensional subspace  $P \subset \mathbb{R}^4$ . This (after a relabeling  $\theta_x \rightarrow \theta_x/2$ ) is our standard 4-vector update, and is therefore *unfrustrated*.

In retrospect we can see what is going on here. We’ve already seen that the *left* update (2.19) for  $SU(2)$  corresponds in the 4-vector language to an update with  $T$  given by (2.54). Likewise, a *right* update for  $SU(2)$  corresponds in the 4-vector language to an update with  $T$  given by (2.58). Now, a *simultaneous* left and right update for  $SU(2)$  corresponds to the *sum* of these two  $T$  matrices: we thus get *twice* the usual entry in the upper block, and zero in the lower block. This explains why we get a single rotation with a doubled angle.

Unfortunately, the update (2.80)/(2.83) for  $N = 4, 6, 8, \dots$  is generically frustrated. Let us choose the configuration  $\{U_x^{old}\}$  so that the matrices  $V_x$  are block-diagonal with  $SU(2)$  matrices in each block. Then, the expressions for the couplings will be just sums of  $SU(2)$ -type couplings, which can each be written in terms of 4-vectors as in (2.33) [since the update in each  $SU(2)$  subspace corresponds to a single plane rotation in 4-vector language]. We have therefore  $k = N/2$  independent angles, so that the couplings are frustrated whenever  $k \geq 2$  and  $N = 2k$ .

This example can be immediately extended to the cases  $k \geq 2$  with  $N > 2k$ : it suffices to choose the matrices  $V_x$  to be block-diagonal, with the uppermost  $2k \times 2k$  block as above,

and the lowermost  $(N - 2k) \times (N - 2k)$  block being an arbitrary  $SU(N - 2k)$  matrix. (For such a *special* configuration one has  $\alpha_{xx'} = \beta_{xx'} = 0$ , even though this does not *in general* happen for  $N > 2k$ .)

The only case left to investigate is  $k = 1$ ,  $N = 3$ . In this case frustration can be proven by making use of configurations taking values in the group's center:

$$U_x = e^{(2\pi i/3)k_x} I \quad (2.87)$$

where  $k_x \in \{0, 1, 2\}$  and  $I$  is the identity matrix. Then the couplings (2.21) become

$$\begin{aligned} \alpha_{xx'} &= \beta_{xx'} = \delta_{xx'} = 0 \\ \gamma_{xx'} &= 2\beta \cos \left[ \frac{2\pi}{3} (k_x - k_{x'}) \right] = \beta (3\delta_{k_x k_{x'}} - 1) \end{aligned} \quad (2.88)$$

The  $\gamma_{xx'}$  are thus *real* numbers, and we will have frustration if their product around a plaquette is negative. But this occurs whenever three of the four sites have different values of  $k_x$ , for example  $\{0, 0, 1, 2\}$ .

In conclusion, the two-sided  $SU(N)$  embedding leads to a frustrated  $XY$  Hamiltonian in all cases *except* the exceptional case  $N = 2$ ,  $k = 1$ .

## 2.5 Summary

In conclusion, we have a *simple* induced Hamiltonian in the following cases:

- (i)  $N$ -vector model, any  $k$
- (ii)  $SU(N)$  principal chiral model, any  $k$
- (iii) complex mixed isovector/isotensor model,  $k = 0$  or  $l = 0$
- (iv)  $RP^{N-1}$  model,  $N$  even,  $k = N/2$
- (v) pure adjoint  $SU(N)$  principal chiral model,  $N$  even,  $k = N/2$
- (vi)  $CP^{N-1}$  model,  $k + l = N$
- (vii)  $SU(N)$  principal chiral model,  $N$  even,  $k = N/2$  two-sided update

In the first three cases the induced  $XY$  Hamiltonian has only isospin-1 terms, while in the latter four cases it has only isospin-2 terms.

Furthermore, we have an *unfrustrated* induced  $XY$  Hamiltonian for the mixed isovector/isotensor models with  $\beta_V \geq \beta_T \geq 0$  and  $k = 1$ , as well as for models equivalent to one of these. We also have an unfrustrated Hamiltonian for the  $RP^2$  model with  $k = 1$ . All other cases appear to lead in general to *frustrated* Hamiltonians.

## 3 Numerical Results

In this section we present our numerical results for the two-dimensional  $N$ -vector models (2.4) with  $N = 3, 4, 8$ .

### 3.1 Observables to be Measured

We wish to study various correlation functions of the isovector field  $\sigma_x$  and the symmetric traceless isotensor field

$$T_x^{(\alpha\beta)} \equiv \sigma_x^{(\alpha)} \sigma_x^{(\beta)} - \frac{1}{N} \delta^{\alpha\beta}. \quad (3.1)$$

Our interest in the isotensor sector arose initially from our work on mixed isovector/isotensor models [45, 46, 44]; but even in the pure  $N$ -vector model it is of some interest to measure isotensor observables. We thus define the isovector and isotensor 2-point correlation functions

$$G_V(x-y) = \langle \sigma_x \cdot \sigma_y \rangle \quad (3.2a)$$

$$\begin{aligned} G_T(x-y) &= \langle \overset{\leftrightarrow}{T}_x \cdot \overset{\leftrightarrow}{T}_y \rangle \equiv \sum_{\alpha,\beta=1}^N \langle T_x^{(\alpha\beta)} T_y^{(\alpha\beta)} \rangle \\ &= \langle (\sigma_x \cdot \sigma_y)^2 \rangle - \frac{1}{N} \end{aligned} \quad (3.2b)$$

Note that  $SO(N)$  invariance (which cannot be spontaneously broken in dimension  $d \leq 2$ ) determines the 1-point and 2-point correlation functions of  $\sigma$  and  $\overset{\leftrightarrow}{T}$  in terms of  $G_V$  and  $G_T$ :

$$\langle \sigma_x^{(\alpha)} \rangle = 0 \quad (3.3a)$$

$$\langle \sigma_x^{(\alpha)} \sigma_y^{(\beta)} \rangle = \frac{1}{N} \delta^{\alpha\beta} G_V(x-y) \quad (3.3b)$$

$$\langle T_x^{(\alpha\beta)} \rangle = 0 \quad (3.3c)$$

$$\langle T_x^{(\alpha\beta)} T_y^{(\kappa\lambda)} \rangle = \frac{1}{N^2 + N - 2} (\delta^{\alpha\kappa} \delta^{\beta\lambda} + \delta^{\alpha\lambda} \delta^{\beta\kappa} - \frac{2}{N} \delta^{\alpha\beta} \delta^{\kappa\lambda}) G_T(x-y) \quad (3.3d)$$

All our numerical work will be done on an  $L \times L$  lattice with periodic boundary conditions. We are interested in the following quantities:

- The isovector and isotensor energies<sup>27</sup>

$$E_V = \langle \sigma_0 \cdot \sigma_{\mathbf{e}} \rangle = G_V(\mathbf{e}) \quad (3.4a)$$

$$E_T = \langle (\sigma_0 \cdot \sigma_{\mathbf{e}})^2 \rangle = G_T(\mathbf{e}) + \frac{1}{N} \quad (3.4b)$$

where  $\mathbf{e}$  stands for any nearest neighbor of the origin.

- The isovector and isotensor magnetic susceptibilities

$$\chi_{\#} = \sum_x G_{\#}(x), \quad (3.5)$$

where  $\# = V$  or  $T$ .

---

<sup>27</sup> Actually  $E_V$  (resp.  $E_T$ ) is  $-1$  (resp.  $-2$ ) times the mean energy per *link*; we have chosen this normalization in order to have  $0 \leq E_{V,T} \leq 1$ , where  $E_{V,T} = 1$  for a totally ordered state. Several other normalizations are in use in the literature.

- The isovector and isotensor correlation functions at the smallest nonzero momentum:

$$F_{\#} = \sum_x e^{ip_0 \cdot x} G_{\#}(x) , \quad (3.6)$$

where  $p_0 = (\pm 2\pi/L, 0)$  or  $(0, \pm 2\pi/L)$ .

- The isovector and isotensor second-moment correlation lengths

$$\xi_{\#}^{(2nd)} = \frac{(\chi_{\#}/F_{\#} - 1)^{1/2}}{2 \sin(\pi/L)} . \quad (3.7)$$

- The isovector and isotensor exponential correlation lengths

$$\xi_{\#}^{(exp)} = \lim_{|x| \rightarrow \infty} \frac{-|x|}{\log G_{\#}(x)} \quad (3.8)$$

and the corresponding mass gaps  $m_{\#} = 1/\xi_{\#}^{(exp)}$ . [These quantities make sense only if the lattice is essentially infinite (i.e.  $L \gg \xi_{\#}^{(exp)}$ ) in at least one direction. We will not *measure* any exponential correlation lengths in this work; but we will use  $\xi_{\#}^{(exp)}$  as a theoretical standard of comparison.]

All these quantities except  $\xi_{\#}^{(exp)}$  can be expressed as expectations involving the following observables:

$$\mathcal{M}_V^2 = \left( \sum_x \boldsymbol{\sigma}_x \right)^2 \quad (3.9a)$$

$$\mathcal{M}_T^2 = \left( \sum_x \vec{\vec{T}}_x \right)^2 \quad (3.9b)$$

$$\mathcal{F}_V = \frac{1}{2} \left[ \left| \sum_x e^{2\pi i x_1/L} \boldsymbol{\sigma}_x \right|^2 + \left| \sum_x e^{2\pi i x_2/L} \boldsymbol{\sigma}_x \right|^2 \right] \quad (3.9c)$$

$$\mathcal{F}_T = \frac{1}{2} \left[ \left| \sum_x e^{2\pi i x_1/L} \vec{\vec{T}}_x \right|^2 + \left| \sum_x e^{2\pi i x_2/L} \vec{\vec{T}}_x \right|^2 \right] \quad (3.9d)$$

$$\mathcal{E}_V = \sum_{\langle xy \rangle} \boldsymbol{\sigma}_x \cdot \boldsymbol{\sigma}_y \quad (3.9e)$$

$$\mathcal{E}_T = \sum_{\langle xy \rangle} (\boldsymbol{\sigma}_x \cdot \boldsymbol{\sigma}_y)^2 \quad (3.9f)$$

Thus,

$$E_{\#} = \frac{1}{2} V^{-1} \langle \mathcal{E}_{\#} \rangle \quad (3.10a)$$

$$\chi_{\#} = V^{-1} \langle \mathcal{M}_{\#}^2 \rangle \quad (3.10b)$$

$$F_{\#} = V^{-1} \langle \mathcal{F}_{\#} \rangle \quad (3.10c)$$

where  $\# = V$  or  $T$ ; here  $V = L^2$  is the number of sites in the lattice.

### 3.2 Autocorrelation Functions and Autocorrelation Times

Let us now define the quantities — autocorrelation functions and autocorrelation times — that characterize the Monte Carlo dynamics. Let  $A$  be an observable (i.e. a function of the field configuration  $\{\varphi_x\}$ ). We are interested in the evolution of  $A$  in Monte Carlo time, and more particularly in the rate at which the system “loses memory” of the past. We define, therefore, the *unnormalized autocorrelation function*<sup>28</sup>

$$C_A(t) = \langle A_s A_{s+t} \rangle - \langle A \rangle^2, \quad (3.11)$$

where expectations are taken *in equilibrium*. The corresponding *normalized autocorrelation function* is

$$\rho_A(t) = C_A(t)/C_A(0). \quad (3.12)$$

We then define the *integrated autocorrelation time*

$$\begin{aligned} \tau_{int,A} &= \frac{1}{2} \sum_{t=-\infty}^{\infty} \rho_A(t) \\ &= \frac{1}{2} + \sum_{t=1}^{\infty} \rho_A(t) \end{aligned} \quad (3.13)$$

[The factor of  $\frac{1}{2}$  is purely a matter of convention; it is inserted so that  $\tau_{int,A} \approx \tau$  if  $\rho_A(t) \approx e^{-|t|/\tau}$  with  $\tau \gg 1$ .] Finally, the *exponential autocorrelation time* for the observable  $A$  is defined as

$$\tau_{exp,A} = \limsup_{t \rightarrow \infty} \frac{|t|}{-\log |\rho_A(t)|}, \quad (3.14)$$

and the exponential autocorrelation time (“slowest mode”) for the system as a whole is defined as

$$\tau_{exp} = \sup_A \tau_{exp,A}. \quad (3.15)$$

Note that  $\tau_{exp} = \tau_{exp,A}$  whenever the observable  $A$  is not orthogonal to the slowest mode of the system.

The integrated autocorrelation time controls the statistical error in Monte Carlo measurements of  $\langle A \rangle$ . More precisely, the sample mean

$$\bar{A} \equiv \frac{1}{n} \sum_{t=1}^n A_t \quad (3.16)$$

has variance

$$\text{var}(\bar{A}) = \frac{1}{n^2} \sum_{r,s=1}^n C_A(r-s) \quad (3.17a)$$

$$= \frac{1}{n} \sum_{t=-(n-1)}^{n-1} \left(1 - \frac{|t|}{n}\right) C_A(t) \quad (3.17b)$$

$$\approx \frac{1}{n} (2\tau_{int,A}) C_A(0) \quad \text{for } n \gg \tau \quad (3.17c)$$

---

<sup>28</sup> In the mathematics and statistics literature, this is called the *autocovariance function*.

Thus, the variance of  $\bar{A}$  is a factor  $2\tau_{int,A}$  larger than it would be if the  $\{A_t\}$  were statistically independent. Stated differently, the number of “effectively independent samples” in a run of length  $n$  is roughly  $n/2\tau_{int,A}$ . The autocorrelation time  $\tau_{int,A}$  (for interesting observables  $A$ ) is therefore a “figure of (de)merit” of a Monte Carlo algorithm.

The integrated autocorrelation time  $\tau_{int,A}$  can be estimated by standard procedures of statistical time-series analysis [47, 48]. These procedures also give statistically valid *error bars* on  $\langle A \rangle$  and  $\tau_{int,A}$ . For more details, see [49, Appendix C]. In this paper we have used a self-consistent truncation window of width  $c\tau_{int,A}$ , where  $c$  is a constant. We have here used  $c = 6$ ; this choice is reasonable whenever the autocorrelation function  $\rho_A(t)$  decays roughly exponentially.

### 3.3 Summary of our Runs

We performed runs on the  $N$ -vector model with  $N = 3, 4, 8$ , using the  $k = 1$   $XY$ -embedding MGMC algorithm described in Section 2.2, on lattices of size  $L = 32, 64, 128, 256$ . We updated the induced  $XY$  model (2.12) using our standard  $XY$ -model MGMC program [7] with  $\gamma = 2$  (W-cycle) and  $m_1 = m_2 = 1$  (one heat-bath pre-sweep and one heat-bath post-sweep). In all cases the coarsest grid is taken to be  $2 \times 2$ . All runs used an ordered initial configuration (“cold start”). The results of these computations are shown in Tables 1–3 (static data) and 4–6 (dynamic data).

For the  $N = 4$  case we made only a few runs, in order to compare  $XY$ -embedding MGMC to our previous detailed study of the direct MGMC algorithm for this model [8]. For  $N = 3$  and  $N = 8$ , by contrast, we made a reasonably extensive set of runs, enough to permit an *ab initio* dynamic finite-size-scaling analysis. Run lengths were in all cases between  $\approx 5000\tau$  and  $\approx 50000\tau$ .

Our static data for  $N = 3, 4, 8$  are in good agreement with data from previous simulations of these models [39, 44, 50, 8, 51]. To check this quantitatively, we made comparisons at each pair  $(\beta, L)$  for which both “old” and “new” data are available, and summed the resulting  $\chi^2$  values. The results are:

- $N = 3$ , comparison with [39, 44, 50]:  
degrees of freedom: 30  
 $\chi^2$  for isovector susceptibility = 38.73, confidence level = 13%  
 $\chi^2$  for isovector correlation length = 34.29, confidence level = 27%  
 $\chi^2$  for isovector energy = 36.18, confidence level = 20%  
 $\chi^2$  for isotensor susceptibility = 40.22, confidence level = 10%  
 $\chi^2$  for isotensor correlation length = 38.23, confidence level = 14%  
 $\chi^2$  for isotensor energy = 37.02, confidence level = 18%
- $N = 4$ , comparison with [8] (isovector sector only)<sup>29</sup>:  
degrees of freedom: 14  
 $\chi^2$  for isovector susceptibility = 18.75, confidence level = 17%  
 $\chi^2$  for isovector correlation length = 21.74, confidence level = 8%  
 $\chi^2$  for isovector energy = 13.70, confidence level = 47%

---

<sup>29</sup> We note that the energy defined in [8] is a factor of 2 larger than the one employed here.

- $N = 8$ , comparison with [51] (isovector sector only):  
degrees of freedom: 4  
 $\chi^2$  for isovector susceptibility = 1.57, confidence level = 81%  
 $\chi^2$  for isovector correlation length = 2.58, confidence level = 63%  
 $\chi^2$  for isovector energy = 6.53, confidence level = 16%

These confidence levels are all individually acceptable, but taken together they are slightly lower than would be expected *a priori*. This may be due to a very slight (e.g.  $\sim 10\%$ ) underestimation of the error bars in either the “old” or the “new” data (or both).

### 3.4 Computational Work

In Table 7 we show the CPU time per iteration for our  $XY$ -embedding MGMC program with  $\gamma = 2$  (W-cycle) and  $m_1 = m_2 = 1$ , running on one processor of a Cray C-90, for  $L = 32, 64, 128, 256$  and  $N = 3, 4, 8$ . We also show, for comparison, the corresponding CPU time for the  $N = 4$  *direct* MGMC algorithm, using our old program [8] recompiled for the Cray C-90. The first timing is for Monte Carlo iterations alone; the second timing includes measurement of observables (isovector only in the old program, isovector and isotensor in the new program). We see that:

(a) For each model these timing data grow *sublinearly* in the volume, in contrast to the theoretical prediction (1.1), because the vectorization is more effective on the larger lattices.<sup>30</sup> However, the ratio  $\text{time}(2L)/\text{time}(L)$  is increasing with  $L$ , and does appear to be approaching the theoretical value of 4 as  $L \rightarrow \infty$ .

(b) At each  $L$ , the CPU time for Monte Carlo iterations grows roughly as  $a + bN$  with  $b/a \approx 0.03$ . This is because the bulk of the CPU time is spent in updating the induced  $XY$  model, which is independent of  $N$ ; while a small fraction of the time is spent computing the induced  $XY$  Hamiltonian and updating the  $N$ -vector spins, which are operations of order  $N$ .

(c) At each  $L$ , the CPU time for measurement of observables (i.e. the difference between the two timings in Table 7) grows roughly as  $aN + bN^2$  with  $b/a$  of order 1. This is because the measurement of isovector (resp. isotensor) observables takes a CPU time of order  $N$  (resp.  $N^2$ ). Our old program [8], by contrast, measured only isovector observables; the time spent in measurement is a factor of  $\approx 4$  smaller.

The running speed on the Cray C-90 for our  $XY$ -embedding MGMC program at  $L = 256$  was about 329 MFlops for the  $N = 3$  case, 322 MFlops for  $N = 4$ , and 317 MFlops for  $N = 8$ . Our old  $N = 4$  direct MGMC program runs on the C-90 at 270 MFlops.

---

<sup>30</sup> Note that the heat-bath subroutine uses von Neumann rejection to generate the desired random variables [7, Appendix A]. The algorithm is vectorized by gathering all the sites of one sublattice (red or black) into a single Cray vector, making one trial of the rejection algorithm, scattering the “successful” outputs, gathering and recompressing the “failures”, and repeating until all sites are successful. Therefore, although the original vector length in this subroutine is  $L^2/2$ , the vector lengths after several rejection steps are much smaller. It is thus advantageous to make the original vector length as large as possible.

Note also that our old  $N = 4$  direct MGMC program [8] used vectors of length  $L^2/4$  instead of  $L^2/2$ . As a result, the ratio  $\text{time}(\text{old program})/\text{time}(\text{new program for } N = 4)$  is slightly higher on the small lattices than on the large lattices.



The total CPU time for the runs reported here was about 2000 Cray C-90 hours, of which about 2/3 were devoted to  $N = 8$  and about 1/3 to  $N = 3$ . The CPU time for  $N = 4$  was comparatively small.

The statistical efficiency of a Monte Carlo algorithm is inversely proportional to the integrated autocorrelation time for the observable(s) of interest, *measured in CPU units*. We can compare our largest values of  $\tau_{int, \mathcal{M}_V^2}$  for the cases  $N = 3, 4, 8$  at lattice size  $L = 128$ : we get  $\tau_{int, \mathcal{M}_V^2} = 2.8, 3.0, 6.0$  Cray C-90 seconds, respectively, for  $N = 3, 4, 8$  (times for Monte Carlo iterations only). Thus, the CPU time to generate one “effectively independent” configuration grows (not surprisingly) with  $N$ , perhaps slightly less than linearly. Note, finally, that for  $N = 4$  the direct MGMC method is about three times as efficient as the  $XY$ -embedding method: while the CPU time per iteration is roughly the same for the two programs (see Table 7), the autocorrelation time  $\tau_{int, \mathcal{M}_V^2}$  is smaller by a factor of  $\approx 3$  for the direct algorithm (see Section 5).

## 4 Finite-Size-Scaling Analysis: Static Quantities

### 4.1 Preliminaries

We shall analyze our static data using a finite-size-scaling extrapolation method due originally to Lüscher, Weisz and Wolff [36] and elaborated recently by our group [38, 39, 40] (see also [37]). An exhaustive study of the  $N = 3$  case has been made elsewhere, using much more precise and extensive data [39, 44, 50]; and our data for  $N = 4$  are too sparse to support this type of analysis. Therefore, our analysis here of the static quantities will be restricted to the case  $N = 8$ .<sup>31</sup>

We wish to test the asymptotic-freedom predictions

$$\xi_{\#}(\beta) = \tilde{C}_{\xi_{\#}} \Lambda^{-1} \left[ 1 + \frac{a_1}{\beta} + \frac{a_2}{\beta^2} + \dots \right] \quad (4.1)$$

$$\chi_V(\beta) = \tilde{C}_{\chi_V} \Lambda^{-2} \left( \frac{2\pi\beta}{N-2} \right)^{-(N-1)/(N-2)} \left[ 1 + \frac{b_1}{\beta} + \frac{b_2}{\beta^2} + \dots \right] \quad (4.2)$$

$$\chi_T(\beta) = \tilde{C}_{\chi_T} \Lambda^{-2} \left( \frac{2\pi\beta}{N-2} \right)^{-2N/(N-2)} \left[ 1 + \frac{d_1}{\beta} + \frac{d_2}{\beta^2} + \dots \right] \quad (4.3)$$

as  $\beta \rightarrow \infty$ , where

$$\Lambda \equiv e^{-2\pi\beta/(N-2)} \left( \frac{2\pi\beta}{N-2} \right)^{1/(N-2)} 2^{5/2} \exp \left[ \frac{\pi}{2(N-2)} \right] \quad (4.4)$$

is the fundamental mass scale<sup>32</sup>; here  $\tilde{C}_{\xi_{\#}}$ ,  $\tilde{C}_{\chi_V}$  and  $\tilde{C}_{\chi_T}$  are *universal* (albeit non-perturbative) quantities characteristic of the continuum theory (and thus depending only on  $N$ ), while the

<sup>31</sup> A preliminary version of this analysis was reported in [52].

<sup>32</sup> In (4.4), the exponential and power of  $\beta$  are universal; the remaining factor is special to the standard nearest-neighbor action (2.4), and comes from a one-loop lattice calculation [53, 54].

$a_k$ ,  $b_k$  and  $d_k$  are nonuniversal constants that can be computed in weak-coupling perturbation theory on the lattice at  $k+2$  loops; and  $\xi_{\#}$  denotes any one of  $\xi_V^{(2nd)}$ ,  $\xi_T^{(2nd)}$ ,  $\xi_V^{(exp)}$ ,  $\xi_T^{(exp)}$ . It is worth emphasizing that the *same* coefficients  $a_k$  occur in all four correlation lengths: this is because the ratios of these correlation lengths take their continuum-limit values plus corrections that are powers of the mass  $m = 1/\xi^{(exp)}$ , hence exponentially small in  $\beta$ .

When analyzing the susceptibilities, it is convenient to study instead the ratios

$$\frac{\chi_V(\beta)}{\xi_{\#}(\beta)^2} = \frac{\tilde{C}_{\chi_V}}{\tilde{C}_{\xi_{\#}}^2} \left( \frac{2\pi\beta}{N-2} \right)^{-(N-1)/(N-2)} \left[ 1 + \frac{c_1}{\beta} + \frac{c_2}{\beta^2} + \frac{c_3}{\beta^3} + \dots \right] \quad (4.5)$$

$$\frac{\chi_T(\beta)}{\xi_{\#}(\beta)^2} = \frac{\tilde{C}_{\chi_T}}{\tilde{C}_{\xi_{\#}}^2} \left( \frac{2\pi\beta}{N-2} \right)^{-2N/(N-2)} \left[ 1 + \frac{e_1}{\beta} + \frac{e_2}{\beta^2} + \dots \right] \quad (4.6)$$

The advantage of this formulation in the case of  $\chi_V$  is that one additional term of perturbation theory is available (i.e.  $c_3$  but not  $a_3$  or  $b_3$ ).

For the standard nearest-neighbor action (2.4), the perturbative coefficients  $a_1$ ,  $a_2$ ,  $c_1$ ,  $c_2$ ,  $c_3$ ,  $e_1$  and  $e_2$  have been computed [55, 56, 57, 41]:

$$a_1 = \frac{1}{4} + \frac{\pi}{16} - 2\pi G_1 + \frac{\frac{1}{4} - \frac{5\pi}{48}}{N-2} \quad (4.7)$$

$$a_2 = \frac{0.0688 - 0.0028 N + 0.0107 N^2 - 0.0129 N^3}{(N-2)^2} \quad (4.8)$$

$$c_1 = \frac{\pi - 2}{4\pi} \frac{N-1}{N-2} \quad (4.9)$$

$$c_2 = \frac{N-1}{(N-2)^2} \left[ -\frac{3N^2 - 23N + 31}{96} + \frac{N-1}{8\pi^2} - \frac{2N-3}{8\pi} + G_1 (N-2)^2 \right] \quad (4.10)$$

$$c_3 = \frac{N-1}{(N-2)^3} (0.0198 + 0.0005N - 0.0011N^2 - 0.0102N^3 + 0.0041N^4) \quad (4.11)$$

$$e_1 = \frac{\pi - 2}{2\pi} \frac{N}{N-2} \quad (4.12)$$

$$e_2 = \frac{(\pi - 2)^2}{8\pi^2} \frac{N^2}{(N-2)^2} + \frac{2N}{N-2} \left[ G_1 (N-2) - \frac{1}{8\pi} - \frac{3N-14}{96} \right] \quad (4.13)$$

where

$$G_1 \approx 0.0461636. \quad (4.14)$$

From these expressions it is straightforward to obtain

$$b_1 = 2a_1 + c_1 \quad (4.15a)$$

$$b_2 = 2a_2 + a_1^2 + 2a_1c_1 + c_2 \quad (4.15b)$$

$$d_1 = 2a_1 + e_1 \quad (4.15c)$$

$$d_2 = 2a_2 + a_1^2 + 2a_1e_1 + e_2 \quad (4.15d)$$

Perturbation theory predicts trivially — or rather, *assumes* — that the lowest mass in the isotensor channel is the scattering state of two isovector particles, i.e. there are no isotensor bound states:

$$\tilde{C}_{\xi_T^{(exp)}}/\tilde{C}_{\xi_V^{(exp)}} = \frac{1}{2}. \quad (4.16)$$

The non-perturbative universal quantity  $\tilde{C}_{\xi_V^{(exp)}} \equiv \Lambda_{\overline{\text{MS}}}/m_V$  for the standard continuum  $S^{N-1}$   $\sigma$ -model has been computed exactly by Hasenfratz, Maggiore and Niedermayer (HMN) [58, 59, 60] using the thermodynamic Bethe Ansatz: it is

$$\tilde{C}_{\xi_V^{(exp)}} = \tilde{C}_{\xi_V^{(exp)}}^{(\text{HMN})} \equiv \left(\frac{e}{8}\right)^{1/(N-2)} \Gamma\left(1 + \frac{1}{N-2}\right). \quad (4.17)$$

For the rest, we know only their values at large  $N$  [61, 62, 41, 63]

$$\tilde{C}_{\xi_V^{(2nd)}}/\tilde{C}_{\xi_V^{(exp)}} = 1 - \frac{0.0032}{N} + O(1/N^2) \quad (4.18)$$

$$\tilde{C}_{\xi_T^{(2nd)}}/\tilde{C}_{\xi_T^{(exp)}} = \sqrt{2/3} \left[1 - \frac{1.2031}{N} + O(1/N^2)\right] \quad (4.19)$$

$$\tilde{C}_{\chi_V} = 2\pi \left[1 + \frac{4 + 3\gamma_C - 3\gamma_E - 7\log 2}{N} + O(1/N^2)\right] \quad (4.20)$$

$$\tilde{C}_{\chi_T} = \pi \left[1 + \frac{-2 + 6\log \frac{\pi}{4} - \frac{36}{\pi^2}\zeta'(2)}{N} + O(1/N^2)\right] \quad (4.21)$$

where  $\gamma_E \approx 0.5772157$  is Euler's constant and

$$\gamma_C = \log\left(\frac{\Gamma(1/3)\Gamma(7/6)}{\Gamma(2/3)\Gamma(5/6)}\right) \approx 0.4861007, \quad (4.22)$$

so that  $4 + 3\gamma_C - 3\gamma_E - 7\log 2 \approx -1.1254$  and  $-2 + 6\log \frac{\pi}{4} - \frac{36}{\pi^2}\zeta'(2) \approx -0.0296$ . From (4.18)/(4.19) combined with (4.16), we get

$$\tilde{C}_{\xi_V^{(2nd)}}/\tilde{C}_{\xi_T^{(2nd)}} = \sqrt{6} \left[1 + \frac{1.1999}{N} + O(1/N^2)\right]. \quad (4.23)$$

We can also write asymptotic scaling in terms of an “improved expansion parameter” [64, 65, 51, 66, 57, 44] based on the energy  $E_V = \langle \sigma_0 \cdot \sigma_1 \rangle$ . First we invert the perturbative expansion [67, 57]

$$E_V(\beta) = 1 - \frac{N-1}{4\beta} - \frac{N-1}{32\beta^2} - \frac{0.005993(N-1)^2 + 0.007270(N-1)}{\beta^3} + O(1/\beta^4) \quad (4.24)$$

and substitute into (4.1); this gives a prediction for  $\xi$  as a function of  $1 - E_V$ :

$$\xi_{\#}(\beta) = \tilde{C}'_{\xi_{\#}} \exp\left[\frac{\pi(N-1)}{2(N-2)}(1 - E_V)^{-1}\right] (1 - E_V)^{1/(N-2)} [1 + a'_1(1 - E_V) + \dots] \quad (4.25)$$

where

$$\tilde{C}'_{\xi\#} = \tilde{C}_{\xi\#} 2^{-5/2} \exp\left[-\frac{\pi}{4(N-2)}\right] \left[\frac{2(N-2)}{\pi(N-1)}\right]^{1/(N-2)} \quad (4.26)$$

$$a'_1 = \frac{4}{N-1} a_1 - \frac{1}{(N-1)(N-2)} \left[\frac{1}{2} + \frac{\pi}{8} - 0.73086 - 0.602482(N-1)\right] \quad (4.27)$$

In a similar way we can obtain “energy-improved” expansions for  $\chi_V$  and  $\chi_T$  and the ratios  $\chi_V/\xi_{\#}^2$  and  $\chi_T/\xi_{\#}^2$ . Note that for the basic observables  $\xi_{\#}$  and  $\chi_{\#}$ , which grow exponentially as  $\beta \rightarrow \infty$ , from the three-loop energy (4.24) we can get at best a three-loop “energy-improved” prediction, no matter how many terms in (4.1)–(4.3) are computed; but for the *ratios*  $\chi_{\#}/\xi_{\#}^2$ , in which the exponential cancels out, we can obtain a four-loop “energy-improved” prediction using our knowledge of  $c_2$  and  $e_2$ .

Our extrapolation method [38] is based on the finite-size-scaling Ansatz

$$\frac{\mathcal{O}(\beta, sL)}{\mathcal{O}(\beta, L)} = F_{\mathcal{O}}(\xi(\beta, L)/L; s) + O(\xi^{-\omega}, L^{-\omega}), \quad (4.28)$$

where  $\mathcal{O}$  is any long-distance observable,  $s$  is a fixed scale factor (usually  $s = 2$ ),  $\xi(\beta, L)$  is a suitably defined finite-volume correlation length,  $L$  is the linear lattice size,  $F_{\mathcal{O}}$  is a scaling function characteristic of the universality class, and  $\omega$  is a correction-to-scaling exponent. Here we will use  $\xi_V^{(2nd)}$  in the role of  $\xi(\beta, L)$ ; for the observables  $\mathcal{O}$  we will use the four “basic observables”  $\xi_V^{(2nd)}$ ,  $\chi_V$ ,  $\xi_T^{(2nd)}$ ,  $\chi_T$  as well as certain combinations of them such as  $\chi_V/(\xi_V^{(2nd)})^2$  and  $\chi_T/(\xi_V^{(2nd)})^2$ .

In an asymptotically free model, the functions  $F_{\mathcal{O}}$  can be computed in perturbation theory, yielding the following expansions [44] in powers of  $1/x^2$ , where  $x \equiv \xi_V^{(2nd)}(\beta, L)/L$ :

$$\frac{\xi_V^{(2nd)}(\beta, sL)}{\xi_V^{(2nd)}(\beta, L)} = s \left[ 1 - \frac{w_0 \log s}{2} \left(\frac{A}{x}\right)^2 - \left(\frac{w_1 \log s}{2} + \frac{w_0^2 \log^2 s}{8}\right) \left(\frac{A}{x}\right)^4 + O(x^{-6}) \right] \quad (4.29a)$$

$$\begin{aligned} \frac{\chi_V(\beta, sL)}{\chi_V(\beta, L)} &= s^2 \left[ 1 - \frac{\log s}{2\pi} x^{-2} \right. \\ &\quad \left. + \frac{1}{N-1} \left( \frac{\log^2 s}{8\pi^2} + \left( \pi I_{3,\infty} + \frac{1}{8\pi^3} \right) \log s \right) x^{-4} + O(x^{-6}) \right] \end{aligned} \quad (4.29b)$$

$$\begin{aligned} \frac{\xi_T^{(2nd)}(\beta, sL)}{\xi_T^{(2nd)}(\beta, L)} &= s \left\{ 1 - \frac{\log s}{4\pi} \frac{N-2}{N-1} x^{-2} \right. \\ &\quad \left. - \frac{(N-2)^2}{(N-1)^2} \left[ \left( \frac{N+1}{2} \left( \pi I_{3,\infty} + \frac{1}{8\pi^3} \right) + \frac{1}{8\pi^2} \right) \frac{\log s}{N-2} + \frac{\log^2 s}{32\pi^2} \right] x^{-4} \right. \\ &\quad \left. + O(x^{-6}) \right\} \end{aligned} \quad (4.29c)$$

$$\frac{\chi_T(\beta, sL)}{\chi_T(\beta, L)} = s^2 \left[ 1 - \frac{\log s}{2\pi} \frac{2N}{N-1} x^{-2} \right]$$

$$+ \frac{N}{(N-1)^2} \left( \frac{N+2}{4\pi^2} \log^2 s + 2 \left( \pi I_{3,\infty} + \frac{1}{8\pi^3} \right) \log s \right) x^{-4} + O(x^{-6}) \Big] \quad (4.29d)$$

and also

$$\frac{\xi_V^{(2nd)}(\beta, L)}{\xi_T^{(2nd)}(\beta, L)} = \left( \frac{2N}{N-1} \right)^{1/2} \left[ 1 + \frac{N+1}{N-1} \pi \left( \pi I_{3,\infty} + \frac{1}{8\pi^3} \right) x^{-2} + O(x^{-4}) \right] \quad (4.30)$$

where  $A = (N-1)^{-1/2}$ ,  $w_0 = (N-2)/2\pi$ ,  $w_1 = (N-2)/(2\pi)^2$  and

$$I_{3,\infty} \approx (2\pi)^{-4} \times 3.709741314407459. \quad (4.31)$$

In the case of the  $N \rightarrow \infty$  limit it is possible to derive exact expressions for the finite-size-scaling functions [63]. We will compare these  $N = \infty$  curves with our empirically obtained finite-size-scaling functions for  $N = 8$ .

Our extrapolation method [38] proceeds as follows: We make Monte Carlo runs at numerous pairs  $(\beta, L)$  and  $(\beta, sL)$ . We plot  $\mathcal{O}(\beta, sL)/\mathcal{O}(\beta, L)$  versus  $\xi(\beta, L)/L$ , using those points satisfying both  $\xi(\beta, L) \geq \text{some value } \xi_{min}$  and  $L \geq \text{some value } L_{min}$ . If all these points fall with good accuracy on a single curve — thus verifying the Ansatz (4.28) for  $\xi \geq \xi_{min}$ ,  $L \geq L_{min}$  — we choose a smooth fitting function  $F_{\mathcal{O}}$ . Then, using the functions  $F_{\xi}$  and  $F_{\mathcal{O}}$ , we extrapolate the pair  $(\xi, \mathcal{O})$  successively from  $L \rightarrow sL \rightarrow s^2L \rightarrow \dots \rightarrow \infty$ .

We have chosen to use functions  $F_{\mathcal{O}}$  of the form

$$F_{\mathcal{O}}(x) = 1 + a_1 e^{-1/x} + a_2 e^{-2/x} + \dots + a_n e^{-n/x}. \quad (4.32)$$

(Other forms of fitting functions can be used instead.) This form is partially motivated by theory, which tells us that in some cases  $F_{\mathcal{O}}(x) \rightarrow 1$  exponentially fast as  $x \rightarrow 0$  [44]. Typically a fit of order  $3 \leq n \leq 15$  is sufficient; the required order depends on the range of  $x$  values covered by the data and on the shape of the curve. Empirically, we increase  $n$  until the  $\chi^2$  of the fit becomes essentially constant. The resulting  $\chi^2$  value provides a check on the systematic errors arising from corrections to scaling and/or from the inadequacies of the form (4.32).

## 4.2 Data Analysis for $N = 8$

We now apply the method described in the previous subsection to our data for the  $N = 8$  case. As mentioned before, since the primary purpose of this paper was to study the MGMC embedding algorithm, and since MGMC is in any case less efficient than Wolff's cluster algorithm [30] for the special case of the  $N$ -vector models, we have made only a modest effort to produce static data, concentrating on the  $N = 8$  case. Moreover, not all of our runs can be used to construct the extrapolation curve<sup>33</sup> (only 20 pairs), since at the beginning of this project we were not yet making use of the extrapolation method in our data analyses.

---

<sup>33</sup> Although all runs with  $\xi \geq \xi_{min}$  can be extrapolated using the curve.

Nevertheless, we get interesting results, which confirm the asymptotic-freedom prediction with the correct nonperturbative constant.

Our data cover the range  $0.08 \leq x \equiv \xi_V^{(2nd)}(L)/L \leq 0.76$ , and we found tentatively that a sixth-order fit is indicated: see Tables 8–11 for the four basic observables  $\xi_V, \chi_V, \xi_T, \chi_T$ .

Next we took  $\xi_{min} = 10$  and sought to choose  $L_{min}$  to avoid any detectable systematic error from corrections to scaling.<sup>34</sup> We began with the conservative choice  $L_{min} = 128$  and plotted the deviations from the fitting curves for the four basic observables: see Figure 1.

Note that in each case there are three  $L = 64$  points (at  $x \approx 0.44, 0.49, 0.54$ ) that deviate upwards from the fitting curve by 1–5 standard deviations. We do not understand the cause of these deviations. They could be due to corrections to scaling, but this explanation seems unlikely to us because: (a) for  $N = 3$  the corrections to scaling are *negative* and smaller in magnitude than those found here [39, 44, 50]; and (b) at  $N = \infty$  the corrections to scaling are extremely small [63]. Possibly there is some instability in the fitting procedure because of the small number of  $L = 128$  pairs at our disposal (only eight). So, not knowing whether to include or exclude these three “deviant” data points, we try both possibilities and treat the discrepancy between the two results as an added systematic error. More precisely, we divided the  $x$  axis into three intervals —  $x < 0.4$ ,  $0.4 \leq x \leq 0.6$ , and  $x > 0.6$  — and allowed different  $L_{min}$  values for each.

See Tables 8–11 for the results of the  $\chi^2$  tests. The best  $\chi^2$  values are obtained, as expected, for the choice  $L_{min} = (64, 128, 64)$ , which eliminates the three “deviant” data points as well as one other point, but leaves intact the rest. But since we don’t really have good cause to eliminate these points, we shall take  $L_{min} = (64, 64, 64)$  to be our *preferred* fit. In any case, we shall carry out the extrapolations using *both* of these fits, and compare the results. In all cases we take  $n = 6$ .

The finite-size-scaling curve for  $\xi_V$  coming from our preferred fit is shown in Figure 2(a) (solid curve). We also show, for comparison, the perturbative prediction (4.29a) through orders  $1/x^2$  and  $1/x^4$  (dashed curves). In Figure 2(b) we show the same solid curve and, for comparison, the corresponding curves for  $N = 3$  (Monte Carlo) [39, 50] and  $N = \infty$  (exact) [63]. In Figures 3–5 we show the analogous curves for the observables  $\chi_V, \xi_T, \chi_T$ . In all cases, the agreement with perturbation theory is excellent for  $x \gtrsim 0.5$  (isovector sector) and  $x \gtrsim 0.6$  (isotensor sector). The  $N = 8$  finite-size-scaling curves fall, as expected, between the  $N = 3$  and  $N = \infty$  curves, and rather closer to the latter.

Next we checked for consistency between the extrapolated values of each observable coming from different lattice sizes at the same  $\beta$ . In most cases these are consistent at better than the 5% level; but in two cases ( $\beta = 6.1, 7.1$ ) they are inconsistent at worse than the 0.1% level (we don’t know why). If we exclude these two  $\beta$  values and sum over the rest, we get  $\chi^2 = 12.09, 15.16, 18.60, 15.00$  (15 degrees of freedom), respectively, for the observables  $\xi_V, \chi_V, \xi_T, \chi_T$ . This corresponds to confidence levels of 67%, 44%, 23%, 45%.

In Table 12 we show the extrapolated values of the four basic observables from our preferred fit  $L_{min} = (64, 64, 64)$  and also from the fit  $L_{min} = (64, 128, 64)$ . The discrepancies between these values (if larger than the statistical errors) can serve as a rough estimate of the remaining systematic errors due to corrections to scaling. The statistical errors in the

---

<sup>34</sup> A choice  $\xi_{min} = 15$  would have been equivalent for our set of data for obtaining the finite-size-scaling functions, since although we have points with  $10 \leq \xi < 15$  that can be extrapolated using these curves, we do not have any *pairs* of points  $(\beta, L)/(\beta, 2L)$  falling in this interval.

extrapolated values from our preferred fit range from about 0.2–0.5% when  $\xi_V \lesssim 20$  to about 2–3% when  $\xi_V \approx 650$ . The systematic errors are of the same order as the statistical errors, or smaller. The statistical errors at different  $\beta$  are strongly positively correlated, but we did not evaluate this correlation quantitatively.

In Figure 6 (points  $+$ ,  $\times$ ,  $\boxplus$ ) we plot  $\xi_{V,\infty,estimate}^{(2nd)}(64,64,64)$  divided by the two-loop, three-loop and four-loop predictions for  $\xi_V^{(exp)}$  given in equations (4.1)/(4.7)/(4.8)/(4.17). This curve is theoretically predicted to converge to a constant as  $\beta \rightarrow \infty$ , and the limiting value is  $\tilde{C}_{\xi_V^{(2nd)}}/\tilde{C}_{\xi_V^{(exp)}}^{(HMN)}$ . We also compare to the prediction (4.25) using the “improved expansion parameter”  $1 - E_V$  (points  $\square$  and  $\diamond$ ). [For  $E_V$  in (4.25) we use the value measured on the largest lattice; the statistical errors and finite-size corrections on  $E_V$  are less than  $5 \times 10^{-5}$ , and therefore induce a negligible error (less than 0.5%) on the predicted  $\xi$ .] We show for comparison the expected limiting value 0.9996 coming from the  $1/N$  expansion (4.18) through order  $1/N$ , evaluated at  $N = 8$ . Both the four-loop and the “improved” 3-loop prediction are in excellent agreement with the data, showing discrepancies of less than 1%.

In Figure 7 we proceed analogously for  $\xi_T$ , by plotting (points  $+$ ,  $\times$ ,  $\boxplus$ )  $\xi_{T,\infty,estimate}^{(2nd)}(64,64,64)$  divided by the two-loop, three-loop and four-loop predictions for  $\xi_T^{(exp)} \equiv \frac{1}{2}\xi_V^{(exp)}$  given in equations (4.1)/(4.7)/(4.8)/(4.16)/(4.17). We also compare to the prediction (4.25) using the “improved expansion parameter”  $1 - E_V$  (points  $\square$  and  $\diamond$ ). The four-loop and improved three-loop data are relatively flat, and suggest a limiting value  $\tilde{C}_{\xi_T^{(2nd)}}/\tilde{C}_{\xi_T^{(exp)}}^{(HMN)} \approx 0.72 \pm 0.01$ . This can be compared with the expected limiting value 0.6937 coming from the  $1/N$  expansion (4.18) through order  $1/N$ , evaluated at  $N = 8$ . Clearly the order- $1/N^2$  corrections are still significant (of order 3–4%), which is not surprising since the order- $1/N$  correction was 15%.

For the susceptibility  $\chi_V$  we proceed in two different ways, using either  $\chi_V$  directly or else using the ratio  $\chi_V/\xi_V^{(2nd)2}$ . The advantage of the latter approach is that one additional term of perturbation theory is available. Thus, in Figure 8(a) we plot  $\chi_{V,\infty,estimate}(64,64,64)$  divided by the theoretical prediction (4.2) *with the prefactor  $\tilde{C}_{\chi_V}$  omitted*; the  $\beta \rightarrow \infty$  limit of this curve thus gives an estimate of  $\tilde{C}_{\chi_V}$ . Here we have two-loop, three-loop and four-loop predictions (points  $+$ ,  $\times$ ,  $\boxplus$ ) as well as “improved” two-loop and three-loop predictions ( $\square$  and  $\diamond$ ). Similarly, we could plot  $\chi_{V,\infty,estimate}(64,64,64)/[\xi_{V,\infty,estimate}^{(2nd)}(64,64,64)]^2$  divided by the theoretical prediction (4.2)/(4.1) with the prefactors  $\tilde{C}_{\chi_V}$  and  $\tilde{C}_{\xi_V^{(2nd)}}$  omitted; the  $\beta \rightarrow \infty$  limit would then give an estimate of  $\tilde{C}_{\chi_V}/(\tilde{C}_{\xi_V^{(2nd)}})^2$ . However, in order to make the vertical scale of this graph more directly comparable to that of Figure 8(a), we have multiplied the quantity being plotted by the factor  $(\tilde{C}_{\xi_V^{(exp)}}^{(HMN)})^2$ . Note that this does not in any way alter the *logic* of the analysis, as  $\tilde{C}_{\xi_V^{(exp)}}^{(HMN)}$  is an explicit number defined in (4.17). The resulting curve is plotted in Figure 8(b); its  $\beta \rightarrow \infty$  limit gives an estimate of  $\tilde{C}_{\chi_V}(\tilde{C}_{\xi_V^{(exp)}}^{(HMN)}/\tilde{C}_{\xi_V^{(2nd)}})^2$ . In this case we have two-loop, three-loop, four-loop and five-loop predictions ( $+$ ,  $\times$ ,  $\boxplus$ ,  $\boxtimes$ ) as well as “improved” two-loop, three-loop and four-loop predictions ( $\square$ ,  $\diamond$ ,  $\boxdot$ ). To convert

this to an estimate for  $\tilde{C}_{\chi_V}$  itself, we need to multiply by

$$\left( \frac{\tilde{C}_{\xi_V^{(2nd)}}}{\tilde{C}_{\xi_V^{(exp)}}^{(\text{HMN})}} \right)^2 = \left( \frac{\tilde{C}_{\xi_V^{(2nd)}}}{\tilde{C}_{\xi_V^{(exp)}}} \right)^2 \left( \frac{\tilde{C}_{\xi_V^{(exp)}}}{\tilde{C}_{\xi_V^{(exp)}}^{(\text{HMN})}} \right)^2 \quad (4.33)$$

The first factor on the right side is theoretically expected to be  $\approx 0.9992$ , and the second factor is theoretically expected to be 1; moreover, our data for  $\xi_V^{(2nd)}$  itself (Figure 6) are consistent with this prediction (of course they are incapable of distinguishing 0.9992 from 1). For all practical purposes the factor (4.33) is 1, and Figures 8(a) and 8(b) can be compared directly. The two approaches give consistent results, but the one based on  $\chi_V/\xi_V^{(2nd)^2}$  seems to work better. We get the value

$$\tilde{C}_{\chi_V} = 5.58 \pm 0.10. \quad (4.34)$$

This can be compared with the predicted value  $\tilde{C}_{\chi_V} = 5.40$  coming from the  $1/N$  expansion (4.20) through order  $1/N$ , evaluated at  $N = 8$ .<sup>35</sup> Clearly the order- $1/N^2$  corrections are still significant (of order 3%), which is not surprising since the order- $1/N$  correction was 14%.

We proceed analogously for  $\chi_T$ , using either  $\chi_T$  directly or else using the ratio  $\chi_T/\xi_V^{(2nd)^2}$ . In Figure 9(a) we plot  $\chi_{T,\infty,estimate(64,64,64)}$  divided by the theoretical prediction (4.3) *with the prefactor  $\tilde{C}_{\chi_T}$  omitted*; the  $\beta \rightarrow \infty$  limit of this curve gives an estimate of  $\tilde{C}_{\chi_T}$ . Here we have two-loop, three-loop and four-loop predictions (points  $+$ ,  $\times$ ,  $\square$ ) as well as “improved” two-loop and three-loop predictions ( $\diamond$  and  $\nabla$ ). In Figure 9(b) we plot  $\chi_{T,\infty,estimate(64,64,64)}/[\xi_{V,\infty,estimate(64,64,64)}^{(2nd)}]^2$  divided by the theoretical prediction (4.3)/(4.1) for this same quantity, with the prefactors  $\tilde{C}_{\chi_T}$  and  $\tilde{C}_{\xi_V^{(2nd)}}$  omitted, and the whole thing finally multiplied by  $(\tilde{C}_{\xi_V^{(exp)}}^{(\text{HMN})})^2$ ; the  $\beta \rightarrow \infty$  limit of this curve gives an estimate of  $\tilde{C}_{\chi_T}(\tilde{C}_{\xi_V^{(exp)}}^{(\text{HMN})}/\tilde{C}_{\xi_V^{(2nd)}})^2$ . As before, this is for all practical purposes equal to  $\tilde{C}_{\chi_T}$ . Here we have two-loop, three-loop and four-loop predictions ( $+$ ,  $\times$ ,  $\square$ ) as well as “improved” two-loop, three-loop and four-loop predictions ( $\diamond$ ,  $\nabla$ ,  $\nabla/\backslash$ ), namely we do not have an additional term of conventional perturbation theory, but we do have an additional term in the “improved” perturbation theory. The two approaches give consistent results, and here the one based on  $\chi_T/\xi_V^{(2nd)^2}$  does not seem to work better. We get the value

$$\tilde{C}_{\chi_T} = 4.1 \pm 0.1. \quad (4.35)$$

This can be compared with the predicted value  $\tilde{C}_{\chi_T} = 3.13$  coming from the  $1/N$  expansion (4.21) through order  $1/N$ , evaluated at  $N = 8$ . Clearly the order- $1/N^2$  corrections are still significant (of order 31%) which is surprising since the order- $1/N$  correction was 0.4%.

## 5 Finite-Size-Scaling Analysis: Dynamic Quantities

---

<sup>35</sup> Our preliminary report [52] mistakenly wrote 5.30 instead of 5.40. We apologize for the arithmetic error!



## 5.1 Integrated Autocorrelation Times

Of all the observables we studied, the slowest mode (by far) is the squared isovector magnetization  $\mathcal{M}_V^2$ : this quantity measures the relative rotations of the spins in different parts of the lattice, and is the prototypical  $O(N)$ -invariant “long-wavelength observable”. For all three values of  $N$ , the autocorrelation time  $\tau_{int, \mathcal{M}_V^2}$  has the same qualitative behavior: as a function of  $\beta$  it first rises to a peak and then falls; the location of this peak shifts towards  $\beta = \infty$  as  $L$  increases; and the height of this peak grows as  $L$  increases. A similar but less pronounced peak is observed in  $\tau_{int, \mathcal{M}_T^2}$ . By contrast, the integrated autocorrelation times of the energies,  $\tau_{int, \mathcal{E}_V}$  and  $\tau_{int, \mathcal{E}_T}$ , are uniformly small — less than 2.5, 3.2, 6.4 for  $N = 3, 4, 8$ , respectively — and vary only weakly with  $\beta$  and  $L$ . This is because the energies are primarily “short-wavelength observables”, and have only weak overlap with the modes responsible for critical slowing-down.

Let us now make these considerations quantitative, by applying finite-size scaling to the dynamic quantities  $\tau_{int, \mathcal{M}_V^2}$  and  $\tau_{int, \mathcal{M}_T^2}$ . We use the Ansatz

$$\tau_{int, A}(\beta, L) \approx \xi(\beta, L)^{z_{int, A}} g_A(\xi(\beta, L)/L) \quad (5.1)$$

for  $A = \mathcal{M}_V^2$  and  $\mathcal{M}_T^2$ . Here  $g_A$  is an unknown scaling function, and  $g_A(0) = \lim_{x \downarrow 0} g_A(x)$  is supposed to be finite and nonzero.<sup>36</sup> We determine  $z_{int, A}$  by plotting  $\tau_{int, A}/\xi_V(L)^{z_{int, A}}$  versus  $\xi_V(L)/L$  and adjusting  $z_{int, A}$  until the points fall as closely as possible onto a single curve (with priority to the larger  $L$  values). We emphasize that the dynamic critical exponent  $z_{int, A}$  is in general *different* from the exponent  $z_{exp}$  associated with the exponential autocorrelation time  $\tau_{exp}$  [1, 68, 4].

Using the procedure just described, we find

$$z_{int, \mathcal{M}_V^2} = \begin{cases} 0.70 \pm 0.08 & \text{for } N = 3 \\ 0.52 \pm 0.10 & \text{for } N = 8 \end{cases} \quad (5.2)$$

(subjective 68% confidence limits). In Figures 10 and 11 we show the “best” finite-size-scaling plots for each case. Note that the corrections to scaling are quite strong: the  $L = 32$  point deviates considerably from the asymptotic scaling curve, and even for  $L = 64$  the deviation is noticeable. However, it is reasonable to hope that these corrections to scaling will have decayed to a small value by  $L = 128$ ; if so, our estimates of  $z_{int, \mathcal{M}_V^2}$  for the W-cycle — which attempt to place the  $L = 128$  and  $L = 256$  points on top of one another — will be afflicted by only a small systematic error. In any case, the error bars in (5.2) take account of this potential systematic error. Similarly, for the isotensor sector we have

$$z_{int, \mathcal{M}_T^2} = \begin{cases} 0.54 \pm 0.08 & \text{for } N = 3 \\ 0.53 \pm 0.10 & \text{for } N = 8 \end{cases} \quad (5.3)$$

---

<sup>36</sup> It is of course equivalent to use the Ansatz

$$\tau_{int, A}(\beta, L) \approx L^{z_{int, A}} h_A(\xi(\beta, L)/L),$$

and indeed the two Ansätze are related by  $h_A(x) = x^{z_{int, A}} g_A(x)$ . However, to determine whether  $\lim_{x \downarrow 0} g_A(x) = \lim_{x \downarrow 0} x^{-z_{int, A}} h_A(x)$  is nonzero, it is more convenient to inspect a graph of  $g_A$  than one of  $h_A$ .

(subjective 68% confidence limits). In Figures 12 and 13 we show the “best” finite-size-scaling plots for each case. It thus appears that, for  $N = 3$ ,  $z_{int, \mathcal{M}_T^2}$  is *strictly smaller than*  $z_{int, \mathcal{M}_V^2}$ . This behavior is by no means surprising; indeed, the exponents  $z_{int, A}$  are expected to vary from one observable to another [1, 4]. On the other hand, for  $N = 8$  we have  $z_{int, \mathcal{M}_T^2} \approx z_{int, \mathcal{M}_V^2}$  within statistical error. We have no explanation for the very different behavior in the two cases. Perhaps  $z_{int, \mathcal{M}_T^2}$  is strictly smaller than  $z_{int, \mathcal{M}_V^2}$  for *all*  $N$ , but the difference between the two exponents goes rapidly to zero as  $N \rightarrow \infty$ .

For the  $N = 4$  case, our data are insufficient to support a good finite-size-scaling analysis. Instead, let us compare our values of  $\tau_{int, \mathcal{M}_V^2}$  to the corresponding values for the direct MGMC algorithm (taken from [8]): see Table 13. We find that the ratio of the two autocorrelation times is compatible with a constant (independent of  $L$  and  $\beta$ ):

$$\frac{\tau_{int, \mathcal{M}_V^2}(XY \text{ embedding})}{\tau_{int, \mathcal{M}_V^2}(\text{direct})} = 3.18 \pm 0.04 \quad (5.4)$$

with  $\chi^2 = 6.55$  (13 DF, level = 92%), using all the data; or  $3.20 \pm 0.04$  with  $\chi^2 = 4.23$  (10 DF, level = 94%), if we use only the data for  $L = 64$  and 128. Therefore, the two algorithms have the same dynamic critical exponent, which was found in [8] to be

$$z_{int, \mathcal{M}_V^2} = 0.60 \pm 0.07 \quad (N = 4) , \quad (5.5)$$

and the same dynamic finite-size-scaling functions; in other words, they belong (as expected) to the same dynamic universality class. It could also have been expected that the ratio of autocorrelation times would be  $\approx 3$ : there are  $N - 1$  distinct internal-spin directions in an  $N$ -vector model, and the  $XY$ -embedding algorithm handles them one at a time, while the direct algorithm handles them all at once.

The dynamic critical exponent  $z_{int, \mathcal{M}_V^2}$  for W-cycle MGMC thus appears to be decreasing as  $N$  increases. (However, our evidence for this is at present on the borderline of statistical significance.) It is tempting to speculate that  $z_{W-cycle, PC}(N\text{-vector})$  tends to zero as  $N \rightarrow \infty$ ; this would be compatible with the vague idea that the  $N = \infty$  model is “essentially Gaussian”. However, it is far from clear that the  $N = \infty$  model is Gaussian *in the sense relevant for MGMC*.

## 5.2 Autocorrelation Functions and Exponential Autocorrelation Times

Finally, we want to test the more detailed dynamic finite-size-scaling Ansatz

$$\rho_A(t; \beta, L) \approx |t|^{-p_A} h_A\left(t/\tau_{exp, A}(\beta, L); \xi(\beta, L)/L\right) , \quad (5.6)$$

where  $p_A$  is an unknown exponent and  $h_A$  is an unknown scaling function. If  $p_A = 0$ , then (5.6) can equivalently be written as

$$\rho_A(t; \beta, L) \approx \hat{h}_A\left(t/\tau_{int, A}(\beta, L); \xi(\beta, L)/L\right) . \quad (5.7)$$

In this latter situation<sup>37</sup>,  $\tau_{int,A}$  and  $\tau_{exp,A}$  have the *same* dynamic critical exponent  $z_{int,A} = z_{exp}$ , and we furthermore have

$$\frac{\tau_{int,A}}{\tau_{exp,A}} \approx F_A(\xi(\beta, L)/L) \quad (5.8)$$

where

$$F_A(x) \equiv \lim_{t \rightarrow +\infty} \frac{1}{t} \log \hat{h}_A(t; x). \quad (5.9)$$

In Figure 14 we test the Ansatz (5.7) for  $A = \mathcal{M}_V^2$  and  $N = 3$ , by plotting  $\rho_{\mathcal{M}_V^2}(t; \beta, L)$  versus  $t/\tau_{int, \mathcal{M}_V^2}(\beta, L)$ , and mapping different ranges of  $\xi(\beta, L)/L$  to different symbols. (For visual clarity we have also “thinned out” the data points; and to reduce the effects of statistical noise, we have included data only from those runs that are longer than  $20000 \tau_{int, \mathcal{M}_V^2}$ .) The data support the Ansatz (5.7) reasonably well, with each range of  $\xi(\beta, L)/L$  defining roughly a single curve (until that curve falls into the statistical noise). The curve for small  $\xi(\beta, L)/L$  is close to straight (i.e. close to a pure exponential), while the curves for larger  $\xi(\beta, L)/L$  are increasingly convex.<sup>38</sup> This means that the ratio  $\tau_{int, \mathcal{M}_V^2}/\tau_{exp, \mathcal{M}_V^2}$  is close to 1 for small  $\xi(\beta, L)/L$ , and less than 1 for larger  $\xi(\beta, L)/L$ . Indeed, our crude estimates of  $\tau_{exp, \mathcal{M}_V^2}$ , based on linear fits (taking proper account of correlations) to the approximately linear regime in Figure 14, suggest that  $\tau_{int, \mathcal{M}_V^2}/\tau_{exp, \mathcal{M}_V^2}$  is  $\approx 0.90$ – $1$  for  $\xi(\beta, L)/L \lesssim 0.1$ , and decreases to  $\approx 0.75$  for  $\xi(\beta, L)/L \approx 0.5$ . It is *conceivable* that  $\tau_{int, \mathcal{M}_V^2}/\tau_{exp, \mathcal{M}_V^2}$  tends to 1 as  $\xi(\beta, L)/L \rightarrow 0$ ; if true, this would mean that  $\mathcal{M}_V^2$  truly becomes the “slowest mode” in the limit  $L \rightarrow \infty$ ,  $\xi/L \rightarrow 0$ .

In Figure 15 we show the analogous plot for  $N = 8$ . Again the Ansatz (5.7) seems to be well verified, but here the dependence on  $\xi(\beta, L)/L$  is much weaker (in truth, it is virtually invisible in our data). We estimate that  $\tau_{int, \mathcal{M}_V^2}/\tau_{exp, \mathcal{M}_V^2}$  is  $\approx 0.98$  for  $\xi(\beta, L)/L \lesssim 0.2$ , and decreases to  $\approx 0.95$  for  $\xi(\beta, L)/L \approx 0.6$ . It is *conceivable* that this dependence on  $\xi(\beta, L)/L$  disappears entirely in the limit  $N \rightarrow \infty$ , i.e. we *might* have  $\tau_{int, \mathcal{M}_V^2}/\tau_{exp, \mathcal{M}_V^2} \rightarrow 1$  for all  $\xi(\beta, L)/L$  in the limit  $L \rightarrow \infty$ ,  $N \rightarrow \infty$ .

## 6 Discussion

### 6.1 Dynamic Critical Behavior of Piecewise-Constant MGMC

Let us now summarize our conclusions about the dynamic critical behavior of W-cycle MGMC with piecewise-constant interpolation:

1) The direct and XY-embedding MGMC algorithms for the 4-vector model fall, as expected, into the same dynamic universality class. Indeed, the ratio of their autocorrelation times is approximately 1:3, as expected from the fact that there are  $N - 1$  distinct internal-spin directions in an  $N$ -vector model.

<sup>37</sup> Contrary to much belief,  $z_{int,A}$  need not equal  $z_{exp}$ . Indeed, if  $p_A > 0$ , we have  $z_{int,A} = (1 - p_A) z_{exp} < z_{exp}$ . See [1, 4] for further discussion.

<sup>38</sup> The rescaled horizontal axis in Figure 14 ensures that the total area under each curve is 1. Therefore, the more convex curves must be below the straight curve for small  $t/\tau_{int, \mathcal{M}_V^2}$ , but *above* it for large  $t/\tau_{int, \mathcal{M}_V^2}$ .

2) The dynamic critical exponent  $z_{int, \mathcal{M}_V^2}$  for W-cycle MGMC with piecewise-constant interpolation is clearly *nonzero* for two-dimensional asymptotically free models: we have

$$z_{W-cycle, PC} = \begin{cases} 0.70 \pm 0.08 & \text{for the 3-vector model [this paper]} \\ 0.60 \pm 0.07 & \text{for the 4-vector model [8, this paper]} \\ 0.52 \pm 0.10 & \text{for the 8-vector model [this paper]} \\ 0.45 \pm 0.02 & \text{for the } SU(3) \text{ chiral model [34, 35]} \end{cases} \quad (6.1)$$

(subjective 68% confidence intervals). Furthermore, this exponent apparently *varies* from one asymptotically free model to another (but the evidence for this is on the borderline of statistical significance, especially in the  $N$ -vector models). Finally, it is *conceivable* that  $z_{W-cycle, PC}(N\text{-vector})$  tends to zero as  $N \rightarrow \infty$ ; testing this will require measurements at larger values of  $N$ .

In [8, Section 4.1] we produced a heuristic explanation of why  $z_{MGMC} \neq 0$ , based on the logarithmically decaying deviations from Gaussianness in an asymptotically free theory. This explanation does not, unfortunately, give a quantitative prediction for  $z_{MGMC}$ ; it merely makes the weak prediction that  $0 < z_{MGMC} < z_{heat-bath}$ . Moreover, our study of MGMC in the *one*-dimensional 4-vector model [9] has cast some doubt on the exactness of this explanation (it seems to be off by at least a logarithm). Clearly, the dynamic critical behavior of MGMC is far from being understood.

## 6.2 Piecewise-Constant vs. Smooth Interpolation

As noted in the Introduction, Mack and collaborators [11, 12, 13, 14, 15] have advocated the use of a smooth interpolation (e.g. piecewise-linear or better) in place of piecewise-constant. The key question is this: Does the MGMC algorithm have a *different dynamic critical exponent* depending on whether smooth or piecewise-constant interpolation is used?

In the Gaussian case, the answer is “yes” for a V-cycle but “no” for a W-cycle (see the Introduction). For non-Gaussian asymptotically free models, we conjecture that the answer is the same as in the Gaussian case, but to date no full-scale test has been made. Some time ago, Hasenbusch, Meyer and Mack [13] reported preliminary data for the 3-vector model suggesting that  $z_{int, \mathcal{M}_V^2} \approx 0.2$  for a V-cycle with smooth interpolation. (These authors did not study a W-cycle, as this would be extremely costly in their unigrid approach, but it is safe to assume that  $z_{W-cycle} \leq z_{V-cycle}$ .) This is considerably lower than our estimate  $z_{int, \mathcal{M}_V^2} \approx 0.7$  for the piecewise-constant W-cycle — suggesting that the smooth interpolation might indeed lead to a smaller dynamic critical exponent than piecewise-constant interpolation, even for a W-cycle. However, the estimate of [13] is based on runs at only four  $(\beta, L)$  pairs, which moreover have different values of  $\xi/L$ , so it is very difficult to perform a correct finite-size-scaling analysis. It would be very useful to have data at additional  $(\beta, L)$  pairs, and with higher statistics.

More recently, Hasenbusch and Meyer [14, 15] have reported data for the  $SU(3)$  and  $CP^3$   $\sigma$ -models, using a V-cycle with piecewise-linear interpolation. For  $CP^3$  the data are consistent with the dynamic finite-size-scaling Ansatz (5.1) with  $z_{int, \mathcal{M}_V^2} \approx 0.2$ . For  $SU(3)$ , however, the data are very erratic, and do not appear to be consistent with (5.1). More data would be very useful here too; both the dynamic critical exponent and the dynamic finite-size-scaling functions could be compared with those for the piecewise-constant W-cycle [34, 35].

### 6.3 Comparison with Other Collective-Mode Algorithms

We have previously [8, Section 4.3] compared the behavior of MGMC with that of Fourier acceleration [69, 70, 71, 72]. To our knowledge, no new data on the dynamic critical behavior of Fourier acceleration has appeared since that discussion, so we have nothing new to add.

A very different approach to collective-mode Monte Carlo is represented by Wolff's [30] cluster algorithm for  $N$ -vector models.<sup>39</sup> This algorithm is based on embedding a field of Ising variables into the  $N$ -vector model, and then simulating the induced Ising model by the Swendsen-Wang [74] algorithm (or its single-cluster variant [30]). It can be argued heuristically [31, 29] that this algorithm is effective at creating long-wavelength spin waves; indeed, extensive numerical tests show that critical slowing-down is *completely eliminated* in the two-dimensional  $N$ -vector models for  $N = 2, 3, 4$  [30, 31, 32, 29, 33].<sup>40</sup>

The principal difference between MGMC and Fourier acceleration on the one hand, and algorithms of Swendsen-Wang and Wolff type on the other, is how proposals are made for updating the long-wavelength modes. MGMC and Fourier acceleration propose additive updates of *fixed* shape (square, triangular or sinusoidal) and variable amplitude, while cluster algorithms like Swendsen-Wang and Wolff allow the system, in some sense, to *choose its own collective modes*.

At present, the Wolff algorithm is clearly the best algorithm for simulating  $N$ -vector models (at least in two dimensions); neither MGMC nor Fourier acceleration appears to be a serious competitor. However, this favorable situation for Wolff-type algorithms probably does *not* extend to other  $\sigma$ -models: indeed, there are strong reasons to believe [29] that a generalized Wolff-type embedding algorithm can have dynamic critical exponent  $z \ll 2$  *only* if the target manifold is a sphere (as in the  $N$ -vector model), a product of spheres, or the quotient of such a space by a discrete group (e.g. real projective space  $RP^{N-1}$ ).<sup>41</sup> By contrast, the MGMC algorithm (especially in its  $XY$ -embedding form) has a straightforward extension to  $\sigma$ -models taking values in an arbitrary homogeneous space  $G/H$ , and it appears to work well quite generally [e.g.  $z \approx 0.45$  for  $SU(3)$ ]. This is a strong motivation for pursuing the study of MGMC algorithms.

## Acknowledgments

We want to thank Martin Hasenbusch and Steffen Meyer for the discussions that initiated this project, and for many helpful comments thereafter. We also wish to thank Gustavo Mana for many discussions. Most of the computations reported here were carried out on the Cray C-90 at the Pittsburgh Supercomputing Center (PSC). This work was supported in part by the U.S. National Science Foundation grants DMS-9200719 and PHY-9520978 (A.D.S.), by the Istituto Nazionale di Fisica Nucleare (A.P.), and by PSC grants PHY890035P and MCA94P032P.

---

<sup>39</sup> This algorithm was also proposed independently by Hasenbusch [73].

<sup>40</sup> For  $N = 2$  the complete elimination of critical slowing-down requires also that the algorithm be effective at creating vortex-antivortex pairs; the mechanism for this is explained in [31].

<sup>41</sup> Moreover, the *practical* Wolff-type embedding algorithm (with one Swendsen-Wang hit on the induced Ising model per iteration) appears to behave rather poorly in the  $RP^{N-1}$  models, with  $z \approx 1$  [75, 33].

# References

- [1] A.D. Sokal, *Monte Carlo Methods in Statistical Mechanics: Foundations and New Algorithms*, Cours de Troisième Cycle de la Physique en Suisse Romande (Lausanne, June 1989).
- [2] S.L. Adler, Nucl. Phys. B (Proc. Suppl.) **9**, 437 (1989).
- [3] U. Wolff, Nucl. Phys. B (Proc. Suppl.) **17**, 93 (1990).
- [4] A.D. Sokal, Nucl. Phys. B (Proc. Suppl.) **20**, 55 (1991).
- [5] J. Goodman and A.D. Sokal, Phys. Rev. Lett. **56**, 1015 (1986).
- [6] J. Goodman and A.D. Sokal, Phys. Rev. **D40**, 2035 (1989).
- [7] R.G. Edwards, J. Goodman and A.D. Sokal, Nucl. Phys. **B354**, 289 (1991).
- [8] R.G. Edwards, S.J. Ferreira, J. Goodman and A.D. Sokal, Nucl. Phys. **B380**, 621 (1992).
- [9] T. Mendes and A. D. Sokal, Phys. Rev. **D53**, 3438 (1996).
- [10] H. Meyer-Ortmanns, Z. Phys. **C27**, 553 (1985).
- [11] G. Mack, in *Nonperturbative Quantum Field Theory*, 1987 Cargèse lectures, edited by G. 't Hooft *et al.* (Plenum, New York, 1988).
- [12] G. Mack and S. Meyer, Nucl. Phys. B (Proc. Suppl.) **17**, 293 (1990).
- [13] M. Hasenbusch, S. Meyer and G. Mack, Nucl. Phys. B (Proc. Suppl.) **20**, 110 (1991).
- [14] M. Hasenbusch and S. Meyer, Phys. Rev. Lett. **68**, 435 (1992).
- [15] M. Hasenbusch and S. Meyer, Phys. Rev. **D45**, 4376 (1992).
- [16] A. Hulsebos, J. Smit and J.C. Vink, Nucl. Phys. **B356**, 775 (1991).
- [17] M.L. Laursen, J. Smit and J.C. Vink, Phys. Lett. **B262**, 467 (1991).
- [18] M.L. Laursen and J.C. Vink, Nucl. Phys. **B401**, 745 (1993).
- [19] M. Grabenstein and K. Pinn, Phys. Rev. **D45**, 4372 (1992).
- [20] M. Grabenstein and K. Pinn, J. Stat. Phys. **71**, 607 (1993).
- [21] M. Grabenstein and B. Mikeska, Phys. Rev. **D47**, 3103 (1993).
- [22] M. Grabenstein, Ph.D. thesis (Universität Hamburg), DESY report 94-007, hep-lat/9401024.
- [23] M. Grabenstein and K. Pinn, Phys. Rev. **D50**, 6998 (1994).
- [24] W. Janke and T. Sauer, J. Stat. Phys. **78**, 759 (1995).

- [25] W. Hackbusch, *Multigrid Methods and Applications* (Springer, Berlin, 1985).
- [26] W.L. Briggs, *A Multigrid Tutorial* (SIAM, Philadelphia, 1987).
- [27] S.F. McCormick and J. Ruge, Math. Comput. **41** (1983) 43.
- [28] J. Goodman and A.D. Sokal, unpublished.
- [29] S. Caracciolo, R.G. Edwards, A. Pelissetto and A.D. Sokal, Nucl. Phys. **B403**, 475 (1993).
- [30] U. Wolff, Phys. Rev. Lett. **62**, 361 (1989).
- [31] R.G. Edwards and A.D. Sokal, Phys. Rev. **D40**, 1374 (1989).
- [32] U. Wolff, Nucl. Phys. **B334**, 581 (1990).
- [33] S. Caracciolo, R.G. Edwards, A. Pelissetto and A.D. Sokal, Dynamic critical behavior of Wolff-type embedding algorithms for  $RP^{N-1}$  and mixed isovector/isotensor  $\sigma$ -models in two dimensions, in preparation.
- [34] G. Mana, T. Mendes, A. Pelissetto and A.D. Sokal, Dynamic critical behavior of multi-grid Monte Carlo for two-dimensional nonlinear  $\sigma$ -models, presented at the Lattice '95 conference, hep-lat/9509030, Nucl. Phys. B (Proc. Suppl.) —, — (1996).
- [35] G. Mana, A. Pelissetto and A.D. Sokal, Multi-grid Monte Carlo via  $XY$  embedding. II. Two-dimensional  $SU(3)$  principal chiral model, in preparation.
- [36] M. Lüscher, P. Weisz and U. Wolff, Nucl. Phys. **B359**, 221 (1991).
- [37] J.-K. Kim, Phys. Rev. Lett. **70**, 1735 (1993); Nucl. Phys. B (Proc. Suppl.) **34**, 702 (1994); Phys. Rev. **D50**, 4663 (1994); Europhys. Lett. **28**, 211 (1994); Phys. Lett. **B345**, 469 (1995).
- [38] S. Caracciolo, R.G. Edwards, S.J. Ferreira, A. Pelissetto and A.D. Sokal, Phys. Rev. Lett. **74**, 2969 (1995).
- [39] S. Caracciolo, R.G. Edwards, A. Pelissetto and A.D. Sokal, Phys. Rev. Lett. **75**, 1891 (1995).
- [40] S. Caracciolo, A. Pelissetto and A.D. Sokal, in preparation.
- [41] S. Caracciolo and A. Pelissetto, Nucl. Phys. **B455**, 619 (1995).
- [42] G. Mack and V.B. Petkova, Ann. Phys. **123**, 442 (1979).
- [43] J. Fröhlich, Phys. Lett. **B83**, 195 (1979).
- [44] S. Caracciolo, R.G. Edwards, A. Pelissetto and A.D. Sokal, Phase diagram and universality classes of  $RP^{N-1}$  and mixed isovector/isotensor  $\sigma$ -models in two dimensions, in preparation.

- [45] S. Caracciolo, R.G. Edwards, A. Pelissetto and A.D. Sokal, Phys. Rev. Lett. **71**, 3906 (1993).
- [46] S. Caracciolo, R.G. Edwards, A. Pelissetto and A.D. Sokal, Nucl. Phys. B (Proc. Suppl.) **34**, 129 (1994).
- [47] M.B. Priestley, *Spectral Analysis and Time Series*, 2 vols. (Academic, London, 1981).
- [48] T.W. Anderson, *The Statistical Analysis of Time Series* (Wiley, New York, 1971).
- [49] N. Madras and A.D. Sokal, J. Stat. Phys. **50**, 109 (1988).
- [50] S. Caracciolo, R.G. Edwards, A. Pelissetto and A.D. Sokal, Asymptotic scaling in the two-dimensional  $O(3)$   $\sigma$ -model at correlation length  $10^5$ : A high-precision Monte Carlo study, in preparation.
- [51] U. Wolff, Phys. Lett. **B248**, 335 (1990); Nucl. Phys. B (Proc. Suppl.) **20**, 682 (1991).
- [52] S. Caracciolo, R.G. Edwards, T. Mendes, A. Pelissetto and A.D. Sokal, Comparison between theoretical four-loop predictions and Monte Carlo calculations in the two-dimensional  $N$ -vector model for  $N = 3, 4, 8$ , presented at the Lattice '95 conference, **hep-lat/9509033**, Nucl. Phys. B (Proc. Suppl.) —, — (1996).
- [53] G. Parisi, Phys. Lett. **B92**, 133 (1980).
- [54] J. Shigemitsu and J.B. Kogut, Nucl. Phys. **B190**[FS3], 365 (1981).
- [55] M. Falcioni and A. Treves, Nucl. Phys. **B265**, 671 (1986).
- [56] P. Weisz and M. Lüscher, unpublished, cited in [51].
- [57] S. Caracciolo and A. Pelissetto, Nucl. Phys. **B420**, 141 (1994).
- [58] P. Hasenfratz, M. Maggiore and F. Niedermayer, Phys. Lett. **B245**, 522 (1990).
- [59] P. Hasenfratz and F. Niedermayer, Phys. Lett. **B245**, 529 (1990).
- [60] P. Hasenfratz and F. Niedermayer, in *Nonperturbative Methods in Low Dimensional Quantum Field Theories* (14<sup>th</sup> Johns Hopkins Workshop on Current Problems in Particle Theory, Debrecen, Hungary, 27–30 August 1990), ed. G. Domokos, Z. Horvath and S. Kovesi-Domokos (World Scientific, Singapore, 1991), pp. 407–411.
- [61] H. Flyvbjerg, Nucl. Phys. **B348**, 714 (1991).
- [62] P. Biscari, M. Campostrini and P. Rossi, Phys. Lett. **B242**, 225 (1990).
- [63] S. Caracciolo and A. Pelissetto, in preparation.
- [64] G. Martinelli, G. Parisi and R. Petronzio, Phys. Lett. **B100**, 485 (1981).
- [65] S. Samuel, O. Martin and K. Moriarty, Phys. Lett. **B153**, 87 (1985).



- [66] G.P. Lepage and P.B. Mackenzie, Phys. Rev. **D48**, 2250 (1993).
- [67] M. Lüscher, unpublished, cited in [51].
- [68] S. Caracciolo, A. Pelissetto and A.D. Sokal, J. Stat. Phys. **60**, 1 (1990).
- [69] G. Parisi, in *Progress in Gauge Field Theory* (1983 Cargèse lectures), ed. G. 't Hooft *et al.* (Plenum, New York, 1984).
- [70] G.G. Batrouni, G.R. Katz, A.S. Kronfeld, G.P. Lepage, B. Svetitsky and K.G. Wilson, Phys. Rev. **D32**, 2736 (1985).
- [71] E. Dagotto and J.B. Kogut, Phys. Rev. Lett. **58**, 299 (1987).
- [72] E. Dagotto and J.B. Kogut, Nucl. Phys. **B290**[FS20], 451 (1987).
- [73] M. Hasenbusch, Nucl. Phys. **B333**, 581 (1990).
- [74] R.H. Swendsen and J.-S. Wang, Phys. Rev. Lett. **58**, 86 (1987).
- [75] S. Caracciolo, R.G. Edwards, A. Pelissetto and A.D. Sokal, Nucl. Phys. B (Proc. Suppl.) **26**, 595 (1992).

$d = 2$ 3-vector model: static data							
$L$	$\beta$	$\chi_V$	$\chi_T$	$\xi_V^{(2nd)}$	$\xi_T^{(2nd)}$	$E_V$	$E_T$
32	1.500	143.20 ( 0.80)	6.34 (0.04)	10.08 (0.06)	3.82 (0.03)	0.603146 (96)	0.497267 (61)
64	1.450	114.61 ( 0.56)	4.03 (0.01)	8.49 (0.06)	2.41 (0.05)	0.582513 (26)	0.484598 (16)
64	1.500	177.31 ( 0.81)	5.33 (0.01)	11.17 (0.06)	3.33 (0.03)	0.601747 (23)	0.496433 (15)
64	1.550	265.44 ( 1.24)	7.40 (0.02)	14.06 (0.07)	4.66 (0.03)	0.619546 (22)	0.508044 (15)
64	1.600	397.54 ( 1.58)	11.10 (0.04)	18.11 (0.07)	6.62 (0.03)	0.636082 (20)	0.519465 (14)
64	1.650	545.23 ( 2.26)	16.85 (0.07)	22.09 (0.10)	8.74 (0.04)	0.651148 (23)	0.530473 (17)
64	1.700	702.27 ( 2.15)	25.02 (0.10)	26.34 (0.10)	10.89 (0.04)	0.664824 (21)	0.540996 (16)
64	1.725	768.21 ( 2.06)	29.55 (0.11)	27.91 (0.09)	11.77 (0.04)	0.671122 (20)	0.546022 (16)
64	1.750	834.56 ( 1.81)	34.51 (0.12)	29.64 (0.08)	12.65 (0.04)	0.677156 (19)	0.550953 (16)
64	1.775	895.44 ( 2.11)	40.06 (0.16)	31.11 (0.10)	13.53 (0.05)	0.682911 (22)	0.555767 (19)
64	1.800	956.71 ( 1.87)	46.13 (0.17)	32.69 (0.10)	14.40 (0.05)	0.688427 (21)	0.560468 (19)
64	1.850	1054.35 ( 1.69)	57.81 (0.19)	34.90 (0.09)	15.76 (0.05)	0.698672 (20)	0.569463 (18)
64	1.900	1147.05 ( 2.09)	70.87 (0.29)	37.09 (0.12)	17.08 (0.07)	0.708203 (27)	0.578129 (26)
64	1.950	1224.55 ( 1.94)	83.83 (0.32)	38.58 (0.12)	18.06 (0.06)	0.717119 (25)	0.586526 (25)
128	1.450	115.43 ( 0.66)	4.01 (0.01)	8.48 (0.18)	2.19 (0.22)	0.582493 (16)	0.484605 (10)
128	1.500	175.61 ( 1.15)	5.17 (0.01)	11.11 (0.17)	2.92 (0.18)	0.601597 (16)	0.496336 (10)
128	1.550	277.80 ( 2.03)	6.95 (0.02)	14.46 (0.18)	4.31 (0.13)	0.619374 (16)	0.507931 (11)
128	1.575	351.79 ( 2.01)	8.07 (0.02)	16.52 (0.13)	4.62 (0.09)	0.627728 (11)	0.513626 ( 7)
128	1.600	451.87 ( 2.78)	9.51 (0.02)	19.22 (0.15)	5.43 (0.09)	0.635722 (10)	0.519229 ( 7)
128	1.650	729.57 ( 4.50)	13.72 (0.04)	25.29 (0.16)	7.76 (0.08)	0.650668 (10)	0.530135 ( 7)
128	1.680	963.04 ( 5.95)	17.74 (0.07)	29.64 (0.18)	9.91 (0.08)	0.659010 ( 9)	0.536485 ( 7)
128	1.700	1159.82 ( 4.95)	21.44 (0.07)	33.23 (0.14)	11.64 (0.06)	0.664314 ( 6)	0.540623 ( 5)
128	1.720	1375.13 ( 5.44)	26.06 (0.08)	36.95 (0.14)	13.48 (0.06)	0.669437 ( 6)	0.544697 ( 5)
128	1.740	1580.42 ( 5.76)	31.49 (0.11)	40.16 (0.15)	15.28 (0.06)	0.674350 ( 6)	0.548676 ( 5)
128	1.750	1707.43 ( 7.99)	34.73 (0.16)	42.28 (0.20)	16.20 (0.09)	0.676748 ( 8)	0.550646 ( 7)
128	1.770	1933.84 ( 7.98)	41.79 (0.19)	45.79 (0.20)	17.98 (0.08)	0.681412 ( 8)	0.554521 ( 7)
128	1.800	2264.75 ( 8.85)	54.13 (0.27)	50.90 (0.23)	20.64 (0.10)	0.688095 ( 9)	0.560202 ( 8)
128	1.850	2774.23 (10.10)	79.97 (0.42)	58.39 (0.27)	24.89 (0.11)	0.698460 (10)	0.569294 ( 9)
128	1.900	3185.97 ( 8.70)	107.63 (0.49)	63.69 (0.24)	27.88 (0.11)	0.708021 (10)	0.577985 ( 9)
128	1.950	3580.66 ( 6.58)	140.95 (0.53)	69.23 (0.20)	31.07 (0.10)	0.716928 ( 9)	0.586342 ( 9)
128	2.000	3915.42 ( 8.57)	175.97 (0.84)	72.99 (0.28)	33.50 (0.15)	0.725183 (12)	0.594332 (12)
256	1.450	116.51 ( 0.59)	4.03 (0.01)	9.05 (0.53)	2.79 (0.68)	0.582516 ( 8)	0.484616 ( 5)
256	1.550	278.41 ( 1.87)	6.92 (0.02)	14.20 (0.47)	4.59 (0.47)	0.619387 ( 8)	0.507942 ( 5)
256	1.650	738.30 ( 6.57)	13.23 (0.04)	25.07 (0.45)	7.53 (0.34)	0.650642 ( 7)	0.530118 ( 5)
256	1.700	1261.53 ( 9.26)	19.02 (0.05)	34.27 (0.34)	9.57 (0.22)	0.664240 ( 5)	0.540568 ( 4)
256	1.750	2151.82 (16.78)	28.55 (0.09)	46.74 (0.39)	14.45 (0.18)	0.676629 ( 4)	0.550554 ( 3)
256	1.800	3550.48 (22.89)	45.81 (0.19)	62.41 (0.39)	21.53 (0.16)	0.687953 ( 3)	0.560088 ( 3)
256	1.850	5468.72 (28.65)	77.19 (0.36)	81.45 (0.42)	30.87 (0.16)	0.698351 ( 3)	0.569199 ( 3)
256	1.900	7422.24 (34.60)	124.83 (0.67)	98.82 (0.51)	39.95 (0.20)	0.707952 ( 3)	0.577921 ( 3)
256	2.000	10832.90 (34.75)	264.76 (1.38)	126.41 (0.54)	54.98 (0.25)	0.725141 ( 4)	0.594293 ( 4)

Table 1: Static data from our runs for the two-dimensional 3-vector model. Error bar (one standard deviation) is shown in parentheses.

$d = 2$ 4-vector model: static data							
$L$	$\beta$	$\chi_V$	$\chi_T$	$\xi_V^{(2nd)}$	$\xi_T^{(2nd)}$	$E_V$	$E_T$
32	2.000	92.57 (0.58)	5.48 (0.03)	7.57 (0.05)	2.76 (0.03)	0.577469 (86)	0.435869 (65)
32	2.100	134.79 (0.72)	8.39 (0.05)	9.65 (0.05)	3.89 (0.03)	0.602061 (86)	0.454645 (69)
32	2.200	180.64 (0.74)	12.75 (0.07)	11.75 (0.05)	5.07 (0.03)	0.623979 (76)	0.472560 (66)
64	2.100	160.69 (1.02)	7.04 (0.02)	10.40 (0.08)	3.26 (0.05)	0.600938 (29)	0.453774 (23)
64	2.150	205.83 (1.09)	8.61 (0.02)	12.13 (0.07)	4.10 (0.04)	0.612116 (23)	0.462739 (19)
64	2.200	257.32 (1.33)	10.57 (0.04)	13.71 (0.07)	4.83 (0.04)	0.622688 (22)	0.471510 (19)
64	2.250	325.27 (1.59)	13.34 (0.05)	15.89 (0.08)	5.89 (0.04)	0.632745 (22)	0.480107 (19)
64	2.300	394.34 (1.36)	16.82 (0.06)	17.81 (0.06)	6.98 (0.03)	0.642221 (16)	0.488456 (15)
64	2.350	471.57 (1.85)	21.36 (0.09)	19.83 (0.08)	8.10 (0.04)	0.651226 (20)	0.496598 (19)
64	2.400	553.20 (1.45)	27.09 (0.09)	21.97 (0.06)	9.33 (0.03)	0.659749 (15)	0.504527 (14)
128	2.250	346.48 (3.88)	11.91 (0.05)	16.20 (0.27)	4.91 (0.17)	0.632545 (19)	0.479943 (17)
128	2.350	577.66 (6.79)	17.74 (0.10)	21.70 (0.29)	6.80 (0.16)	0.650918 (18)	0.496337 (16)
128	2.450	939.66 (7.63)	28.32 (0.16)	28.74 (0.24)	10.35 (0.12)	0.667481 (12)	0.511894 (11)
128	2.550	1457.27 (9.77)	47.68 (0.32)	37.45 (0.26)	14.93 (0.12)	0.682445 (11)	0.526619 (11)
128	2.650	2004.60 (9.45)	77.35 (0.47)	45.51 (0.24)	19.54 (0.12)	0.695981 (10)	0.540488 (11)

Table 2: Static data from our runs for the two-dimensional 4-vector model. Error bar (one standard deviation) is shown in parentheses.

$d = 2$ 8-vector model: static data							
$L$	$\beta$	$\chi_V$	$\chi_T$	$\xi_V^{(2nd)}$	$\xi_T^{(2nd)}$	$E_V$	$E_T$
64	4.000	53.89 ( 0.27)	5.19 (0.01)	5.46 (0.07)	1.91 (0.04)	0.543613 (29)	0.347690 (26)
64	4.600	148.63 ( 0.46)	11.37 (0.02)	9.84 (0.04)	3.56 (0.02)	0.603866 (13)	0.405040 (14)
64	4.800	208.47 ( 0.54)	15.40 (0.02)	12.02 (0.04)	4.60 (0.02)	0.620987 (10)	0.422834 (11)
64	5.000	284.97 ( 0.68)	21.34 (0.04)	14.33 (0.04)	5.86 (0.02)	0.636812 (10)	0.439888 (11)
64	5.200	381.17 ( 0.81)	30.39 (0.07)	17.05 (0.04)	7.50 (0.02)	0.651454 ( 9)	0.456198 (11)
64	5.400	487.41 ( 0.88)	43.18 (0.10)	19.75 (0.04)	9.26 (0.02)	0.664983 ( 9)	0.471718 (11)
64	5.800	706.90 ( 1.46)	80.34 (0.27)	24.91 (0.06)	12.77 (0.04)	0.689116 (15)	0.500489 (18)
64	6.100	858.53 ( 1.37)	116.18 (0.33)	28.11 (0.06)	15.07 (0.04)	0.705067 (14)	0.520279 (17)
64	6.400	1005.06 ( 1.27)	159.23 (0.38)	31.30 (0.06)	17.35 (0.04)	0.719367 (13)	0.538548 (17)
64	6.600	1092.16 ( 1.00)	189.00 (0.34)	33.08 (0.05)	18.63 (0.03)	0.728185 (10)	0.550059 (13)
64	6.800	1177.94 ( 0.97)	221.60 (0.36)	34.86 (0.05)	19.94 (0.03)	0.736470 (10)	0.561049 (13)
64	7.100	1298.91 ( 0.90)	272.69 (0.38)	37.48 (0.05)	21.80 (0.03)	0.747930 ( 9)	0.576527 (13)
64	7.400	1405.80 ( 0.90)	323.59 (0.43)	39.62 (0.05)	23.35 (0.03)	0.758452 ( 9)	0.591024 (12)
64	7.800	1540.37 ( 0.97)	394.93 (0.53)	42.60 (0.06)	25.47 (0.04)	0.771157 (10)	0.608890 (15)
64	8.200	1660.89 ( 0.96)	466.20 (0.58)	45.26 (0.07)	27.36 (0.04)	0.782591 (10)	0.625310 (14)
64	8.700	1798.68 ( 0.88)	556.16 (0.59)	48.52 (0.07)	29.65 (0.04)	0.795351 ( 9)	0.644016 (14)
128	4.000	53.92 ( 0.26)	5.19 (0.01)	5.47 (0.21)	1.74 (0.18)	0.543583 (14)	0.347665 (13)
128	4.600	148.57 ( 0.66)	11.21 (0.01)	9.68 (0.13)	3.55 (0.08)	0.603836 ( 9)	0.405005 (10)
128	4.900	254.22 ( 1.32)	17.12 (0.03)	13.39 (0.13)	4.74 (0.07)	0.629018 ( 9)	0.431414 ( 9)
128	5.200	430.36 ( 1.73)	26.62 (0.04)	18.01 (0.10)	6.50 (0.04)	0.651306 ( 6)	0.456032 ( 7)
128	5.500	726.74 ( 2.03)	43.17 (0.07)	24.23 (0.08)	9.34 (0.04)	0.671168 ( 4)	0.478960 ( 5)
128	5.800	1175.09 ( 2.89)	74.24 (0.17)	31.96 (0.08)	13.73 (0.04)	0.688918 ( 4)	0.500251 ( 4)
128	5.930	1412.55 ( 4.41)	94.97 (0.32)	35.66 (0.12)	16.03 (0.07)	0.696030 ( 5)	0.508995 ( 6)
128	6.100	1731.01 ( 4.59)	128.76 (0.43)	40.07 (0.12)	18.94 (0.07)	0.704853 ( 5)	0.520012 ( 6)
128	6.400	2330.01 ( 6.27)	211.82 (0.89)	48.11 (0.16)	24.38 (0.10)	0.719216 ( 7)	0.538353 ( 9)
128	6.800	3080.42 ( 5.92)	359.97 (1.23)	56.98 (0.15)	30.75 (0.10)	0.736312 ( 6)	0.560839 ( 8)
128	7.100	3607.80 ( 5.57)	495.51 (1.45)	63.13 (0.15)	35.15 (0.10)	0.747807 ( 6)	0.576359 ( 8)
128	7.400	4093.51 ( 5.05)	644.66 (1.58)	68.54 (0.15)	39.01 (0.09)	0.758335 ( 5)	0.590861 ( 8)
128	7.800	4686.97 ( 6.87)	861.07 (2.58)	75.05 (0.21)	43.68 (0.14)	0.771073 ( 7)	0.608771 (10)
128	8.200	5227.49 ( 6.30)	1091.37 (2.74)	81.01 (0.22)	47.98 (0.14)	0.782502 ( 7)	0.625181 (10)
128	8.700	5857.80 ( 5.58)	1401.51 (2.83)	88.31 (0.21)	53.18 (0.14)	0.795294 ( 7)	0.643931 (10)
256	5.200	433.09 ( 3.29)	26.39 (0.06)	18.31 (0.45)	6.38 (0.29)	0.651300 ( 6)	0.456024 ( 7)
256	5.800	1291.13 ( 7.12)	66.30 (0.13)	33.48 (0.27)	11.91 (0.13)	0.688885 ( 3)	0.500210 ( 4)
256	6.100	2220.50 (12.62)	109.15 (0.32)	45.26 (0.30)	17.09 (0.13)	0.704805 ( 3)	0.519952 ( 4)
256	6.400	3650.42 (15.65)	188.23 (0.67)	59.60 (0.27)	24.87 (0.14)	0.719168 ( 2)	0.538291 ( 3)
256	6.600	4930.58 (21.44)	279.33 (1.32)	71.09 (0.33)	32.07 (0.19)	0.727985 ( 2)	0.549797 ( 3)
256	6.800	6250.21 (19.41)	399.68 (1.58)	81.14 (0.28)	38.54 (0.16)	0.736265 ( 2)	0.560776 ( 3)
256	7.100	8345.02 (26.99)	655.40 (3.32)	96.18 (0.38)	48.79 (0.23)	0.747763 ( 3)	0.576300 ( 4)
256	7.800	13095.48 (22.82)	1583.24 (5.25)	126.95 (0.35)	70.85 (0.22)	0.771032 ( 3)	0.608712 ( 4)
256	8.200	15497.34 (29.21)	2255.87 (8.48)	141.80 (0.47)	81.41 (0.30)	0.782477 ( 4)	0.625145 ( 5)

Table 3: Static data from our runs for the two-dimensional 8-vector model. Error bar (one standard deviation) is shown in parentheses.

$d = 2$ 3-vector model: dynamic data							
$L$	$\beta$	Sweeps	Discard	$\tau_{int, \mathcal{M}_V^2}$	$\tau_{int, \mathcal{M}_T^2}$	$\tau_{int, \mathcal{E}_V}$	$\tau_{int, \mathcal{E}_T}$
32	1.500	105000	5000	7.16 (0.30)	3.43 (0.10)	2.45 (0.06)	2.00 (0.04)
64	1.450	305000	5000	6.54 (0.15)	1.43 (0.02)	2.12 (0.03)	1.75 (0.02)
64	1.500	405000	5000	8.92 (0.21)	2.04 (0.02)	2.24 (0.03)	1.85 (0.02)
64	1.550	405000	5000	11.42 (0.30)	3.42 (0.05)	2.38 (0.03)	1.94 (0.02)
64	1.600	485000	5000	14.35 (0.38)	5.42 (0.09)	2.38 (0.03)	1.96 (0.02)
64	1.650	305000	5000	14.69 (0.50)	6.27 (0.14)	2.29 (0.03)	1.93 (0.02)
64	1.700	300000	5000	12.96 (0.42)	6.15 (0.14)	1.98 (0.03)	1.74 (0.02)
64	1.725	300000	5000	12.13 (0.38)	5.99 (0.13)	1.94 (0.02)	1.74 (0.02)
64	1.750	300000	5000	10.12 (0.29)	5.46 (0.12)	1.86 (0.02)	1.68 (0.02)
64	1.775	200000	5000	9.20 (0.31)	5.27 (0.13)	1.71 (0.02)	1.57 (0.02)
64	1.800	200000	5000	7.85 (0.24)	5.07 (0.13)	1.66 (0.02)	1.57 (0.02)
64	1.850	200000	5000	6.76 (0.20)	4.55 (0.11)	1.59 (0.02)	1.50 (0.02)
64	1.900	100000	5000	5.52 (0.21)	4.27 (0.14)	1.54 (0.03)	1.47 (0.03)
64	1.950	100000	5000	4.95 (0.18)	4.03 (0.13)	1.48 (0.03)	1.43 (0.03)
128	1.450	200000	5000	4.99 (0.12)	1.14 (0.01)	2.12 (0.03)	1.75 (0.03)
128	1.500	200000	5000	6.75 (0.19)	1.33 (0.02)	2.25 (0.04)	1.86 (0.03)
128	1.550	200000	5000	9.03 (0.30)	1.64 (0.02)	2.25 (0.04)	1.88 (0.03)
128	1.575	400000	5000	11.48 (0.30)	1.97 (0.02)	2.24 (0.03)	1.87 (0.02)
128	1.600	400000	5000	14.29 (0.42)	2.38 (0.03)	2.24 (0.03)	1.88 (0.02)
128	1.650	400000	5000	17.93 (0.59)	3.99 (0.06)	2.21 (0.03)	1.87 (0.02)
128	1.680	400000	5000	21.34 (0.77)	5.99 (0.11)	2.10 (0.02)	1.80 (0.02)
128	1.700	800000	5000	24.08 (0.65)	7.38 (0.11)	2.06 (0.02)	1.78 (0.01)
128	1.720	800000	5000	24.80 (0.68)	8.44 (0.13)	2.04 (0.02)	1.79 (0.01)
128	1.740	800000	5000	24.73 (0.68)	9.14 (0.15)	1.93 (0.01)	1.73 (0.01)
128	1.750	400000	5000	23.06 (0.86)	9.32 (0.22)	1.95 (0.02)	1.74 (0.02)
128	1.770	400000	5000	21.99 (0.80)	9.07 (0.21)	1.90 (0.02)	1.71 (0.02)
128	1.800	300000	5000	19.79 (0.79)	9.11 (0.25)	1.81 (0.02)	1.65 (0.02)
128	1.850	200000	5000	17.86 (0.84)	8.27 (0.26)	1.66 (0.02)	1.58 (0.02)
128	1.900	200000	5000	14.10 (0.59)	7.39 (0.22)	1.60 (0.02)	1.55 (0.02)
128	1.950	200000	5000	9.09 (0.30)	6.16 (0.17)	1.52 (0.02)	1.47 (0.02)
128	2.000	100000	5000	7.71 (0.34)	5.56 (0.21)	1.44 (0.03)	1.41 (0.03)
256	1.450	200000	5000	3.83 (0.08)	1.05 (0.01)	2.06 (0.03)	1.74 (0.03)
256	1.550	200000	5000	6.83 (0.20)	1.36 (0.02)	2.27 (0.04)	1.90 (0.03)
256	1.650	200000	5000	12.87 (0.51)	2.06 (0.03)	2.08 (0.03)	1.79 (0.03)
256	1.700	400000	5000	19.52 (0.67)	2.80 (0.04)	2.06 (0.02)	1.78 (0.02)
256	1.750	400000	5000	26.65 (1.07)	4.74 (0.08)	1.87 (0.02)	1.66 (0.02)
256	1.800	600000	5000	36.89 (1.42)	9.90 (0.20)	1.81 (0.02)	1.66 (0.01)
256	1.850	600000	5000	39.86 (1.60)	13.09 (0.30)	1.71 (0.01)	1.59 (0.01)
256	1.900	400000	5000	34.30 (1.57)	13.57 (0.39)	1.61 (0.02)	1.54 (0.01)
256	2.000	200000	5000	19.26 (0.94)	9.64 (0.33)	1.47 (0.02)	1.43 (0.02)

Table 4: Dynamic data from our runs for the two-dimensional 3-vector model. “Sweeps” is the total number of MGMC iterations performed; “Discard” is the number of iterations discarded prior to beginning the analysis. Error bar (one standard deviation) is shown in parentheses.

$d = 2$ 4-vector model: dynamic data							
$L$	$\beta$	Sweeps	Discard	$\tau_{int, \mathcal{M}_V^2}$	$\tau_{int, \mathcal{M}_T^2}$	$\tau_{int, \mathcal{E}_V}$	$\tau_{int, \mathcal{E}_T}$
32	2.000	105000	5000	7.84 (0.34)	3.88 (0.12)	2.98 (0.08)	2.70 (0.07)
32	2.100	105000	5000	8.91 (0.41)	5.37 (0.19)	3.19 (0.09)	2.88 (0.08)
32	2.200	105000	5000	8.50 (0.38)	5.86 (0.22)	2.86 (0.07)	2.69 (0.07)
64	2.100	205000	5000	11.03 (0.40)	3.23 (0.06)	2.95 (0.06)	2.70 (0.05)
64	2.150	305000	5000	12.92 (0.42)	4.39 (0.08)	2.94 (0.05)	2.72 (0.04)
64	2.200	305000	5000	14.17 (0.48)	5.78 (0.12)	2.95 (0.05)	2.71 (0.04)
64	2.250	305000	5000	15.70 (0.56)	7.20 (0.17)	2.94 (0.05)	2.72 (0.04)
64	2.300	505000	5000	15.90 (0.44)	8.47 (0.17)	2.90 (0.03)	2.72 (0.03)
64	2.350	305000	5000	15.59 (0.55)	8.91 (0.24)	2.86 (0.04)	2.70 (0.04)
64	2.400	525000	5000	15.50 (0.41)	9.48 (0.20)	2.77 (0.03)	2.63 (0.03)
128	2.250	100000	5000	14.33 (0.86)	3.31 (0.10)	2.82 (0.08)	2.68 (0.07)
128	2.350	100000	5000	18.82 (1.30)	5.49 (0.20)	2.74 (0.07)	2.60 (0.07)
128	2.450	200000	5000	24.15 (1.32)	9.82 (0.34)	2.77 (0.05)	2.62 (0.05)
128	2.550	200000	5000	26.08 (1.48)	13.60 (0.56)	2.61 (0.05)	2.50 (0.04)
128	2.650	200000	5000	21.34 (1.09)	12.97 (0.52)	2.53 (0.04)	2.46 (0.04)

Table 5: Dynamic data from our runs for the two-dimensional 4-vector model. “Sweeps” is the total number of MGMC iterations performed; “Discard” is the number of iterations discarded prior to beginning the analysis. Error bar (one standard deviation) is shown in parentheses.

$d = 2$ 8-vector model: dynamic data							
$L$	$\beta$	Sweeps	Discard	$\tau_{int, \mathcal{M}_V^2}$	$\tau_{int, \mathcal{M}_T^2}$	$\tau_{int, \mathcal{E}_V}$	$\tau_{int, \mathcal{E}_T}$
64	4.000	200000	5000	10.60 (0.38)	3.79 (0.08)	6.03 (0.16)	5.89 (0.16)
64	4.600	800000	5000	20.57 (0.51)	9.39 (0.16)	6.33 (0.09)	6.21 (0.08)
64	4.800	1200000	5000	25.99 (0.59)	14.42 (0.25)	6.30 (0.07)	6.21 (0.07)
64	5.000	1200000	5000	27.99 (0.66)	18.92 (0.37)	6.35 (0.07)	6.25 (0.07)
64	5.200	1200000	5000	29.59 (0.72)	22.69 (0.48)	6.24 (0.07)	6.16 (0.07)
64	5.400	1200000	5000	29.62 (0.72)	24.13 (0.53)	6.26 (0.07)	6.19 (0.07)
64	5.800	400000	5000	25.42 (1.00)	22.92 (0.86)	6.12 (0.12)	6.10 (0.12)
64	6.100	400000	5000	22.39 (0.83)	20.78 (0.74)	5.96 (0.11)	5.97 (0.11)
64	6.400	400000	5000	20.49 (0.72)	19.66 (0.68)	5.98 (0.11)	5.98 (0.11)
64	6.600	600000	5000	19.65 (0.55)	18.88 (0.52)	5.86 (0.09)	5.85 (0.09)
64	6.800	600000	5000	19.29 (0.54)	18.54 (0.51)	5.74 (0.09)	5.73 (0.09)
64	7.100	600000	5000	17.69 (0.47)	17.29 (0.46)	5.92 (0.09)	5.91 (0.09)
64	7.400	600000	5000	18.73 (0.51)	18.26 (0.50)	5.72 (0.09)	5.72 (0.09)
64	7.800	400000	5000	15.87 (0.49)	15.65 (0.48)	5.87 (0.11)	5.87 (0.11)
64	8.200	400000	5000	16.55 (0.52)	16.29 (0.51)	5.67 (0.11)	5.68 (0.11)
64	8.700	400000	5000	15.52 (0.48)	15.31 (0.47)	5.66 (0.10)	5.66 (0.10)
128	4.000	200000	5000	8.96 (0.30)	3.15 (0.06)	5.88 (0.16)	5.69 (0.15)
128	4.600	400000	5000	16.71 (0.53)	5.24 (0.09)	6.36 (0.12)	6.23 (0.12)
128	4.900	400000	5000	24.29 (0.93)	7.74 (0.17)	6.23 (0.12)	6.13 (0.12)
128	5.200	800000	5000	33.07 (1.04)	12.81 (0.25)	6.14 (0.08)	6.07 (0.08)
128	5.500	1600000	5000	40.85 (1.01)	22.58 (0.42)	6.18 (0.06)	6.12 (0.06)
128	5.800	1600000	5000	47.01 (1.25)	33.91 (0.77)	6.13 (0.06)	6.10 (0.06)
128	5.930	800000	5000	46.46 (1.74)	35.31 (1.15)	6.23 (0.09)	6.20 (0.08)
128	6.100	800000	5000	44.74 (1.64)	36.74 (1.22)	5.89 (0.08)	5.87 (0.08)
128	6.400	400000	5000	38.53 (1.86)	33.70 (1.53)	6.06 (0.12)	6.03 (0.12)
128	6.800	400000	5000	33.82 (1.53)	31.20 (1.36)	5.97 (0.11)	5.96 (0.11)
128	7.100	400000	5000	31.04 (1.35)	29.30 (1.24)	5.88 (0.11)	5.87 (0.11)
128	7.400	400000	5000	27.46 (1.12)	26.54 (1.07)	5.77 (0.11)	5.78 (0.11)
128	7.800	200000	5000	26.19 (1.49)	25.61 (1.44)	5.70 (0.15)	5.69 (0.15)
128	8.200	200000	5000	23.24 (1.24)	22.75 (1.20)	5.79 (0.15)	5.79 (0.15)
128	8.700	200000	5000	20.75 (1.05)	20.43 (1.02)	5.82 (0.16)	5.82 (0.16)
256	5.200	200000	5000	23.83 (1.29)	7.76 (0.24)	6.19 (0.17)	6.15 (0.17)
256	5.800	600000	5000	45.04 (1.92)	16.72 (0.43)	6.16 (0.10)	6.11 (0.10)
256	6.100	600000	5000	58.70 (2.86)	29.10 (1.00)	6.01 (0.09)	5.98 (0.09)
256	6.400	800000	5000	63.40 (2.77)	43.93 (1.60)	6.08 (0.08)	6.07 (0.08)
256	6.600	600000	5000	65.95 (3.40)	51.56 (2.35)	5.74 (0.09)	5.74 (0.09)
256	6.800	800000	5000	64.12 (2.82)	51.32 (2.02)	5.86 (0.08)	5.87 (0.08)
256	7.100	400000	5000	56.07 (3.27)	49.35 (2.70)	5.91 (0.11)	5.91 (0.11)
256	7.800	400000	5000	40.33 (2.00)	38.33 (1.85)	5.76 (0.11)	5.75 (0.11)
256	8.200	200000	5000	35.39 (2.34)	34.03 (2.20)	5.89 (0.16)	5.92 (0.16)

Table 6: Dynamic data from our runs for the two-dimensional 8-vector model. “Sweeps” is the total number of MGMC iterations performed; “Discard” is the number of iterations discarded prior to beginning the analysis. Error bar (one standard deviation) is shown in parentheses.

CPU timings (Cray C-90, ms/iteration)				
$L$	$XY$ -embedding			direct
	$N = 3$	$N = 4$	$N = 8$	$N = 4$
32	14/15	14.5/17	16/24	19/20
64	38/42	39/45	42/61	50/52
128	113/123	116/135	128/178	136/140
256	380/405	388/432	426/580	400/410

Table 7: CPU times in milliseconds per iteration for MGMC algorithm for the two dimensional  $N$ -vector models with  $N = 3, 4, 8$ , on a Cray C-90. In all cases we have taken  $\gamma = 2$  (W-cycle) and  $m_1 = m_2 = 1$  (one heat-bath pre-sweep and one heat-bath post-sweep). The first timing is for Monte Carlo iterations alone; the second timing includes measurement of observables (see text).



$\xi_V$ FSS curve, $d = 2$ $O(8)$ model										
$L_{min}$	$\xi_{min}$	DF	$n = 3$	$n = 4$	$n = 5$	$n = 6$	$n = 7$	$n = 8$	$n = 9$	$n = 10$
( 64, 64, 64)	10	$18 - n$	123.06 0.0%	26.08 2.5%	25.99 1.7%	24.67 1.6%	20.73 3.6%	20.72 2.3%	18.37 3.1%	18.33 1.9%
( 64,128, 64)	10	$14 - n$	56.82 0.0%	8.82 55.0%	7.89 54.5%	7.82 45.1%	7.51 37.8%	7.28 29.6%	4.70 45.4%	4.70 32.0%
( 64,128,128)	10	$10 - n$	10.95 14.1%	5.92 43.2%	5.65 34.2%	4.87 30.1%	3.59 30.9%	3.58 16.7%	0.00 97.7%	0.00 —
(128,128, 64)	10	$12 - n$	45.04 0.0%	8.66 37.2%	6.76 45.4%	6.55 36.5%	5.93 31.3%	5.84 21.1%	1.73 63.1%	1.59 45.1%
(128,128,128)	10	$8 - n$	8.01 15.6%	5.62 23.0%	4.33 22.8%	3.18 20.4%	0.41 52.0%	0.00 —	0.00 —	0.00 —

Table 8:  $\chi^2$  and confidence level for the fit of  $\xi_V(\beta, 2L)/\xi_V(\beta, L)$  versus  $\xi_V(\beta, L)/L$ . The first (resp. second, third)  $L_{min}$  value applies for  $\xi_V(\beta, L)/L < 0.4$  (resp. between 0.4 and 0.6,  $> 0.6$ ). DF = number of degrees of freedom;  $n$  = order of polynomial (4.32).

$\chi_V$ FSS curve, $d = 2$ $O(8)$ model										
$L_{min}$	$\xi_{min}$	DF	$n = 3$	$n = 4$	$n = 5$	$n = 6$	$n = 7$	$n = 8$	$n = 9$	$n = 10$
( 64, 64, 64)	10	$18 - n$	576.45 0.0%	57.82 0.0%	56.79 0.0%	44.84 0.0%	37.59 0.0%	37.58 0.0%	32.73 0.0%	32.57 0.0%
( 64,128, 64)	10	$14 - n$	311.04 0.0%	21.20 2.0%	13.29 15.0%	11.09 19.7%	10.97 14.0%	10.54 10.4%	6.83 23.4%	6.77 14.9%
( 64,128,128)	10	$10 - n$	22.43 0.2%	11.84 6.6%	8.54 12.9%	6.89 14.2%	3.93 26.9%	3.81 14.9%	0.84 35.9%	0.00 —
(128,128, 64)	10	$12 - n$	252.40 0.0%	18.95 1.5%	13.24 6.6%	10.01 12.4%	9.82 8.0%	9.68 4.6%	3.86 27.7%	3.19 20.3%
(128,128,128)	10	$8 - n$	19.43 0.2%	11.72 2.0%	7.56 5.6%	5.94 5.1%	0.36 54.8%	0.00 —	0.00 —	0.00 —

Table 9:  $\chi^2$  and confidence level for the fit of  $\chi_V(\beta, 2L)/\chi_V(\beta, L)$  versus  $\xi_V(\beta, L)/L$ . The first (resp. second, third)  $L_{min}$  value applies for  $\xi_V(\beta, L)/L < 0.4$  (resp. between 0.4 and 0.6,  $> 0.6$ ). DF = number of degrees of freedom;  $n$  = order of polynomial (4.32).

$\xi_T$ FSS curve, $d = 2$ $O(8)$ model										
$L_{min}$	$\xi_{min}$	DF	$n = 3$	$n = 4$	$n = 5$	$n = 6$	$n = 7$	$n = 8$	$n = 9$	$n = 10$
( 64, 64, 64)	10	$18 - n$	909.07 0.0%	96.54 0.0%	35.33 0.1%	30.35 0.2%	30.20 0.1%	29.92 0.1%	25.12 0.3%	23.80 0.2%
( 64,128, 64)	10	$14 - n$	618.69 0.0%	57.94 0.0%	23.47 0.5%	10.31 24.4%	9.56 21.5%	9.55 14.5%	4.97 42.0%	4.03 40.3%
( 64,128,128)	10	$10 - n$	173.90 0.0%	22.91 0.1%	7.31 19.9%	7.26 12.3%	3.57 31.2%	1.68 43.2%	0.06 80.5%	0.00 —
(128,128, 64)	10	$12 - n$	401.75 0.0%	27.17 0.1%	15.38 3.1%	9.45 15.0%	8.70 12.2%	8.64 7.1%	2.36 50.1%	1.53 46.6%
(128,128,128)	10	$8 - n$	86.43 0.0%	13.64 0.9%	6.75 8.0%	6.68 3.5%	0.01 91.8%	0.00 —	0.00 —	0.00 —

Table 10:  $\chi^2$  and confidence level for the fit of  $\xi_T(\beta, 2L)/\xi_T(\beta, L)$  versus  $\xi_V(\beta, L)/L$ . The first (resp. second, third)  $L_{min}$  value applies for  $\xi_V(\beta, L)/L < 0.4$  (resp. between 0.4 and 0.6,  $> 0.6$ ). DF = number of degrees of freedom;  $n$  = order of polynomial (4.32).

$\chi_T$ FSS curve, $d = 2$ $O(8)$ model										
$L_{min}$	$\xi_{min}$	DF	$n = 3$	$n = 4$	$n = 5$	$n = 6$	$n = 7$	$n = 8$	$n = 9$	$n = 10$
( 64, 64, 64)	10	$18 - n$	97.29 0.0%	83.32 0.0%	38.71 0.0%	38.67 0.0%	38.67 0.0%	36.42 0.0%	31.28 0.0%	30.90 0.0%
( 64,128, 64)	10	$14 - n$	48.65 0.0%	47.81 0.0%	16.19 6.3%	9.71 28.6%	9.22 23.7%	9.21 16.2%	3.66 60.0%	3.60 46.3%
( 64,128,128)	10	$10 - n$	10.21 17.7%	6.04 41.8%	5.90 31.6%	5.84 21.1%	1.51 67.9%	1.12 57.1%	0.81 36.7%	0.00 —
(128,128, 64)	10	$12 - n$	46.85 0.0%	43.03 0.0%	15.19 3.4%	9.37 15.4%	8.60 12.6%	8.58 7.2%	2.59 45.9%	2.45 29.3%
(128,128,128)	10	$8 - n$	8.69 12.2%	5.81 21.3%	5.67 12.9%	5.53 6.3%	0.18 66.9%	0.00 —	0.00 —	0.00 —

Table 11:  $\chi^2$  and confidence level for the fit of  $\chi_T(\beta, 2L)/\chi_T(\beta, L)$  versus  $\xi_V(\beta, L)/L$ . The first (resp. second, third)  $L_{min}$  value applies for  $\xi_V(\beta, L)/L < 0.4$  (resp. between 0.4 and 0.6,  $> 0.6$ ). DF = number of degrees of freedom;  $n$  = order of polynomial (4.32).

$d = 2$ 8-vector model					
$L_{min}$	$\beta$	$\chi_V$	$\xi_V^{(2nd)}$	$\chi_T$	$\xi_T^{(2nd)}$
( 64, 128, 64 )	4.80	212.99 ( 0.74)	12.13 ( 0.05)	14.86 ( 0.03)	4.37 (0.02)
( 64, 64, 64 )	4.80	212.98 ( 0.73)	12.13 ( 0.05)	14.88 ( 0.03)	4.37 (0.02)
( 64, 128, 64 )	4.90	254.30 ( 1.31)	13.39 ( 0.13)	17.11 ( 0.03)	4.74 (0.07)
( 64, 64, 64 )	4.90	254.30 ( 1.33)	13.39 ( 0.13)	17.11 ( 0.03)	4.74 (0.07)
( 64, 128, 64 )	5.00	301.04 ( 1.34)	14.68 ( 0.08)	19.73 ( 0.06)	5.28 (0.03)
( 64, 64, 64 )	5.00	300.89 ( 1.30)	14.68 ( 0.08)	19.76 ( 0.06)	5.29 (0.03)
( 64, 128, 64 )	5.20	432.63 ( 1.41)	18.08 ( 0.09)	26.43 ( 0.03)	6.44 (0.04)
( 64, 64, 64 )	5.20	432.30 ( 1.42)	18.07 ( 0.09)	26.44 ( 0.03)	6.44 (0.04)
( 64, 128, 64 )	5.40	621.49 ( 2.90)	22.16 ( 0.13)	35.73 ( 0.12)	7.94 (0.05)
( 64, 64, 64 )	5.40	620.71 ( 2.93)	22.12 ( 0.13)	35.67 ( 0.12)	7.93 (0.05)
( 64, 128, 64 )	5.50	743.24 ( 2.67)	24.47 ( 0.11)	41.61 ( 0.09)	8.85 (0.04)
( 64, 64, 64 )	5.50	743.19 ( 2.62)	24.47 ( 0.10)	41.66 ( 0.09)	8.86 (0.04)
( 64, 128, 64 )	5.80	1290.93 ( 4.98)	33.36 ( 0.17)	66.11 ( 0.12)	11.94 (0.07)
( 64, 64, 64 )	5.80	1290.50 ( 4.95)	33.37 ( 0.17)	66.16 ( 0.12)	11.96 (0.07)
( 64, 128, 64 )	5.93	1650.44 ( 9.02)	38.34 ( 0.26)	81.27 ( 0.34)	13.69 (0.10)
( 64, 64, 64 )	5.93	1647.92 ( 8.94)	38.29 ( 0.26)	81.23 ( 0.34)	13.67 (0.10)
( 64, 128, 64 )	6.10	2245.25 ( 9.97)	45.36 ( 0.24)	106.26 ( 0.28)	16.31 (0.10)
( 64, 64, 64 )	6.10	2236.29 ( 9.60)	45.15 ( 0.23)	105.93 ( 0.26)	16.21 (0.09)
( 64, 128, 64 )	6.40	3917.72 ( 20.15)	61.67 ( 0.38)	172.30 ( 0.60)	22.27 (0.14)
( 64, 64, 64 )	6.40	3917.57 ( 19.28)	61.64 ( 0.36)	172.53 ( 0.56)	22.26 (0.13)
( 64, 128, 64 )	6.60	5748.46 ( 37.56)	76.37 ( 0.61)	239.31 ( 1.30)	27.38 (0.23)
( 64, 64, 64 )	6.60	5711.84 ( 34.80)	75.75 ( 0.52)	237.66 ( 1.02)	27.06 (0.19)
( 64, 128, 64 )	6.80	8181.57 ( 48.89)	92.09 ( 0.62)	327.82 ( 1.33)	33.14 (0.21)
( 64, 64, 64 )	6.80	8203.61 ( 47.71)	92.35 ( 0.58)	328.73 ( 1.22)	33.26 (0.20)
( 64, 128, 64 )	7.10	14186.62 ( 129.08)	124.39 ( 1.10)	535.73 ( 2.94)	44.82 (0.34)
( 64, 64, 64 )	7.10	14442.55 ( 115.01)	126.32 ( 0.95)	542.57 ( 2.52)	45.45 (0.30)
( 64, 128, 64 )	7.40	25107.76 ( 545.38)	169.58 ( 2.78)	884.22 ( 10.56)	60.68 (0.78)
( 64, 64, 64 )	7.40	25478.71 ( 327.09)	171.33 ( 1.65)	894.13 ( 7.01)	61.55 (0.53)
( 64, 128, 64 )	7.80	53454.83 ( 949.80)	255.26 ( 3.62)	1742.55 ( 16.91)	91.72 (0.98)
( 64, 64, 64 )	7.80	54631.29 ( 676.83)	259.06 ( 2.50)	1769.85 ( 12.66)	93.29 (0.75)
( 64, 128, 64 )	8.20	114828.43 ( 2825.84)	385.50 ( 6.83)	3459.45 ( 49.17)	138.89 (1.97)
( 64, 64, 64 )	8.20	117744.40 ( 2150.12)	391.93 ( 4.97)	3516.35 ( 42.02)	141.65 (1.54)
( 64, 128, 64 )	8.70	302299.08 (10890.33)	648.17 (15.33)	8300.80 (208.42)	231.74 (4.57)
( 64, 64, 64 )	8.70	306388.42 (10315.52)	654.85 (13.69)	8384.16 (202.32)	234.93 (4.31)

Table 12: Estimated values at  $\infty$  for the four basic observables as functions of  $\beta$ , from two different extrapolations. Error bar is one standard deviation (statistical errors only). All extrapolations use  $s = 2$ ,  $\xi_{min} = 10$ ,  $n = 6$ . Our preferred fit is  $L_{min} = (64, 64, 64)$ .

$d = 2$ $O(4)$ model, comparison with direct method						
		XY embed		direct MGMC		
$L$	$\beta$	RRL	$\tau_{int, \mathcal{M}_V^2}$	RRL	$\tau_{int, \mathcal{M}_V^2}$	RATIO
32	2.00	12762	7.84 (0.34)	35984	2.64 (0.07)	2.97 (0.15)
32	2.10	11222	8.91 (0.41)	34671	2.74 (0.07)	3.25 (0.17)
32	2.20	11767	8.50 (0.38)	35714	2.66 (0.07)	3.19 (0.17)
64	2.10	18129	11.03 (0.40)	56686	3.44 (0.07)	3.21 (0.13)
64	2.15	23212	12.92 (0.42)	50257	3.88 (0.09)	3.33 (0.13)
64	2.20	21166	14.17 (0.48)	44419	4.39 (0.10)	3.23 (0.13)
64	2.30	31446	15.90 (0.44)	39000	5.00 (0.13)	3.18 (0.12)
64	2.35	19244	15.59 (0.55)	38844	5.02 (0.13)	3.11 (0.14)
64	2.40	33555	15.50 (0.41)	40372	4.83 (0.12)	3.21 (0.12)
128	2.25	6631	14.33 (0.86)	44930	4.34 (0.10)	3.30 (0.21)
128	2.35	5046	18.82 (1.30)	32392	6.02 (0.17)	3.13 (0.23)
128	2.45	8074	24.15 (1.32)	25624	7.61 (0.24)	3.17 (0.20)
128	2.55	7476	26.08 (1.48)	25064	7.78 (0.24)	3.35 (0.22)
128	2.65	9136	21.34 (1.09)	27045	7.21 (0.22)	2.96 (0.18)

Table 13: Comparison of autocorrelation times  $\tau_{int, \mathcal{M}_V^2}$  for the 4-vector model, using XY-embedding MGMC (Table 5 above) versus direct MGMC [8]. RRL = Relative Run Length  $\equiv$  run length divided by  $\tau_{int, \mathcal{M}_V^2}$ . RATIO =  $\tau_{int, \mathcal{M}_V^2}(XY \text{ embedding})/\tau_{int, \mathcal{M}_V^2}(\text{direct})$ .

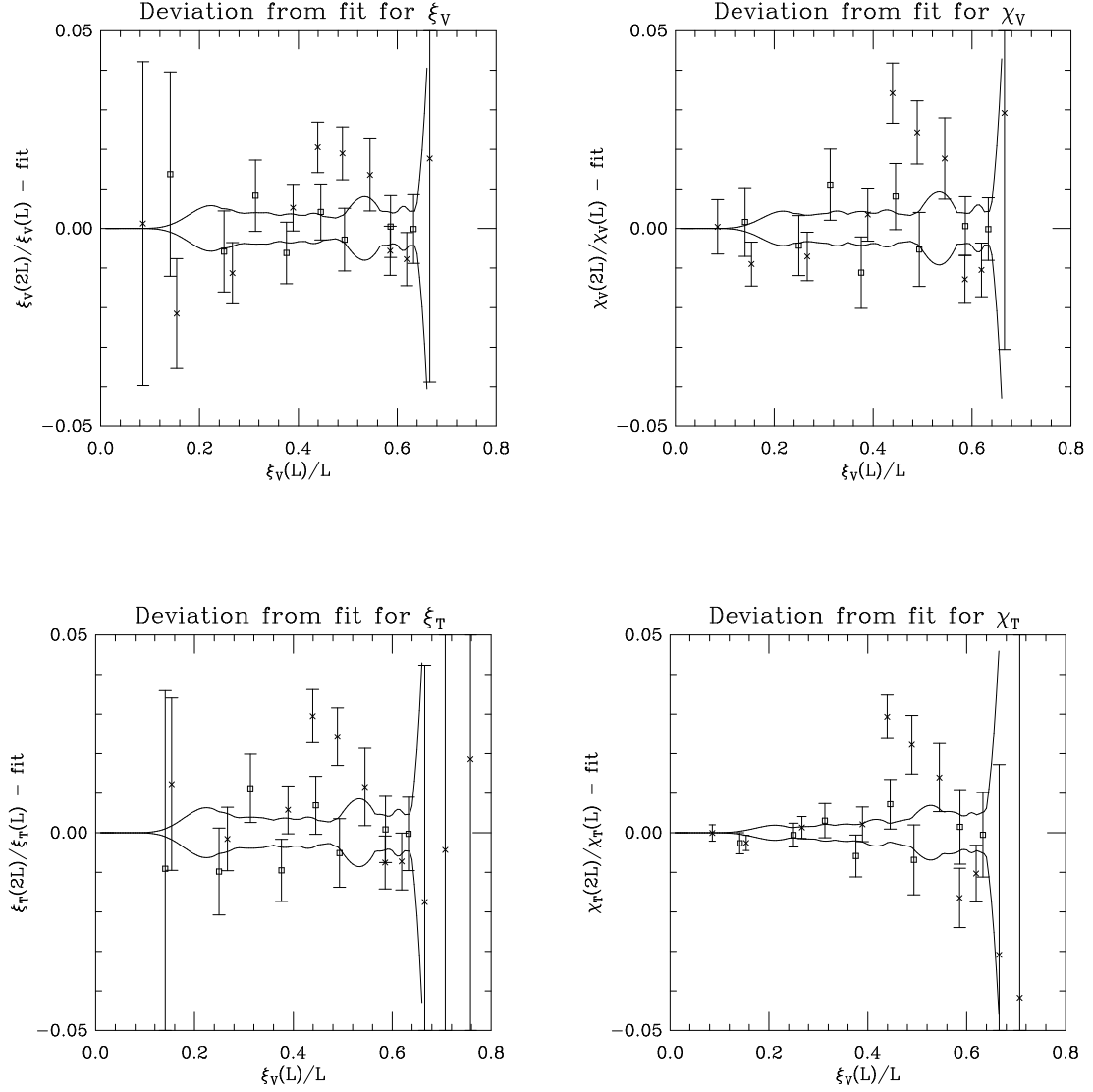


Figure 1: Deviation of points from fit to extrapolation curve  $F_{\#}$  with  $s = 2$ ,  $\xi_{min} = 10$ ,  $n = 6$  and  $L_{min} = (128, 128, 128)$ . Symbols indicate  $L = 64$  ( $\times$ ) and  $L = 128$  ( $\square$ ). Error bars are one standard deviation. Curves near zero indicate statistical error bars ( $\pm$  one standard deviation) on the function  $F_{\#}$ . Observables are (a)  $\xi_V$ , (b)  $\chi_V$ , (c)  $\xi_T$ , (d)  $\chi_T$ .

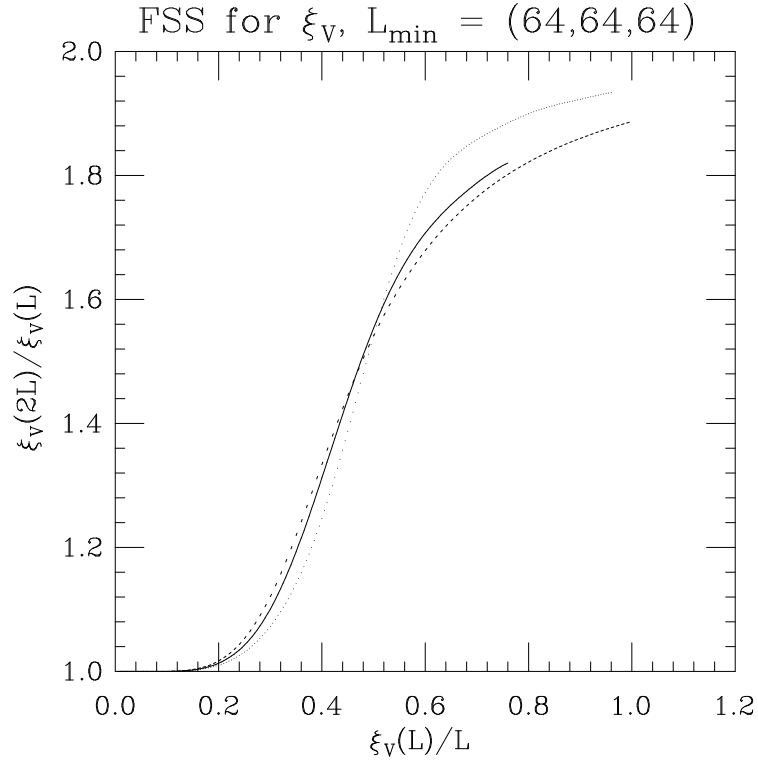
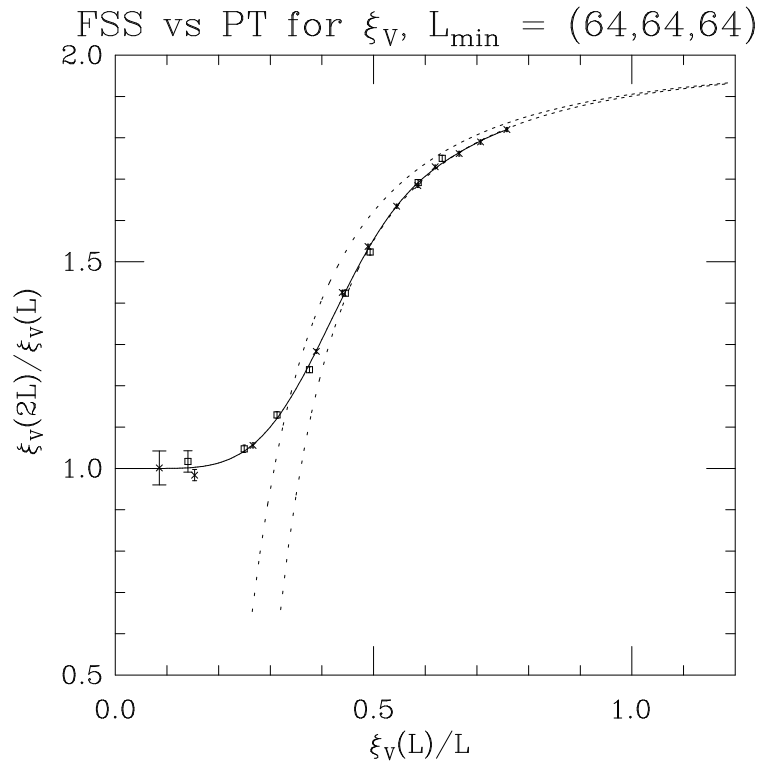


Figure 2:  $\xi_V^{(2nd)}(\beta, 2L)/\xi_V^{(2nd)}(\beta, L)$  versus  $\xi_V^{(2nd)}(\beta, L)/L$ . Symbols indicate  $L = 64$  ( $\times$ ) and  $L = 128$  ( $\square$ ). Error bars are one standard deviation. Solid curve is a sixth-order fit, with  $\xi_{\min} = 10$  and  $L_{\min} = (64, 64, 64)$ . (a) Dashed curves are the perturbative predictions through orders  $1/x^2$  (lower dashed curve) and  $1/x^4$  (upper dashed curve). (b) Dashed line is the exact FSS curve for  $N = \infty$ , and dotted line is the empirical FSS curve [63, 50] for  $N = 3$ .

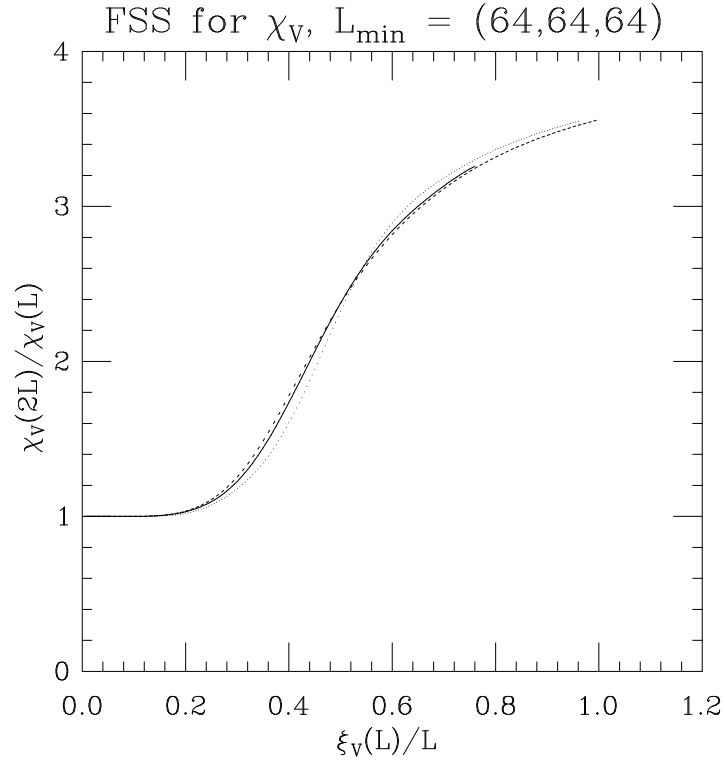
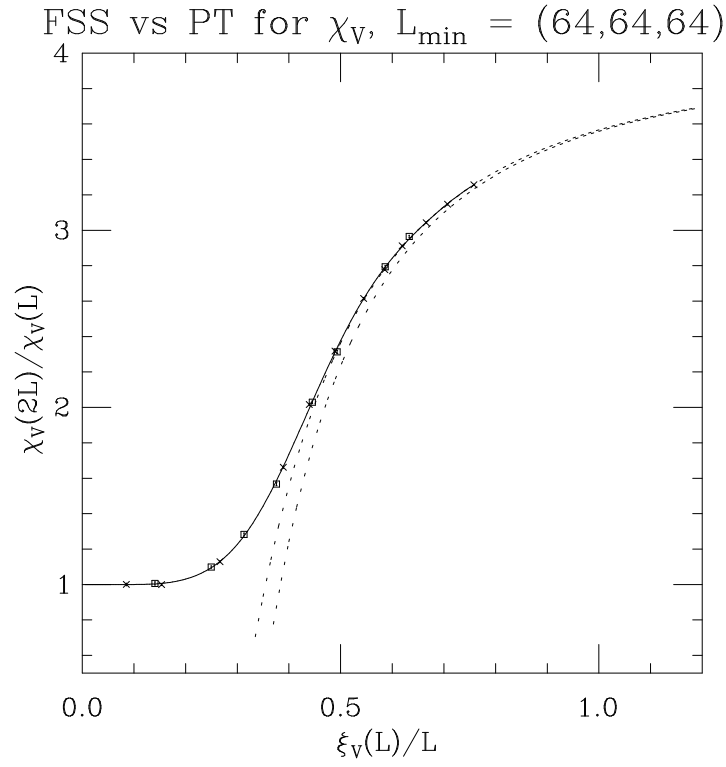


Figure 3:  $\chi_V(\beta, 2L)/\chi_V(\beta, L)$  versus  $\xi_V^{(2nd)}(\beta, L)/L$ . Symbols indicate  $L = 64$  ( $\times$ ) and  $L = 128$  ( $\square$ ). Error bars are one standard deviation. Solid curve is a sixth-order fit, with  $\xi_{\min} = 10$  and  $L_{\min} = (64, 64, 64)$ . (a) Dashed curves are the perturbative predictions through orders  $1/x^2$  (lower dashed curve) and  $1/x^4$  (upper dashed curve). (b) Dashed line is the exact FSS curve for  $N = \infty$ , and dotted line is the empirical FSS curve [63, 50] for  $N = 3$ .

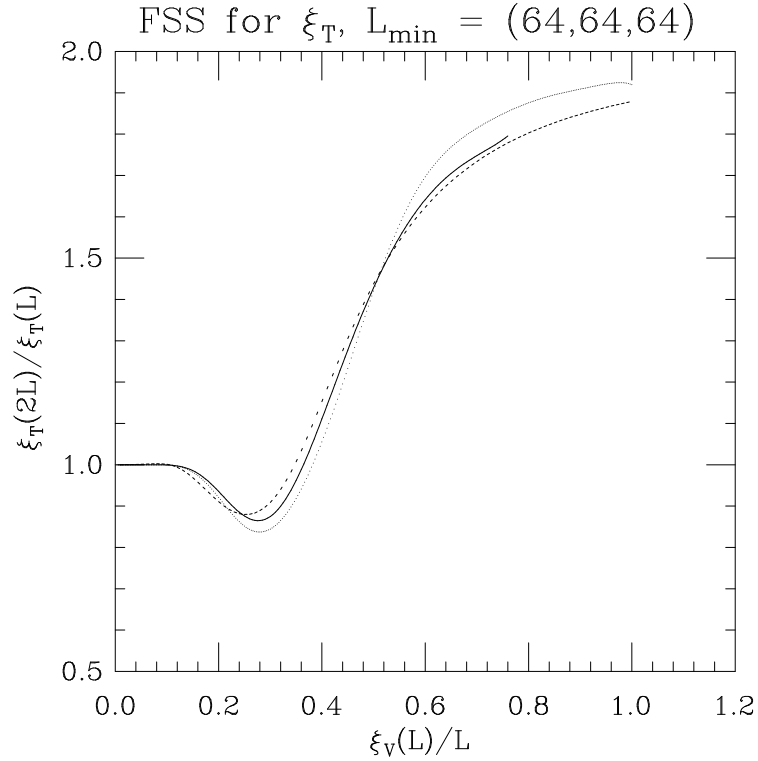
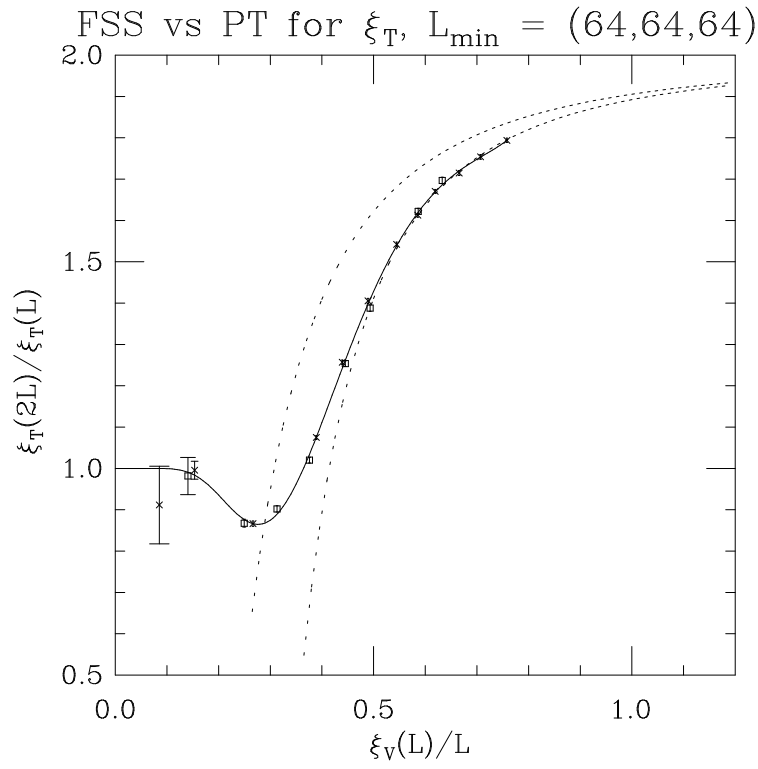


Figure 4:  $\xi_T^{(2nd)}(\beta, 2L)/\xi_T^{(2nd)}(\beta, L)$  versus  $\xi_V^{(2nd)}(\beta, L)/L$ . Symbols indicate  $L = 64$  ( $\times$ ) and  $L = 128$  ( $\square$ ). Error bars are one standard deviation. Solid curve is a sixth-order fit, with  $\xi_{\min} = 10$  and  $L_{\min} = (64, 64, 64)$ . (a) Dashed curves are the perturbative predictions through orders  $1/x^2$  (lower dashed curve) and  $1/x^4$  (upper dashed curve). (b) Dashed line is the exact FSS curve for  $N = \infty$ , and dotted line is the empirical FSS curve [63, 50] for  $N = 3$ .



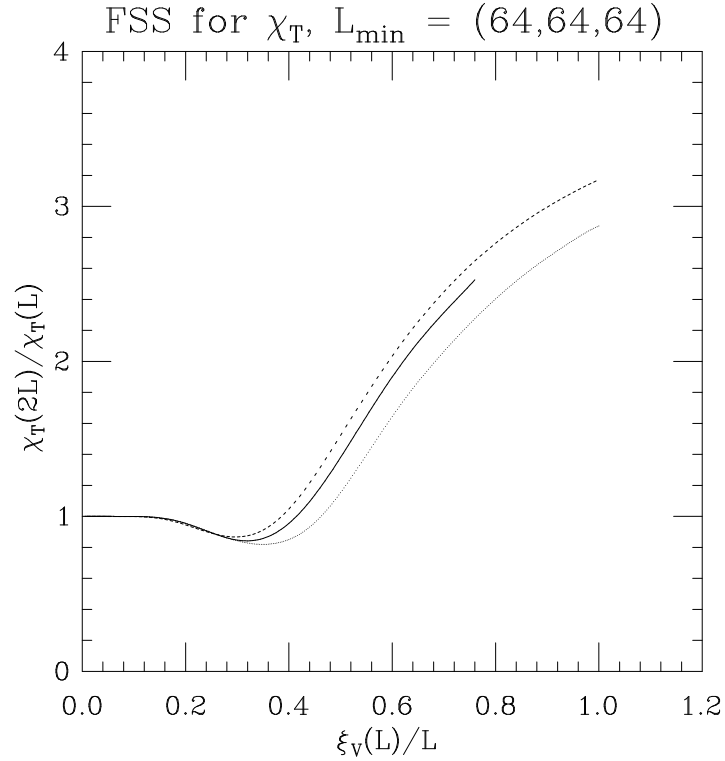
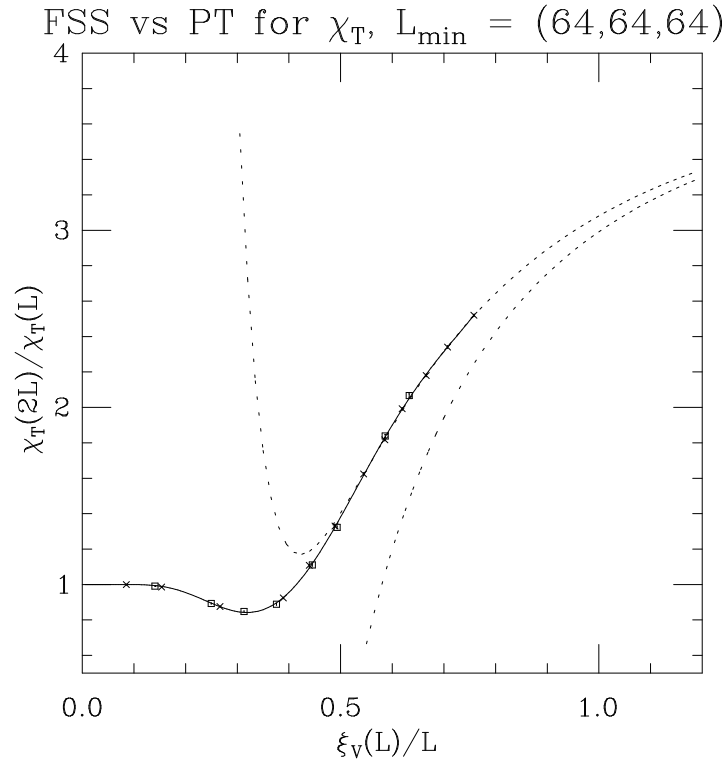


Figure 5:  $\chi_T(\beta, 2L)/\chi_T(\beta, L)$  versus  $\xi_V^{(2nd)}(\beta, L)/L$ . Symbols indicate  $L = 64$  ( $\times$ ) and  $L = 128$  ( $\square$ ). Error bars are one standard deviation. Solid curve is a sixth-order fit, with  $\xi_{\min} = 10$  and  $L_{\min} = (64, 64, 64)$ . (a) Dashed curves are the perturbative predictions through orders  $1/x^2$  (lower dashed curve) and  $1/x^4$  (upper dashed curve). (b) Dashed line is the exact FSS curve for  $N = \infty$ , and dotted line is the empirical FSS curve [63, 50] for  $N = 3$ .

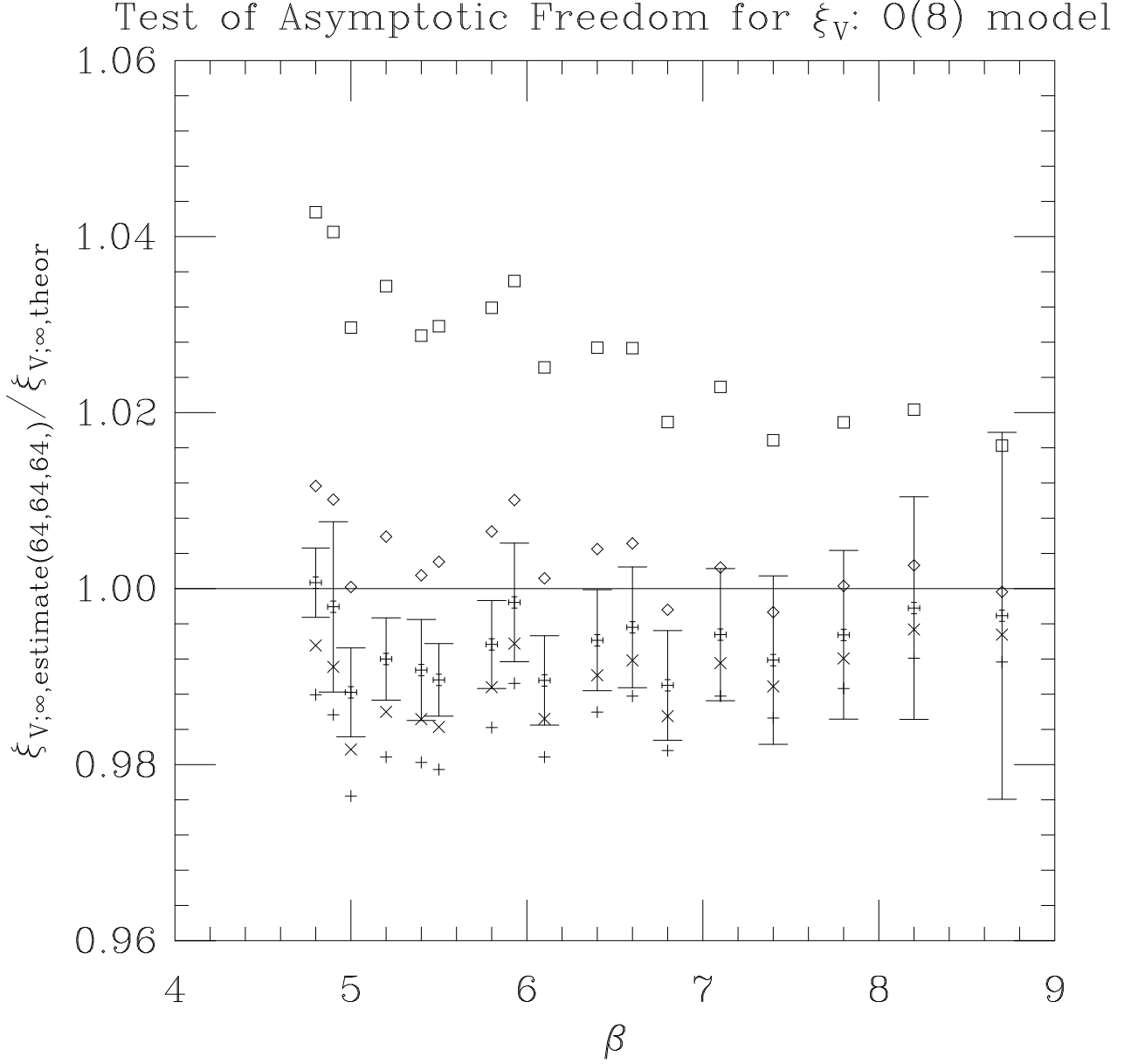


Figure 6:  $\xi_{V;\infty,estimate(64,64,64)}^{(2nd)}/\xi_{V;\infty,theor}^{(exp)}$  versus  $\beta$ . Error bars are one standard deviation (statistical error only). There are five versions of  $\xi_{V;\infty,theor}^{(exp)}$ : standard perturbation theory in  $1/\beta$  gives points + (2-loop),  $\times$  (3-loop) and  $=$  (4-loop); “improved” perturbation theory in  $1 - E$  gives points  $\square$  (2-loop) and  $\diamond$  (3-loop). The horizontal straight line indicates the predicted limiting value 0.9996 from the  $1/N$  expansion (4.18). For clarity, error bars are shown for the 4-loop prediction only.

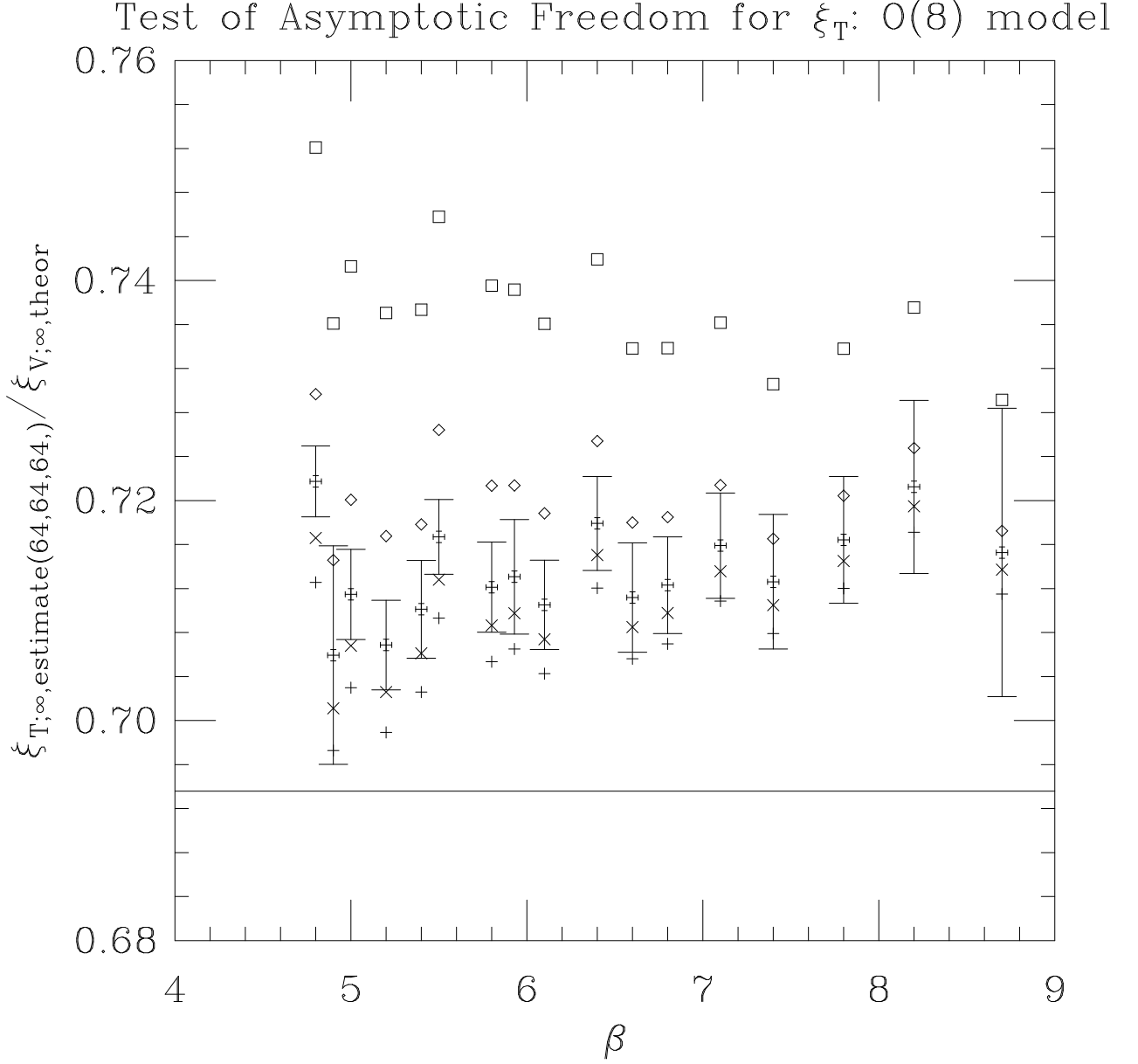


Figure 7:  $\xi_{T;\infty,estimate(64,64,64)}^{(2nd)}/\xi_{V;\infty,theor}^{(exp)}$  versus  $\beta$ . Error bars are one standard deviation (statistical error only). There are five versions of  $\xi_{V;\infty,theor}^{(exp)}$  standard perturbation theory in  $1/\beta$  gives points + (2-loop),  $\times$  (3-loop) and  $\equiv$  (4-loop); “improved” perturbation theory in  $1 - E$  gives points  $\square$  (2-loop) and  $\diamond$  (3-loop). The horizontal straight line indicates the predicted limiting value 0.6937 from the  $1/N$  expansion (4.19). For clarity, error bars are shown for the 4-loop prediction only.

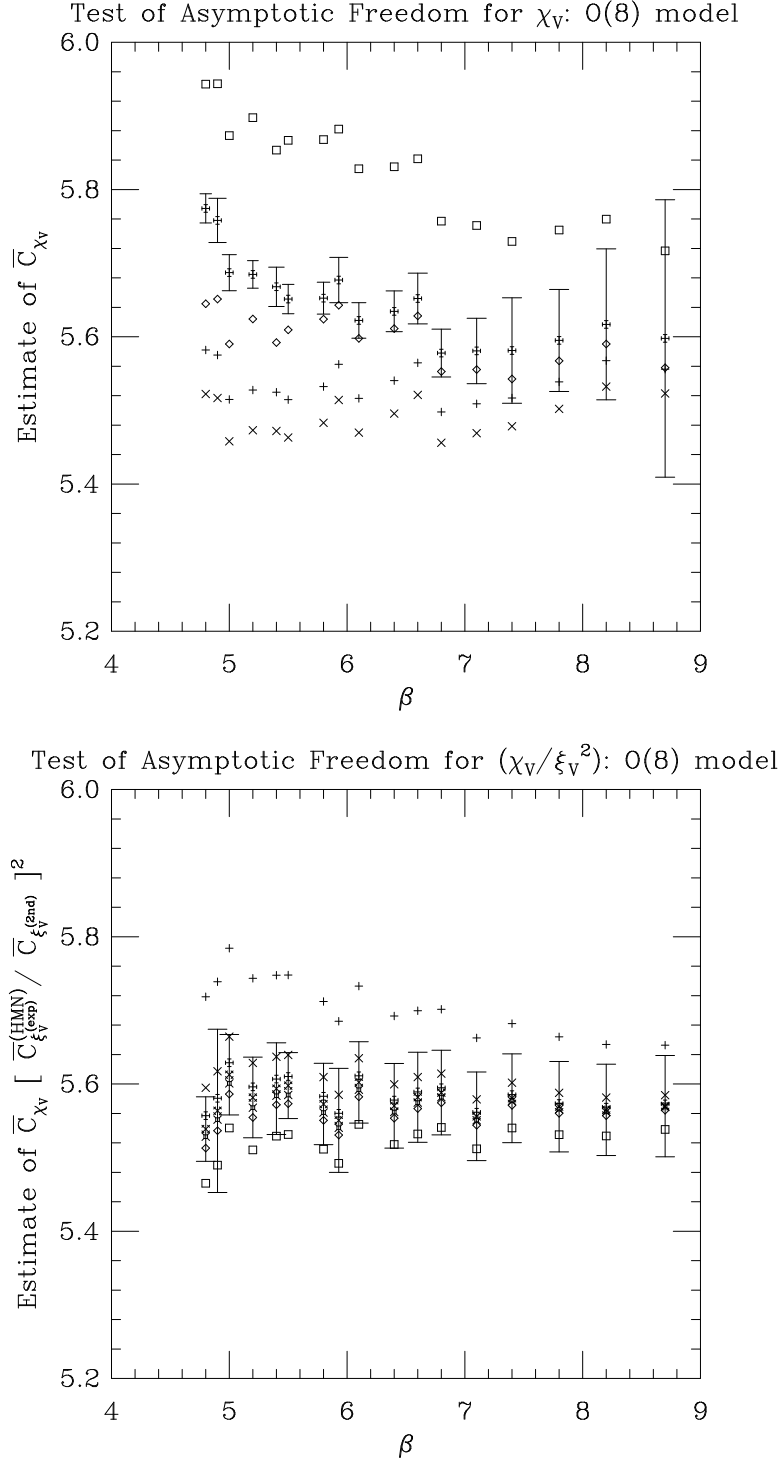


Figure 8: (a) Estimate of  $\tilde{C}_{\chi_V}$  versus  $\beta$ . Error bars are one standard deviation (statistical error only). There are five versions of the theoretical prediction: standard perturbation theory in  $1/\beta$  gives points  $+$  (2-loop),  $\times$  (3-loop) and  $=$  (4-loop); “improved” perturbation theory in  $1 - E$  gives points  $\square$  (2-loop) and  $\diamond$  (3-loop). (b) Estimate of  $\tilde{C}_{\chi_V} [\tilde{C}_{\xi_V^{(exp)}}^{(HMN)} / \tilde{C}_{\xi_V^{(2nd)}}]^2$  versus  $\beta$ . For this theoretical prediction we have an additional version of standard perturbation theory, points  $\times$  (5-loop) and “improved” points  $\square$  (4-loop). For clarity, error bars are shown for the 5-loop prediction only.

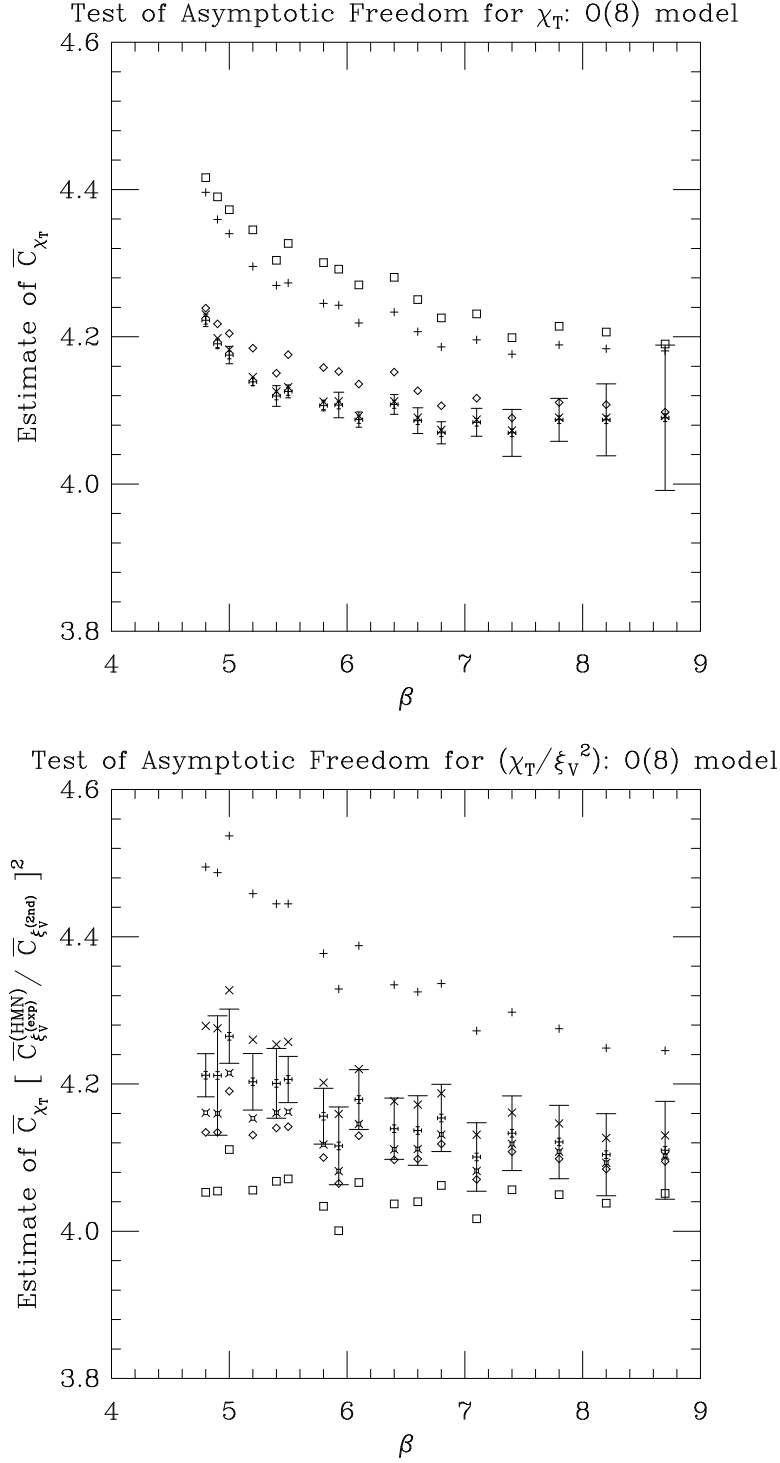


Figure 9: (a) Estimate of  $\tilde{C}_{\chi_T}$  versus  $\beta$ . Error bars are one standard deviation (statistical error only). There are five versions of the theoretical prediction: standard perturbation theory in  $1/\beta$  gives points  $+$  (2-loop),  $\times$  (3-loop) and  $=$  (4-loop); “improved” perturbation theory in  $1 - E$  gives points  $\square$  (2-loop) and  $\diamond$  (3-loop). (b) Estimate of  $\tilde{C}_{\chi_T} [\tilde{C}_{\xi_V^{(exp)}}^{(HMN)} / \tilde{C}_{\xi_V^{(2nd)}}]^2$  versus  $\beta$ . For this theoretical prediction we have an additional version of “improved” perturbation theory, points  $\square \diagdown$  (4-loop). For clarity, error bars are shown for the 4-loop prediction only.

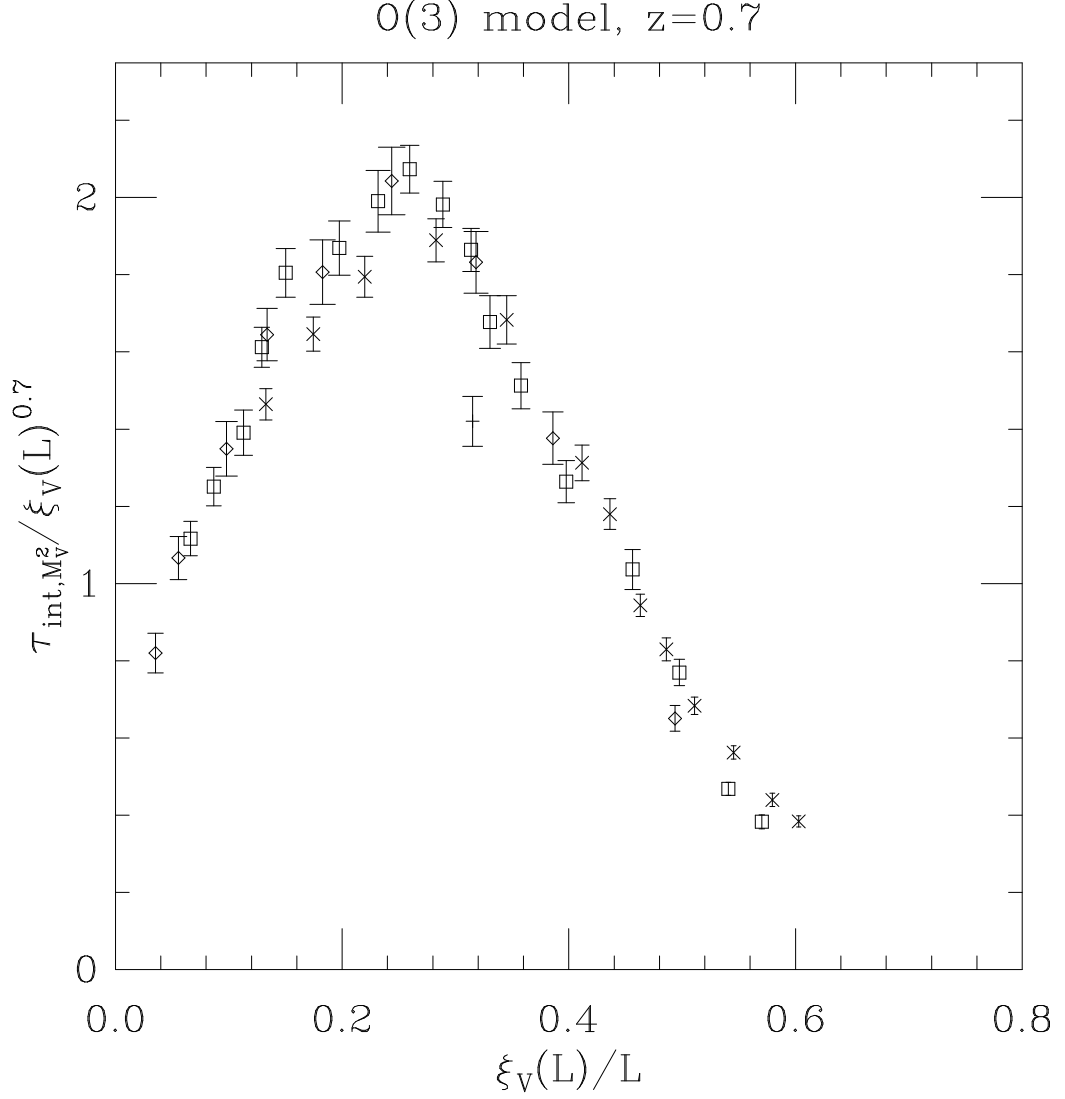


Figure 10: Dynamic finite-size-scaling plot of  $\tau_{int, \mathcal{M}_V^2} [\xi_V^{(2nd)}]^{-z_{int, \mathcal{M}_V^2}}$  versus  $\xi_V^{(2nd)}(\beta, L)/L$  for the two-dimensional 3-vector model. Lattice sizes are  $L = 32$  (+),  $64$  ( $\times$ ),  $128$  ( $\square$ ) and  $256$  ( $\diamond$ ). Here  $z_{int, \mathcal{M}_V^2} = 0.7$ .

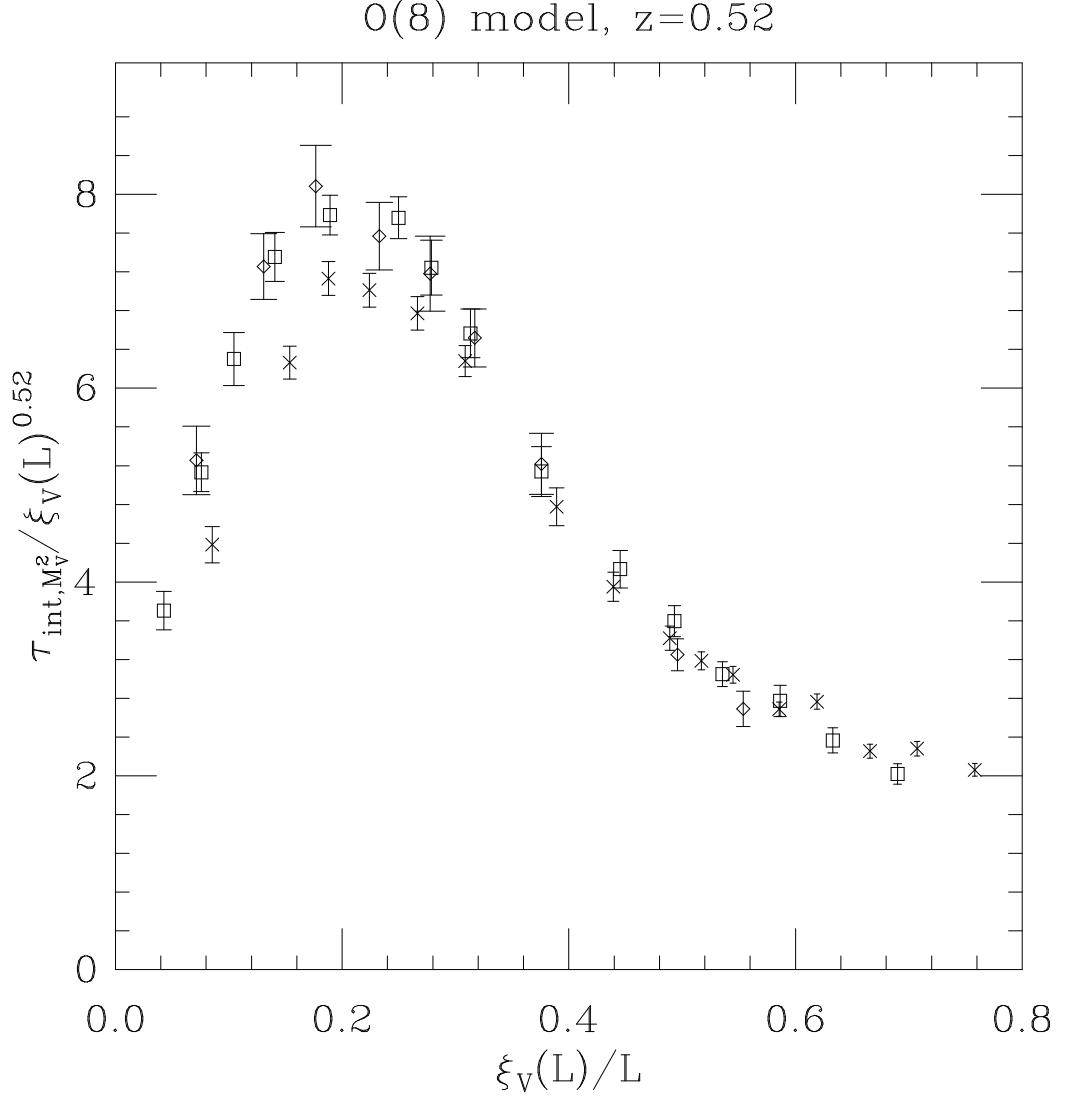


Figure 11: Dynamic finite-size-scaling plot of  $\tau_{int, \mathcal{M}_V^2} [\xi_V^{(2nd)}]^{-z_{int, \mathcal{M}_V^2}}$  versus  $\xi_V^{(2nd)}(\beta, L)/L$  for the two-dimensional 8-vector model. Lattice sizes are  $L = 64$  ( $\times$ ),  $128$  ( $\square$ ) and  $256$  ( $\diamond$ ). Here  $z_{int, \mathcal{M}_V^2} = 0.52$ .

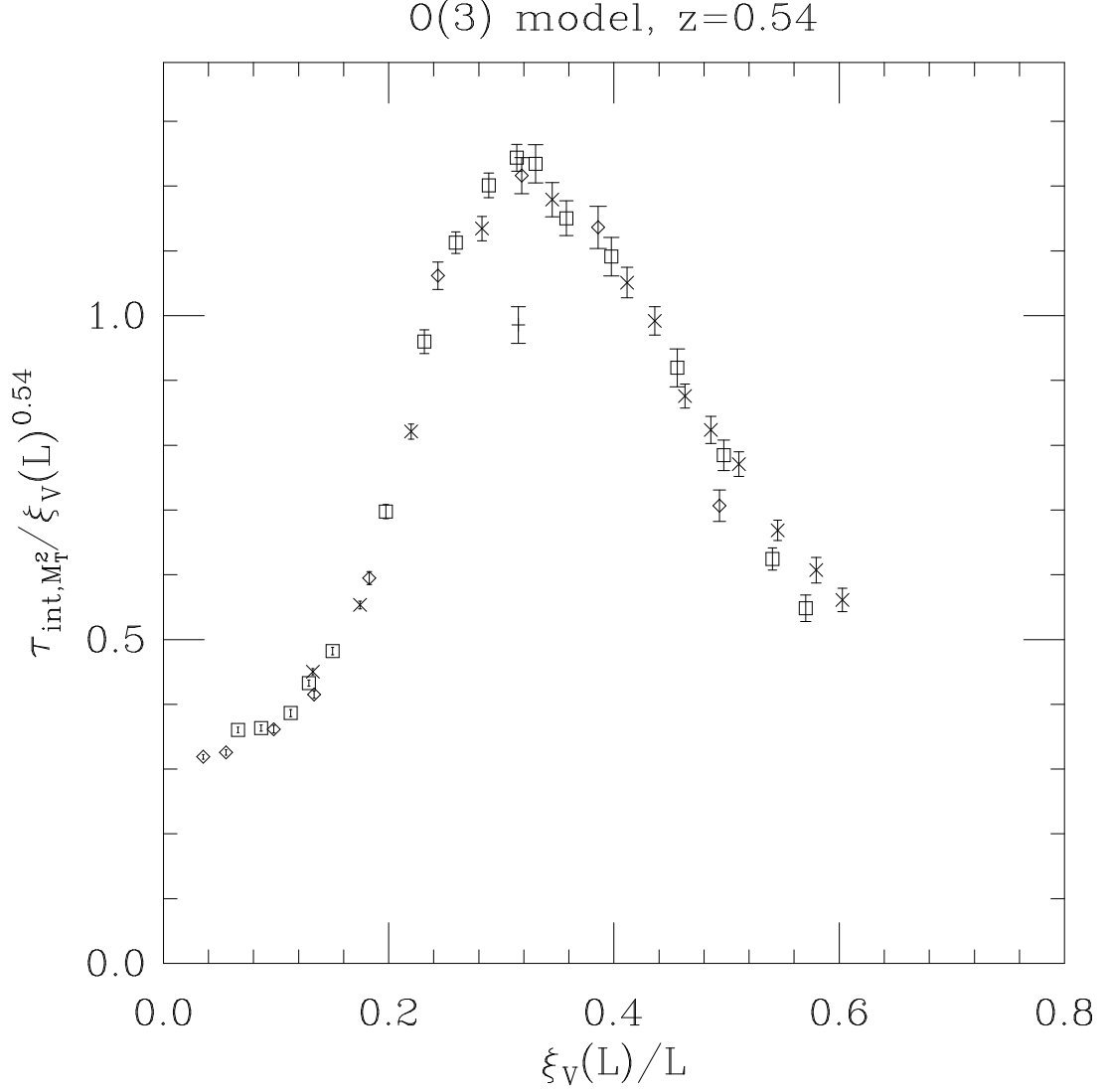


Figure 12: Dynamic finite-size-scaling plot of  $\tau_{int, \mathcal{M}_T^2} [\xi_V^{(2nd)}]^{-z_{int, \mathcal{M}_T^2}}$  versus  $\xi_V^{(2nd)}(\beta, L)/L$  for the two-dimensional 3-vector model. Lattice sizes are  $L = 32$  (+),  $64$  ( $\times$ ),  $128$  ( $\square$ ) and  $256$  ( $\diamond$ ). Here  $z_{int, \mathcal{M}_T^2} = 0.54$ .



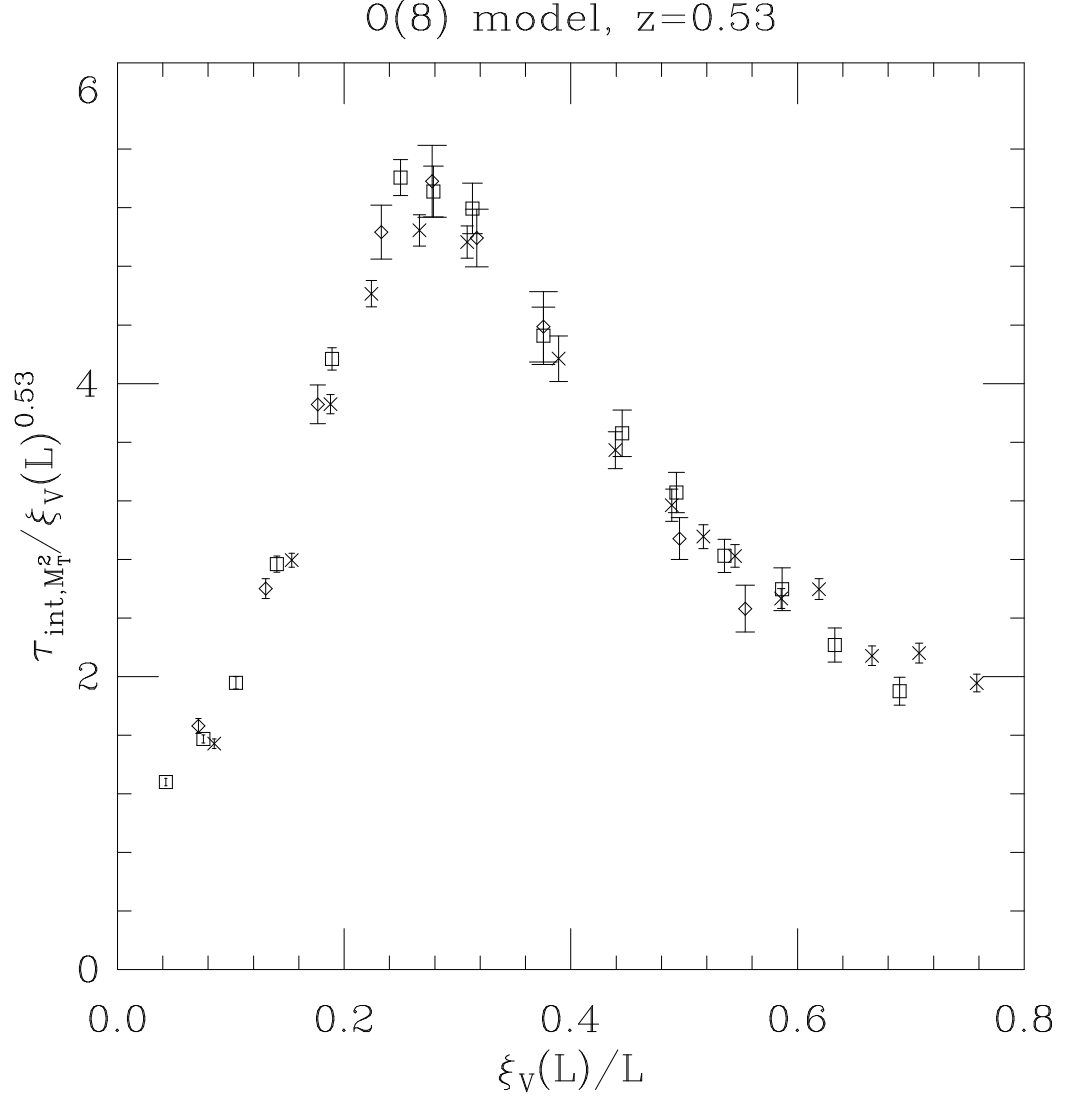


Figure 13: Dynamic finite-size-scaling plot of  $\tau_{int, \mathcal{M}_T^2} [\xi_V^{(2nd)}]^{-z_{int, \mathcal{M}_T^2}}$  versus  $\xi_V^{(2nd)}(\beta, L)/L$  for the two-dimensional 8-vector model. Lattice sizes are  $L = 64$  ( $\times$ ),  $128$  ( $\square$ ) and  $256$  ( $\diamond$ ). Here  $z_{int, \mathcal{M}_T^2} = 0.53$ .

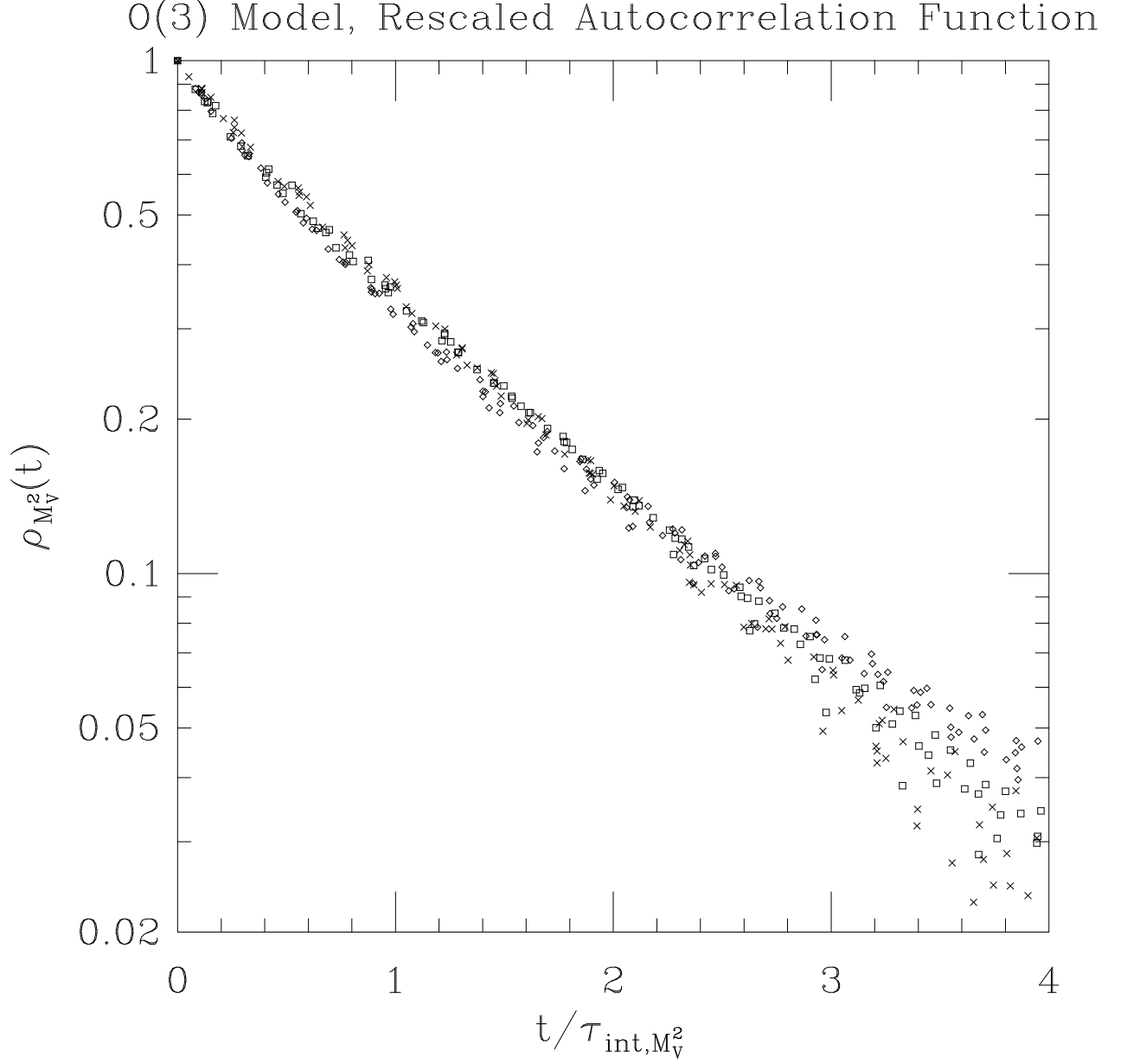


Figure 14: Autocorrelation function  $\rho_{M_V^2}$  as a function of time rescaled by  $\tau_{\text{int}, M_V^2}$  for  $N = 3$ . Only runs longer than  $20000 \tau_{\text{int}, M_V^2}$  are included. Symbols  $\times$  (resp.  $\square$ ,  $\diamond$ ) correspond to  $\xi(\beta, L)/L < 0.2$  (resp. between 0.2 and 0.4,  $> 0.4$ ).

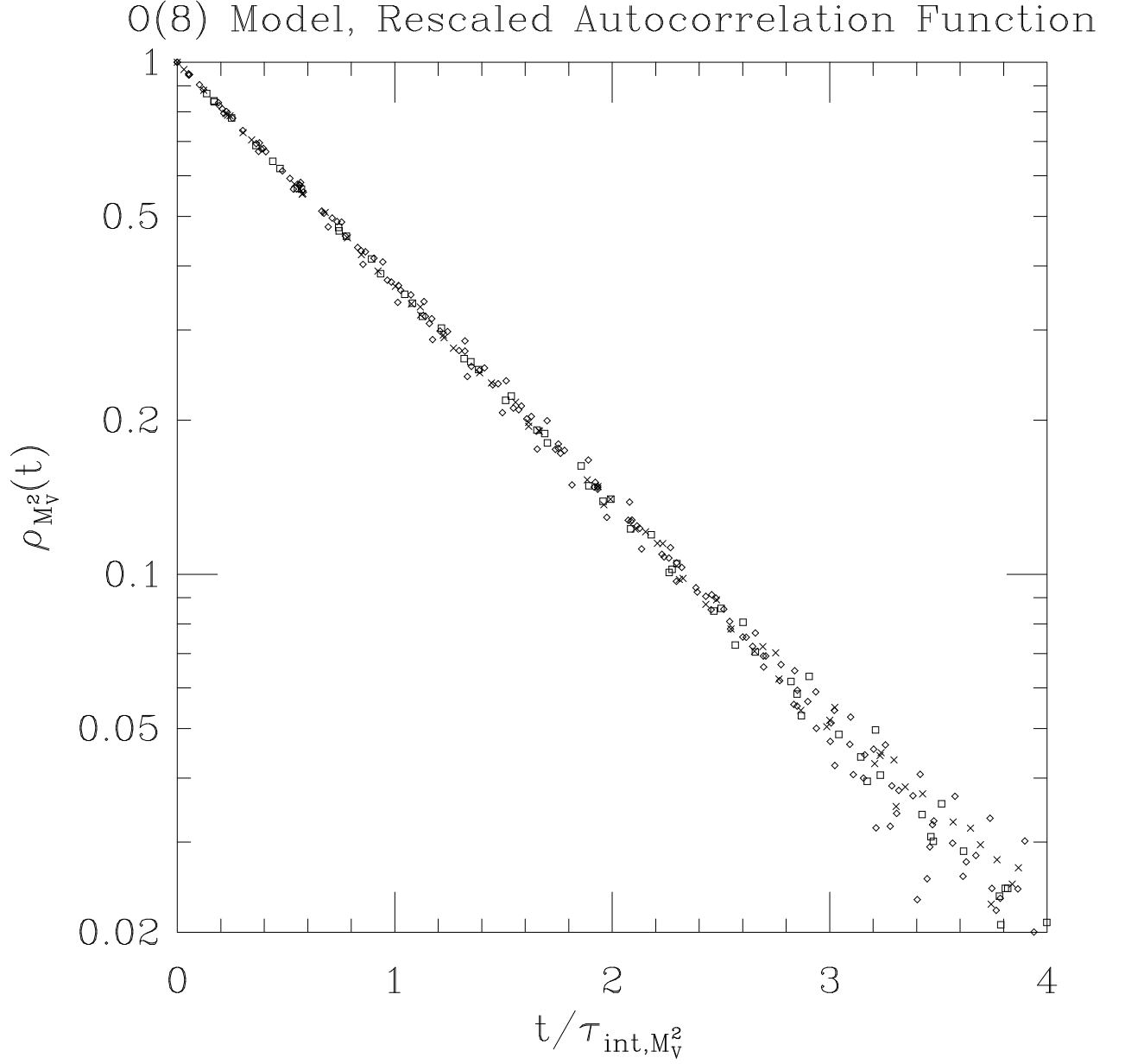


Figure 15: Autocorrelation function  $\rho_{M_V^2}$  as a function of time rescaled by  $\tau_{\text{int}, M_V^2}$  for  $N = 8$ . Only runs longer than  $20000 \tau_{\text{int}, M_V^2}$  are included. Symbols  $\times$  (resp.  $\square$ ,  $\diamond$ ) correspond to  $\xi(\beta, L)/L < 0.2$  (resp. between 0.2 and 0.4,  $> 0.4$ ).